

**NAVAL POSTGRADUATE SCHOOL**  
**Monterey, California**



**THESIS**

**EVALUATION OF THE CMARC PANEL CODE  
SOFTWARE SUITE FOR THE DEVELOPMENT OF A UAV  
AERODYNAMIC MODEL**

by

Stephen J. Pollard

June, 1997

Thesis Advisor:

Co-Advisor:

Max F. Platzer

Ismail H. Tuncer

**Approved for public release; distribution is unlimited.**

**DTIC QUALITY INSPECTED 4**

**19980102 097**

# REPORT DOCUMENTATION PAGE

Form Approved  
OMB No. 0704-0188

Public reporting burden for this collection of information is estimated to average 1 hour per response, including the time for reviewing instruction, searching existing data sources, gathering and maintaining the data needed, and completing and reviewing the collection of information. Send comments regarding this burden estimate or any other aspect of this collection of information, including suggestions for reducing this burden, to Washington headquarters Services, Directorate for Information Operations and Reports, 1215 Jefferson Davis Highway, Suite 1204, Arlington, VA 22202-4302, and to the Office of Management and Budget, Paperwork Reduction Project (0704-0188) Washington DC 20503.

<b>1. AGENCY USE ONLY (Leave blank)</b>		<b>2. REPORT DATE</b> June 1997	<b>3. REPORT TYPE AND DATES COVERED</b> Master's Thesis	
<b>4. TITLE AND SUBTITLE</b> EVALUATION OF THE CMARC PANEL CODE SOFTWARE SUITE FOR THE DEVELOPMENT OF A UAV AERODYNAMIC MODEL			<b>5. FUNDING NUMBERS</b>	
<b>6. AUTHOR(S)</b> Pollard, Stephen J.				
<b>7. PERFORMING ORGANIZATION NAME(S) AND ADDRESS(ES)</b> Naval Postgraduate School Monterey, CA 93943-5000			<b>8. PERFORMING ORGANIZATION REPORT NUMBER</b>	
<b>9. SPONSORING / MONITORING AGENCY NAME(S) AND ADDRESS(ES)</b>			<b>10. SPONSORING / MONITORING AGENCY REPORT NUMBER</b>	
<b>11. SUPPLEMENTARY NOTES</b> The views expressed in this thesis are those of the author and do not reflect the official policy or position of the Department of Defense or the U.S. Government.				
<b>12a. DISTRIBUTION / AVAILABILITY STATEMENT</b> Approved for public release; distribution unlimited.			<b>12b. DISTRIBUTION CODE</b>	
<b>13. ABSTRACT (maximum 200 words)</b> The CMARC panel code is evaluated to verify its accuracy and suitability for the development of an aerodynamic model of the Naval Postgraduate School (NPS) FROG Unmanned Air Vehicle (UAV). CMARC is a DOS personal computer based version of the NASA Panel Method Ames Research Center (PMARC) panel code. The core processing algorithms in CMARC are equivalent to PMARC. CMARC enhancements include improved memory management and command line functionality. Both panel codes solve for inviscid, incompressible flow over complex three-dimensional bodies using potential flow theory. Emphasis is first placed on verifying CMARC against the PMARC and NPS Unsteady Potential Flow (UPOT) panel codes. CMARC boundary layer calculations are then compared to experimental data for an inclined prolate spheroid. Finally, a complex three-dimensional panel model is developed for aerodynamic modeling of the FROG UAV. CMARC off-body flow field calculations are used to generate static-source and angle-of-attack vane position corrections. Position corrections are provided in look-up table and curve fit formats. Basic longitudinal and lateral-directional stability derivatives are also developed with CMARC data. CMARC derived stability derivatives are sufficiently accurate for incorporation into an initial aerodynamic model. Adjustments through analysis of flight test data may be required. Future CMARC studies should concentrate on the development of the damping and control power derivatives.				
<b>14. SUBJECT TERMS</b> Unmanned Aerial Vehicles, UAV, CMARC, PMARC, UPOT, Panel Code, Stability Derivatives, Boundary Layer Code, Computational Fluid Dynamics, CFD			<b>15. NUMBER OF PAGES</b> 151	
			<b>16. PRICE CODE</b>	
<b>17. SECURITY CLASSIFICATION OF REPORT</b> Unclassified	<b>18. SECURITY CLASSIFICATION OF THIS PAGE</b> Unclassified	<b>19. SECURITY CLASSIFICATION OF ABSTRACT</b> Unclassified	<b>20. LIMITATION OF ABSTRACT</b> UL	



Approved for public release; distribution is unlimited

**EVALUATION OF THE CMARC PANEL CODE SOFTWARE SUITE FOR THE  
DEVELOPMENT OF A UAV AERODYNAMIC MODEL**

Stephen J. Pollard  
Lieutenant Commander, United States Navy  
B.S., United States Naval Academy, 1982

Submitted in partial fulfillment of the  
requirements for the degree of

**MASTER OF SCIENCE IN AERONAUTICAL ENGINEERING**

from the

**NAVAL POSTGRADUATE SCHOOL**

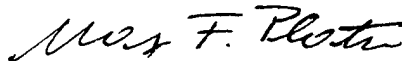
**June 1997**

Author:



Stephen J. Pollard

Approved by:



Max F. Platzer, Thesis Advisor



Ismail H. Tuncer, Co-Advisor



Daniel J. Collins, Chairman  
Department of Aeronautics and Astronautics



## ABSTRACT

The CMARC panel code is evaluated to verify its accuracy and suitability for the development of an aerodynamic model of the Naval Postgraduate School (NPS) FROG Unmanned Air Vehicle (UAV). CMARC is a DOS personal computer based version of the NASA Panel Method Ames Research Center (PMARC) panel code. The core processing algorithms in CMARC are equivalent to PMARC. CMARC enhancements include improved memory management and command line functionality. Both panel codes solve for inviscid, incompressible flow over complex three-dimensional bodies using potential flow theory. Emphasis is first placed on verifying CMARC against the PMARC and NPS Unsteady Potential Flow (UPOT) panel codes. CMARC boundary layer calculations are then compared to experimental data for an inclined prolate spheroid. Finally, a complex three-dimensional panel model is developed for aerodynamic modeling of the FROG UAV. CMARC off-body flow field calculations are used to generate static-source and angle-of-attack vane position corrections. Position corrections are provided in look-up table and curve fit formats. Basic longitudinal and lateral-directional stability derivatives are also developed with CMARC data. CMARC derived stability derivatives are sufficiently accurate for incorporation into an initial aerodynamic model. Adjustments through analysis of flight test data may be required. Future CMARC studies should concentrate on the development of the damping and control power derivatives.



## TABLE OF CONTENTS

I. INTRODUCTION.....	1
A. BACKGROUND.....	1
B. REQUIREMENTS.....	2
C. STATEMENT OF OBJECTIVES.....	2
II. OVERVIEW OF PERSONAL SIMULATION WORKS.....	5
A. GENERAL.....	5
B. LOFTSMAN.....	5
1. Streamlined Bodies.....	5
2. Wings and Control Surfaces.....	6
3. Patches.....	6
C. CMARC.....	6
D. POSTMARC.....	7
III. CMARC PANEL CODE THEORY.....	9
A. POTENTIAL FLOW PANEL CODE THEORY (CMARC/PMARC).....	9
B. CMARC BOUNDARY LAYER ANALYSIS THEORY.....	12
IV. CMARC VERIFICATION.....	17
A. VERIFICATION OF CMARC AGAINST PMARC.....	17
B. COMPARISON OF CMARC AND PMARC PROCESSING TIMES.....	20
C. COMPARISON OF CMARC TO THE UPOT BOUNDARY LAYER.....	23
CODE	
1. UPOT Boundary Layer Calculations.....	23
2. High AR Wing Model.....	23
3. Boundary Layer Results and Analysis (CMARC vs. UPOT).....	24
a. Boundary Layer Transition.....	24
b. Separation.....	25
c. Skin Friction Coefficient near the Stagnation Point.....	35
D. COMPARISON OF CMARC TO INCLINED PROLATE SPHEROID.....	36
EXPERIMENTAL DATA	



1. Inclined 6:1 Prolate Spheroid - AGARD AR-303 Case C-2.....	37
a. Wind Tunnel Experiment Setup.....	37
b. Experimental Data.....	38
c. Integration of Local Forces to Provide Lift Drag and Pitching Moment.....	40
2. CMARC Model of 6:1 Prolate Spheroid.....	42
3. Data Extraction.....	43
4. Prolate Spheroid Pressure Distribution.....	43
5. Boundary Layer Separation Locations.....	47
6. Boundary Layer Skin Friction Coefficient.....	49
7. Integrated Skin Friction Forces.....	51
8. Total Integrated Forces.....	52
V. AERODYNAMIC MODEL OF THE FROG UAV.....	55
A. BACKGROUND.....	55
B. FROG UAV DESCRIPTION.....	55
C. FROG UAV MODELING.....	58
1. General.....	58
2. Modeling Coordinate System.....	60
3. LOFTSMAN Patches.....	60
a. Fuselage Model.....	61
b. Main Wing Patch.....	61
c. Horizontal Stabilizer Patch.....	62
d. Vertical Stabilizer Patch.....	62
e. Tail Boom Patch.....	62
f. Engine Pod Patch.....	63
g. Engine Pylon Patch.....	63
4. Common CMARC Input File Errors.....	63
D. STATIC-PRESSURE SOURCE AND YAW VANE CORRECTIONS THROUGH OFF-BODY FLOW ANALYSIS.....	64
1. Description of the FROG UAV Pitot-Static and AOA Systems.....	64
2. Modeling Off-Body Streamlines.....	64

3. Analysis of Static Source Position Errors.....	66
4. Analysis of Alpha Vane Position Error.....	72
5. Summary of Off-Body Flow Field Analysis.....	72
E. DEVELOPMENT OF BASIC STABILITY DERIVATIVES.....	75
1. Longitudinal Stability Derivatives.....	75
a. Longitudinal Stability Derivative Methods.....	75
b. Analysis of Longitudinal Stability Data.....	78
2. Lateral Directional Stability Derivatives.....	79
a. Lateral-Directional Stability Derivative Methods.....	79
b. Analysis of Lateral-Directional Stability Data.....	81
3. Summary of CMARC Stability Derivative Analysis.....	81
VI. CONCLUSIONS AND RECOMMENDATIONS.....	83
APPENDIX A. DEVELOPMENT OF THE MOMENTUM INTEGRAL.....	85
EQUATION	
APPENDIX B. INTEGRATION OF AERODYNAMIC FORCES OVER THE.....	89
SURFACE OF A PROLATE SPHEROID	
APPENDIX C. MATLAB PROGRAMS TO INTEGRATE AERODYNAMIC.....	93
FORCES OVER THE SURFACE OF A PROLATE	
SPHEROID	
APPENDIX D. REPRESENTATIVE CMARC/PMARC SPEED TEST FILE.....	95
APPENDIX E. MATLAB PROGRAM FOR REORDERING AGARD DATA.....	97
FILE	
APPENDIX F. CMARC PROLATE SPHEROID INPUT FILE.....	99
APPENDIX G. CMARC/PMARC DATA EXTRACTION PROGRAM.....	107
APPENDIX H. LOFTSMAN INPUT FILES.....	109
APPENDIX I. FROG UAV CMARC INPUT FILE.....	117
LIST OF REFERENCES.....	137
INITIAL DISTRIBUTION LIST.....	139



## I. INTRODUCTION

### A. BACKGROUND

Computational fluid dynamics (CFD) is increasingly used as a design and analysis tool. As the price of computer hardware drops and computational power increases, CFD becomes more attractive to a larger audience. CFD tools range from the high end three-dimensional (3D) Navier-Stokes solvers for compressible, viscous fluids to potential flow solvers for incompressible, inviscid flows. This paper discusses the development of a DOS personal computer hosted panel code model for the Naval Postgraduate School (NPS) Fiber Optic Guided (FROG) Unmanned Air Vehicle (UAV) program.

The Personal Simulation Works software suite, consisting of LOFTSMAN, CMARC and POSTMARC, is used for all aspects of the study. The software provides for panel model development, input file processing and the visualization of results. Emphasis is placed on verifying both the accuracy and suitability of the CFD programs for aerodynamic modeling.

Until recently, personal computers (PC) did not have the computational power or memory to be practical for panel code CFD programs. Things have changed with the introduction of the Pentium class PC and low cost RAM. AeroLogic capitalized on the power of the Pentium class PC and developed Personal Simulation Works (PSW). PSW is centered around the 3D low order, inviscid potential flow solver named CMARC. CMARC is a re-hosted version of NASA's Panel Method Ames Research Code (PMARC). PMARC was re-written in the C language and compiled for IBM compatible PCs. CMARC runs under the DOS operating system. CMARC will also run in a DOS window under the WINDOWS 3.x, 95 or NT operating systems. CMARC has enhanced capabilities that include; improved memory management, an expanded set of command line switches and provisions for expanded boundary layer post-processing capabilities. However, the core processing algorithms remain the same as implemented in PMARC.

LOFTSMAN, the PSW pre-processing program, is used to mesh complex 3D bodies and create input file patches. The program runs under the DOS operating system and allows the user to loft conics based 3D surfaces. The program automatically creates CMARC, PMARC or VSAERO input patches based on desired panel densities and distribution.

POSTMARC is used for flow visualization and integration of resultant forces. It runs under the Windows 3.x, 95 and NT operating systems. POSTMARC reads CMARC or PMARC output files and provides for the visualization of model geometry, wake stepping, on and off-body streamlines and surface phenomena.

## **B. REQUIREMENTS**

The Naval Postgraduate School Aeronautics Department is integrating UAV hardware and software to demonstrate autonomous flight, trajectory tracking and automatic landing. A core requirement for flight control development is a valid aerodynamic truth model for the UAV airframe. The introduction of each new airframe requires the development of a new aerodynamic truth model. Most recently, Papageorgiou [Ref. 1] developed and tested an aerodynamic model for the NPS FROG UAV based on classical methods. His model produced a close match to flight test results in the longitudinal axis. However, the lateral-directional axis required modifications based on measured flight test data to produce acceptable results. With the availability of low cost panel code CFD capabilities, it is suggested that a panel code model of the FROG UAV is an alternative for estimating many of the stability derivatives required for an aerodynamic truth model.

Accurate pitot-static and angle-of-attack sensors are required for highly augmented flight control systems. CMARC is well suited for solving on-body static pressure distributions and off-body flow velocities over the predominately attached flow fields of fuselage fore bodies. This proves particularly useful for generating pitot static and angle of attack correction curves and look-up tables.

## **C. STATEMENT OF OBJECTIVES**

The Naval Postgraduate School Aeronautics Department has both active CFD research and avionics development programs. The primary purpose of this investigation is to verify the accuracy and suitability of the PSW software suite while developing a panel code model for the NPS FROG UAV program. Specific objectives are as follows:

- Demonstrate panel code modeling, processing and visualization on a Pentium PC using the PSW software package.

- Verify CMARC results against PMARC.
- Investigate the CMARC integral boundary layer calculations through comparison to validated 2D CFD codes and 3D experimental data.
- Develop and analyze a panel code model for the NPS FROG UAV using PSW to estimate basic stability derivatives and produce angle-of-attack vane and pitot-static correction curves.
- Compare relative speed of CMARC hosted on 150 MHz Pentium personal computer to PMARC hosted on a Silicon Graphics Indigo<sup>2</sup> workstation.



## II. OVERVIEW OF PERSONAL SIMULATION WORKS

### A. GENERAL

Personal Simulation Works is a PC based software suite that provides for the three primary CFD requirements; 3D modeling of an aircraft (LOFTSMAN), panel code flow solver (CMARC), and post-processing of the computed flow field (POSTMARC). The software package contains three applications hosted on the IBM compatible personal computer. Each software program is discussed separately.

### B. LOFTSMAN

LOFTSMAN is a 3D modeling tool that generates surface panel distributions for CMARC or PMARC input files. The program is based on conics, which allows rapid lofting of streamlined bodies such as aircraft fuselages and engine nacelles. In addition, wing and control surfaces can be designed with the extensive library of airfoil templates or with user specified coordinates. The software is well documented, including a tutorial, in the Personal Simulation Works User Guide [Ref. 2]. LOFTSMAN is primarily designed for creating new objects, but an existing airframe can be matched quite closely with just a detailed three-view drawing that includes frame cross sections.

#### 1. Streamlined Bodies

LOFTSMAN functionality is divided into Body Objects and Wing Objects. In general, they remain separate unless the intersection between a wing and body is required.

Body Objects are created using a family of curves called second-degree conics. Circles, ellipses, parabolas and hyperbolas are among this group. An entire fuselage is described by specifying just four lines. These are the top waterline (TW), bottom waterline (BW), the maximum breadth line (MB) and the waterline of the maximum breadth line (WW). For each line, the beginning, ending and a few points along the line are specified. Control points are also specified with a curvature factor that allows LOFTSMAN to generate a smooth conic between the points. The power of conic lofting will become evident when discussing the modeling of the complex FROG UAV fuselage in Chapter V.



## **2. Wings and Control Surfaces**

Wings and control surfaces are easily specified in LOFTSMAN using a short input file created with any text editor. The file specifies root, intermediate and tip rib section, location, axis, chord and incidence. LOFTSMAN then fairs a smooth surface through the rib sections. Washout is specified by varying the incidence of the root and tip ribs. Sweep-back is controlled by staggering the tip rib location with respect to the root rib. Once the general wing surface is specified, control surfaces such as ailerons, flaps and elevators can be deflected and meshed.

## **3. Patches**

LOFTSMAN automatically meshes 3D surfaces and creates patches for CMARC/PMARC input files. The distinction between a mesh and a patch is important. A mesh is a set of quadrilateral and triangular panels that represent the surface of a wing or body. When the set of panels is organized and formatted to create a sub-component portion of a CMARC or PMARC input file, it is called a patch.

A body or wing surface is first meshed at a density specified by the user. Cosine and half-cosine spacing are among the compression options. After meshing the object, one saves it to a text file as a formatted patch. One then opens the patch file with any text editor and copies/pastes the patch text into the appropriate location in the CMARC input file.

Each control surface deflection requires a separate mesh and formatted patch. For instance, to evaluate roll performance one needs to separately mesh an upward aileron deflection on the right wing and a downward deflection on the left wing. If multiple deflections of a single control surface are required, each deflection must be meshed separately.

## **C. CMARC**

CMARC is the C version of the Panel Method NASA Ames Research Center (PMARC) low order, 3D panel code. Inviscid, irrotational, incompressible, potential flow is assumed. Low order means that source and doublet strength distribution is constant across a panel. There is no attempt to match the source or doublet strength of an adjacent

panel at a common edge. Advanced features include internal flow modeling and time stepping wake models.

PMARC version 12.19 was released as FORTRAN 77 source code in 1992. CMARC was rewritten in the C language and compiled for hosting on IBM compatible personal computers by AeroLogic, Inc. The program runs under the DOS operating system. It will also run in a DOS window from Windows 3.1, 95 or NT. Enhanced features include command line options and flexible memory management. Command line options simplify batch processing by adding an extensive set of switches that can be set external to the CMARC input file. Flexible memory management provides for the automatic sizing of arrays without having to recompile the source code.

#### **D. POSTMARC**

POSTMARC is a Windows post-processing program for the visualization of CMARC and PMARC output files. Capabilities include body geometry, wake stepping, surface pressure and streamline visualization. POSTMARC also provides the capability to integrate pressure and skin friction forces over the model geometry. This proves particularly useful when one desires to recalculate loads around a different center of gravity.

An interesting feature for design work integrates panel surface area to obtain total wetted area. After lofting a new geometry in LOFTSMAN, a quick check of geometry is made by running CMARC with the -g command line toggle. The total wetted area is then checked in POSTMARC. This function is particularly useful when working to reduce skin friction drag.

Versions 1.17.3 and later of POSTMARC include the capability to integrate skin friction drag coefficient over the model geometry. It is important to note that a key piece of the drag equation is missing from a POSTMARC solution. CMARC provides induced drag from the surface pressure distribution and skin friction drag from the 2D boundary layer code. Skin friction is only calculated up to the point of boundary layer separation. Pressure drag due to separation, a major portion of the drag equation, is missing from a CMARC/POSTMARC solution.

In fact, if one isn't careful, POSTMARC drag calculations can be misleading. Take for instance two similar model configurations with only minor geometry differences that do not affect wetted area. It is possible for the model with more flow separation to

have less skin friction drag because there is no CMARC output for skin friction coefficient after the boundary layer code predicts separation. During iterative design work, this could lead to the incorrect conclusion that the design team is reducing overall drag. Perhaps a better function for LOFTSMAN than integrated skin friction drag would be a function that predicts the percentage of attached flow and laminar flow. Iterative design changes could be made that maximize laminar flow and minimize separated flow.

### III. CMARC PANEL CODE THEORY

#### A. POTENTIAL FLOW PANEL CODE THEORY (CMARC/PMARC)

Potential flow theory involves the superposition of sources and doublets to generate the desired flow field around a 3D body. It assumes inviscid, irrotational and incompressible flow. As such, valid solutions are only obtained at low Mach numbers and for flow fields without large areas of separation.

The basic concept of panel methods, as outlined by Bertin and Smith [Ref. 3], requires the modeling of the desired 3D configuration with a large number of quadrilateral and triangular panels representing the surface of the aircraft. A series of sources, doublets and vortices is then distributed on each panel. Superposition allows the simultaneous computation of the singularity strengths required to satisfy flow tangency on the surface. The inviscid, irrotational and incompressible flow field represented by the superposition of sources and doublets satisfies the Laplace equation:

$$\nabla^2 \Phi = 0 \quad 3.1$$

Using Green's Theorem, the potential at any point P in the flow is represented by:

$$\Phi_P = \frac{1}{4\pi} \iint_{S+W} (\Phi - \Phi_i) \bar{n} \nabla \left( \frac{1}{r} \right) dS - \frac{1}{4\pi} \iint_{S+W} \left( \frac{1}{r} \right) \bar{n} \cdot (\nabla \Phi - \nabla \Phi_i) dS \quad 3.2$$

Where  $(\Phi - \Phi_i)$  represents the potential from the doublet distribution and  $\bar{n} \cdot (\nabla \Phi - \nabla \Phi_i)$  represents the potential from the source distributions.

CMARC is a low order panel code that assumes constant source and doublet strength distributions across each panel. Figure 3.1 shows a panel layout for a generic 3D wing fuselage configuration. It is important to note that for a 3D solution, there is an equivalence to surface doublet and surface vortex distributions. CMARC implements source and doublet distributions.

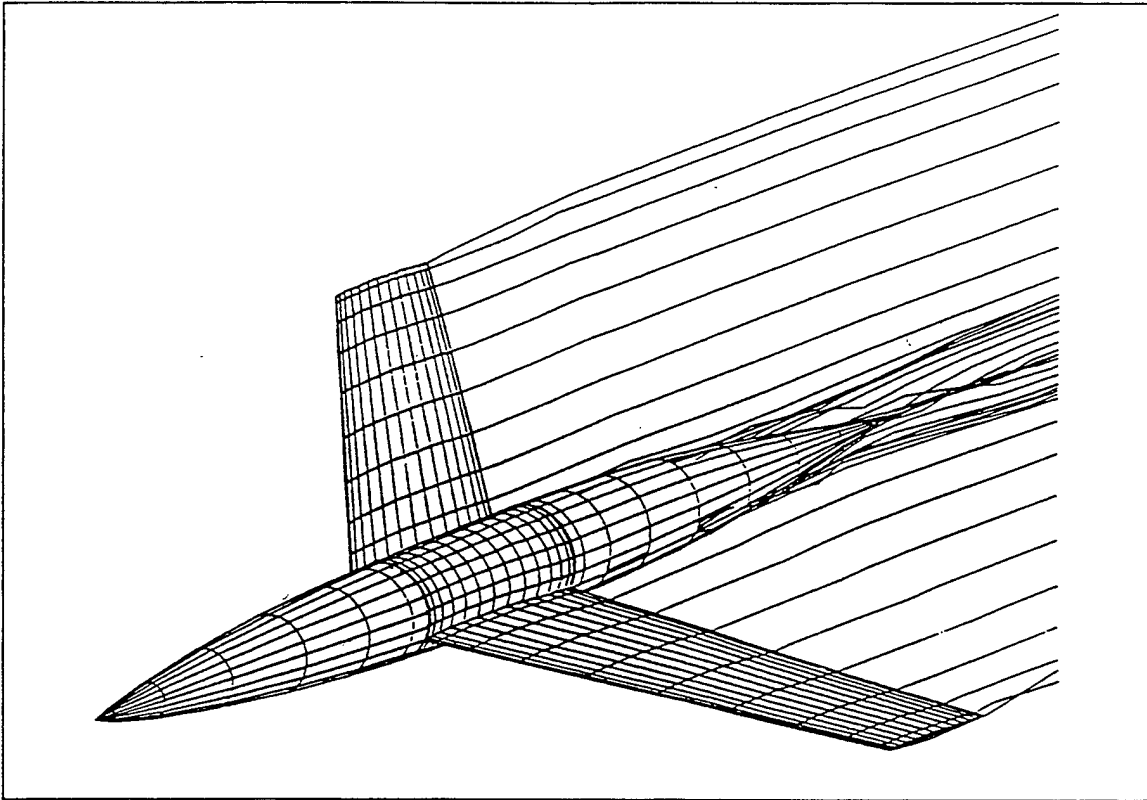


**Figure 3.1 Typical Wing-Body Panel Code Configuration, from Ref. [4].**

As mentioned previously, the general boundary condition imposed is tangential flow at the surface. CMARC, as outlined in Ref. [2], allows the modification of this boundary condition on individual panels or groups of panels. A normal surface velocity distribution may be specified to simulate flow into or out of ducts.

In order to produce lift, a potential flow panel code requires a method to implement the Kutta condition. As noted in Anderson [Ref. 5], the Kutta condition at the trailing edge implies that the circulation,  $\Gamma$ , around an airfoil is such that the flow exits the trailing edge smoothly. In addition, the velocities leaving the top and bottom surfaces are finite and equal in magnitude and direction.

Panel codes impose the Kutta condition by the shedding of wake panels along the trailing edges or separation lines. Wake panels are similar to a surface panel with only a doublet distribution. The doublet strength of the attached wake panel equals the difference in doublet strengths of the two adjacent surface panels.

The CMARC core panel code processing engine is functionally equivalent to the PMARC panel code module. The implemented equations are well documented by Ashby et al. [Ref. 4]. The PMARC documentation includes a wing-body combination, shown in Figure 3.1, evaluated by PMARC with good correlation to experimental data. The results are shown in Figures 3.2 and 3.3. In addition, Lambert [Ref. 6] compared PMARC panel code results to several theoretical and experimental test cases with good correlation at low angle-of-attack. Sensitivity to wake placement is highlighted by his studies.

Wake positioning can have a large influence on potential flow solutions. A wake is obviously attached to the trailing edge of wings and control surfaces with sharp, thin trailing edges to produce the Kutta condition. However, wake positioning on streamlined fuselages, missile airframes and nacelles is more of an art than science. Recently, Tuncer and Platzer [Ref. 7] investigated generalized wake placement techniques for cylindrical bodies of revolution with good correlation to experimental data at up to 20 degrees angle-of-attack. The techniques are used in this study with success for the verification of CMARC calculations for flow over an inclined 6:1 prolate spheroid.

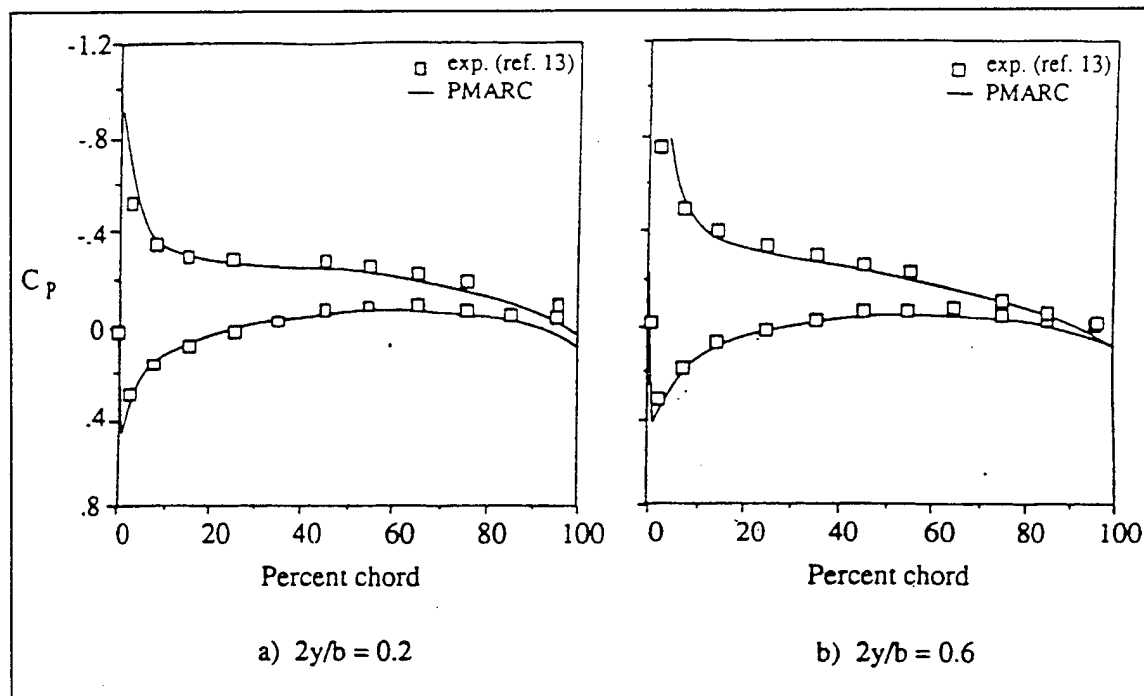


**Figure 3.2 Comparison of Experimental Data and PMARC Results for Two Spanwise Stations of the Wing/Body ( $\alpha = 4^\circ$ ), from Ref. [4].**

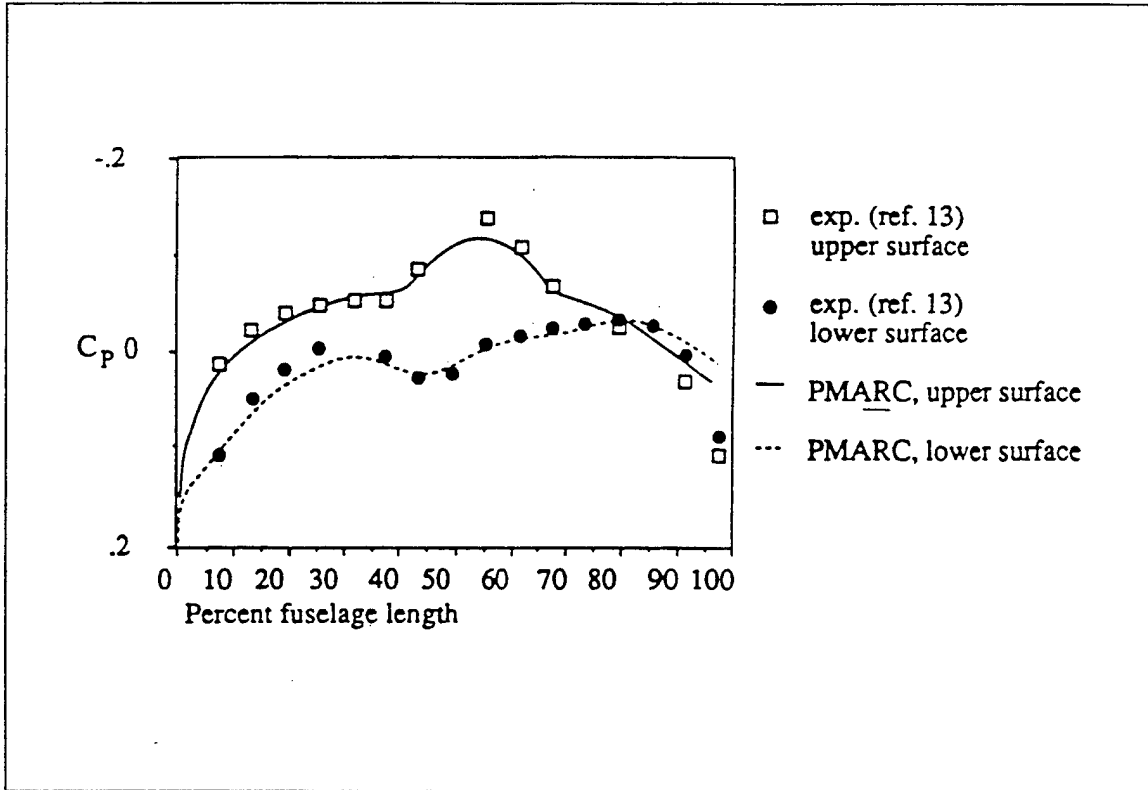


**Figure 3.3 Comparison of Experimental Data and PMARC Along the Fuselage Centerline of the Wing/Body Configuration ( $\alpha = 4^\circ$ ), from Ref. [4].**

## B. CMARC BOUNDARY LAYER ANALYSIS THEORY

CMARC and PMARC use the same two-dimensional integral method to calculate boundary layer characteristics along a surface streamline. A transition model automatically switches from laminar to turbulent calculations. The developers of the PMARC code chose a 2D integral routine over a 3D finite difference grid method due to speed and robustness of the calculations [Ref. 4]. Building a finite difference grid is a difficult and time consuming process requiring the user to develop grids over complex 3D surfaces. In addition, boundary layer calculation times can easily exceed that required for the basic potential flow solution. Reference [8] gives a good outline of three-dimensional finite difference methods.

The CMARC and PMARC User's Guides [Refs. 2 and 4] contain detailed discussions on the development of the CMARC/PMARC boundary layer code starting from the two-dimensional momentum equation:

$$\frac{d\theta}{d\eta} + (2 + H) \frac{\theta}{U} \frac{dU}{d\eta} = \frac{1}{2} C_f \quad 3.3$$

The momentum integral equation is numerically integrated along a surface streamline. The derivation leading to Equation 3.3 is developed in Appendix A for completeness.

The laminar region of the boundary layer is modeled by numerically integrating the following exact differential equation. The equation is solved iteratively through numerical integration along a streamline starting at a stagnation point [Ref. 4]:

$$\theta(\eta)^2 = \frac{0.45\nu}{U(\eta)^6} \int_0^\eta (1 + 2.222g(K, \mu)) U(\eta)^5 d\eta + \theta(0)^2 \left( \frac{U(0)}{U(\mu)} \right)^6 \quad 3.4$$

Where: U - velocity at outer edge of boundary layer  
 $\theta$  - momentum thickness  
 $K = \frac{\theta^2}{\nu} \frac{dU}{d\eta}$   
 $\eta$  - generalized coordinate along a streamline

The value  $g(K, \mu)$  is based on exact solutions for a number of pressure distributions. Initial work was conducted by Thwaites with improvements by Curle [Ref. 9]:

$$g(K, \mu) = F_0(K) - \mu G_0(K) - 0.45 + 6K \quad 3.5$$

CMARC uses an empirical transition model based on the average pressure gradient,  $\bar{K}$ , for predicting laminar to turbulent transition. The following relations are used to calculate the transition point [Ref. 4]:



$$\bar{K} = \frac{\int_{\eta_{ins}}^{\eta} K d\eta}{\eta - \eta_{ins}} \quad 3.6$$

Where  $\eta_{ins}$  is the streamline coordinate at instability. And, K is the local pressure gradient at boundary layer instability [Ref. 4]:

$$K = -0.4709 + 0.11066 * \ln(\text{Re}_\theta) + 0.0058591 * \ln^2(\text{Re}_\theta) \quad (0 \leq \text{Re}_\theta \leq 650) \quad 3.7$$

$$K = 0.69412 - 0.23992 * \ln(\text{Re}_\theta) + 0.0205 * \ln^2(\text{Re}_\theta) \quad (650 < \text{Re}_\theta \leq 10000)$$

The local Reynolds number at transition is correlated to  $\bar{K}$  with the following expressions [Ref. 4]:

$$\bar{K} = -0.0925 + 0.00007 * \text{Re}_\theta \quad (0 \leq \text{Re}_\theta \leq 750)$$

$$\bar{K} = -0.12571 + 0.000114286 * \text{Re}_\theta \quad (750 < \text{Re}_\theta \leq 1100) \quad 3.8$$

$$\bar{K} = 1.59381 - 0.45543 * \ln(\text{Re}_\theta) + 0.032534 * \ln^2(\text{Re}_\theta) \quad (1100 < \text{Re}_\theta \leq 3000)$$

At transition, the initial turbulent shape factor, H, is given by the following empirical formula that is a fit to data developed by Coles [Ref. 9]:

$$H = \frac{1.4754}{\log_{10}(\text{Re}_\theta)} + 0.9698 \quad 3.9$$

Provisions are made to check for turbulent reattachment if laminar separation is encountered. At laminar separation, a point calculation is made to determine if the boundary layer will reattach. If reattachment is predicted, the boundary layer code immediately switches to turbulent calculations. No attempt is made to model the laminar separation bubble or provide a transition length. After laminar separation is predicted, the following empirical relations are used to determine if reattachment occurs [Ref. 4]:

$$\begin{aligned}
 K &= 0.0227 - 0.007575 * Re_{\theta} - 0.000001157 * Re_{\theta}^2 && (Re_{\theta} \geq 125) \\
 K &= -0.09 && (Re_{\theta} < 125)
 \end{aligned}
 \tag{3.10}$$

The boundary layer code in CMARC uses a point transition model. No attempt is made to model a more representative transition length. Turbulent calculations begin at transition using the Nash-Hicks model [Ref. 4]. Calculations continue along the streamline until turbulent separation is predicted or the end of the streamline is reached. No boundary layer data is available after separation.

The authors of PMARC caveat that their boundary layer calculations are quite accurate for predominately 2D flow but break down in regions of large cross flow near separation. This premise will be first tested by comparing predominately 2D flow over the inboard region of a high aspect ratio wing to the finite difference calculations performed by the Naval Postgraduate School Unsteady Potential Flow Code (UPOT). Then a comparison is made to experimental data for flow over an inclined prolate spheroid. The 6:1 prolate spheroid is chosen because of the availability of extensive experimental data. In addition, three-dimensional flow around the prolate spheroid is similar to flow around a streamlined slender fuselage.



## IV. CMARC VERIFICATION

### A. VERIFICATION OF CMARC AGAINST PMARC

The first step in CMARC verification is comparison with NASA's PMARC panel code. CMARC is PMARC-12 rewritten in C from FORTRAN. Additionally, CMARC is compiled for hosting on an IBM compatible PC. Other than some added command line functionality and significant memory management improvements, the CMARC basic panel code and boundary layer routines are equivalent to PMARC and should produce the same results. However, due to the recent fielding of CMARC, the author felt it prudent to spot check the solutions to verify equivalency.

CMARC and PMARC were both fed an identical input file for a straight NACA 2415 wing with a 6.4 aspect ratio at 5 degrees angle of attack. The input file is listed in full in Appendix C. Figures 4.1 and 4.2 show CMARC and PMARC pressure coefficients cross-plotted for chordwise and spanwise wing stations respectively. The results overlay as an identical match. Figure 4.3 and 4.4 display the boundary layer calculations for skin friction coefficient and displacement thickness. Again the results overlay. Integrated forces and moment listings were also identical. From this, it is inferred that CMARC and PMARC produce equivalent results.

Although both programs produce equivalent results, it is worthy to note that there are occasionally small, insignificant differences in floating point calculations and rounding. Some results differ by a digit in the sixth decimal place. In addition, with identical input files, there can be a difference in convergence likelihood. Occasionally, PMARC failed to converge when CMARC did. Again, floating point differences are the most likely source of the disparity. Regardless, difference in the rates of convergence were slight and relatively transparent to the user. However, in all cases CMARC was better behaved with a higher likelihood of convergence. It is concluded that CMARC and PMARC results are interchangeable.

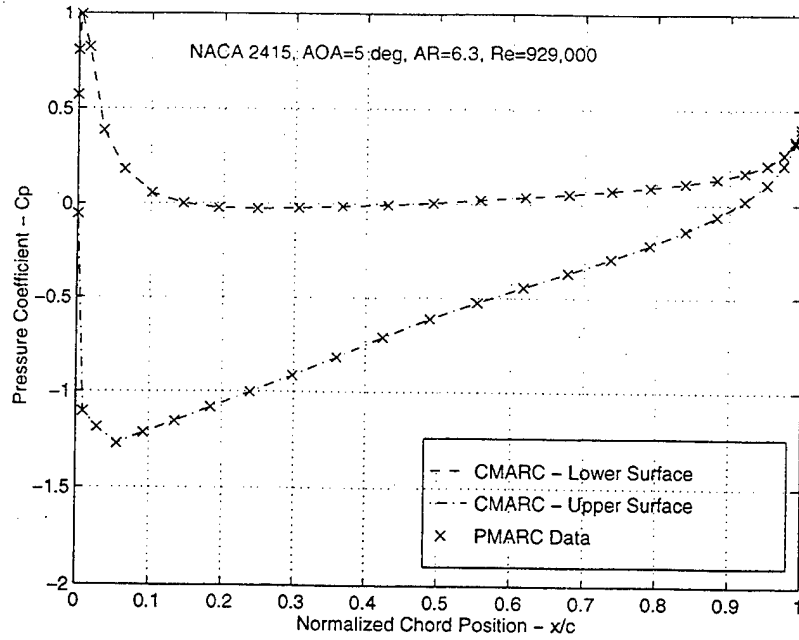


**Figure 4.1 Comparison of CMARC and PMARC Pressure Coefficients For a Chordwise Wing Station.**

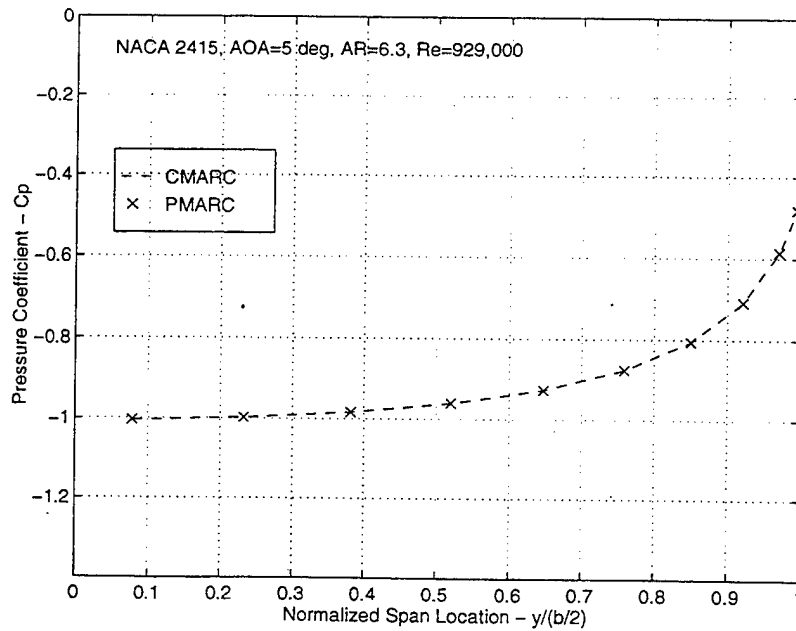


**Figure 4.2 Comparison of CMARC and PMARC Pressure Coefficients For a Spanwise Wing Station.**

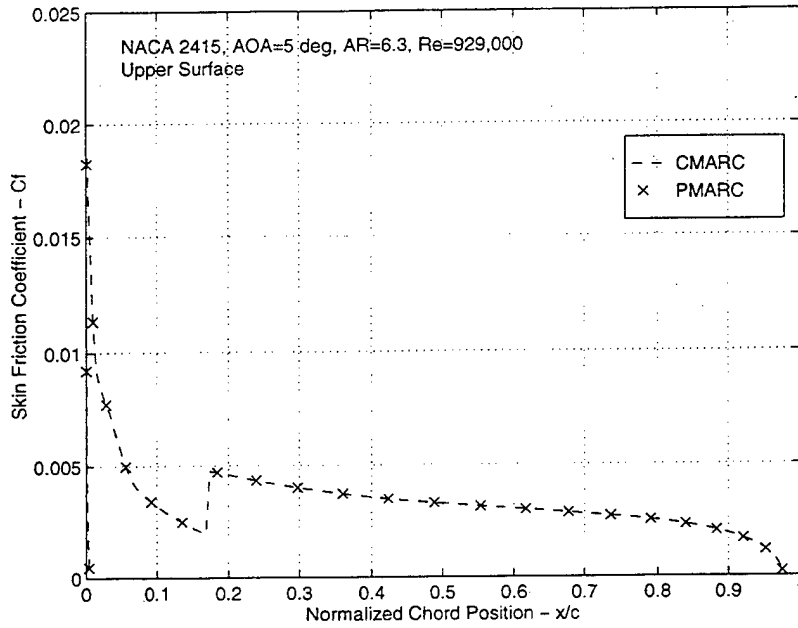


**Figure 4.3 Comparison of CMARC and PMARC Skin Friction Coefficient for an Upper Wing Surface Streamline.**

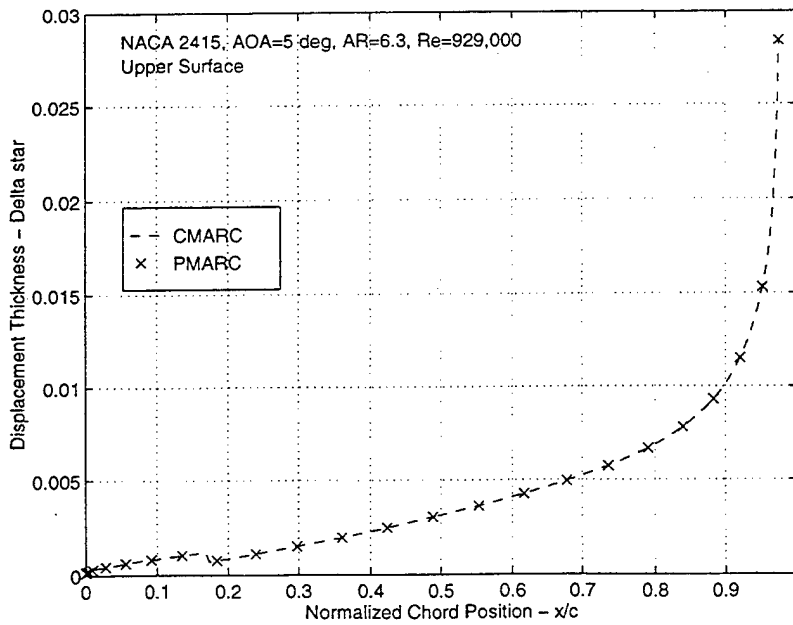


**Figure 4.4 Comparison of CMARC and PMARC Boundary Layer Displacement Thickness for an Upper Wing Surface Streamline.**

## B. COMPARISON OF CMARC AND PMARC PROCESSING TIMES

One of the primary metrics in determining suitability of a panel code hosted on an inexpensive PC is processing time. CMARC's processing speed should be within an order of magnitude of PMARC hosted on the NPS Aeronautics Department Silicon Graphics (SGI) workstations to be of much utility. To this end, processing times were compared for identical input models ranging from 200 to 1600 panels. Comparisons were performed between a 150 MHz/48 MB Pentium PC and two configurations of networked SGI Indigo<sup>2</sup> workstations. One workstation was the 150 MHz/64 MB Indigo<sup>2</sup> (Viper) running the IRIX 5.3 operating system and the other a 250 MHz/128 MB SGI Indigo<sup>2</sup> (Aurora) workstation running IRIX 6.2. With both workstations, file input/output is addressed through the network to the server.

Three versions of PMARC were tested. The first version, "pmarc12" located in the local/usr/bin, was compiled in FORTRAN to run on the older IRIX 5.3 operating system. The second version, "pmarc-inram," was compiled with Dynamic Linked Libraries (DLLs) to run on the new IRIX 6.2 operating system. These first two PMARC executable codes were compiled with the "in RAM" flag selected for matrix storage. This considerably reduced hard disk accessing time. PMARC either keeps all the matrices in RAM or all on the file server depending on whether the RAM flag is when compiled. Flexible memory management allows CMARC to fill available RAM and then automatically spill over to the hard drive. This reduces user memory management requirements.

A third version, "pmarc\_dll," was compiled with DLLs, but the matrix storage flag was inadvertently set to hard drive instead of RAM. Processing times were considerably longer with this option selected. It is not recommended unless the computer is RAM limited.

The input model used was a NACA 2415 finite wing with four time steps. The panel density was varied to obtain the desired panel count. Appendix D contains a representative input file.

The processing benchmarks showed that CMARC, hosted on a PC, is significantly faster than all three versions of PMARC hosted on the networked SGI workstations. Table 4.1 summarizes results for identical models ranging from 200 - 1600 panels.

Figure 4.5 is a plot of processing time vs. panel count for models ranging from 200 to 1600 panels. For small sized models, all configurations are relatively close to the

same speed. As the model size increases, processing time increases roughly as the square of model size. However, as model size increases, all versions of PMARC on the networked SGI workstations become significantly slower than CMARC on the PC. This is most likely due to the slower file read/write access times to the file server. The version of PMARC with the matrix storage flag set to hard drive required considerably more processing time than the two versions with RAM selected.

Platform CPU / RAM Program	Pentium PC 150 MHz / 48 MB	SGI Indigo <sup>2</sup> 150 MHz / 64 MB		SGI Indigo <sup>2</sup> 250 MHz / 128 MB	
	CMARC	PMARC	PMARC-DLL	PMARC	PMARC-DLL
Panel Count	min:sec	min:sec	min:sec	min:sec	min:sec
200	0:11	0:12	0:15	N/A	0:13
400	0:27	0:43	0:53	N/A	0:29
800	1:29	2:46	3:10	N/A	1:51
1600	5:54	9:31	17:30	N/A	10:04

**Table 4.1 CMARC and PMARC Processing Times for Models Ranging from 200 to 1600 Panels.**

It is important to note that the models compared in this study only differed in panel count. Panel count is not the only factor in determining processing time. The number of time steps selected, solution resolution, convergence rate and boundary layer calculations will all impact processing speed. As a result, the times presented should only be viewed as representative of the relative impact of panel density and not as the time required to process any other model geometry.

In conclusion, CMARC hosted on a dedicated 150 MHz Pentium PC is significantly faster than PMARC hosted on a similar or faster networked SGI workstation. In some cases, over twice as fast. Clearly, executing the CMARC panel code on the PC is a suitable alternative to running PMARC on the SGI workstations. Low cost 200-300 MHz Pentium II PCs are now available which will allow further reductions in CMARC processing times.



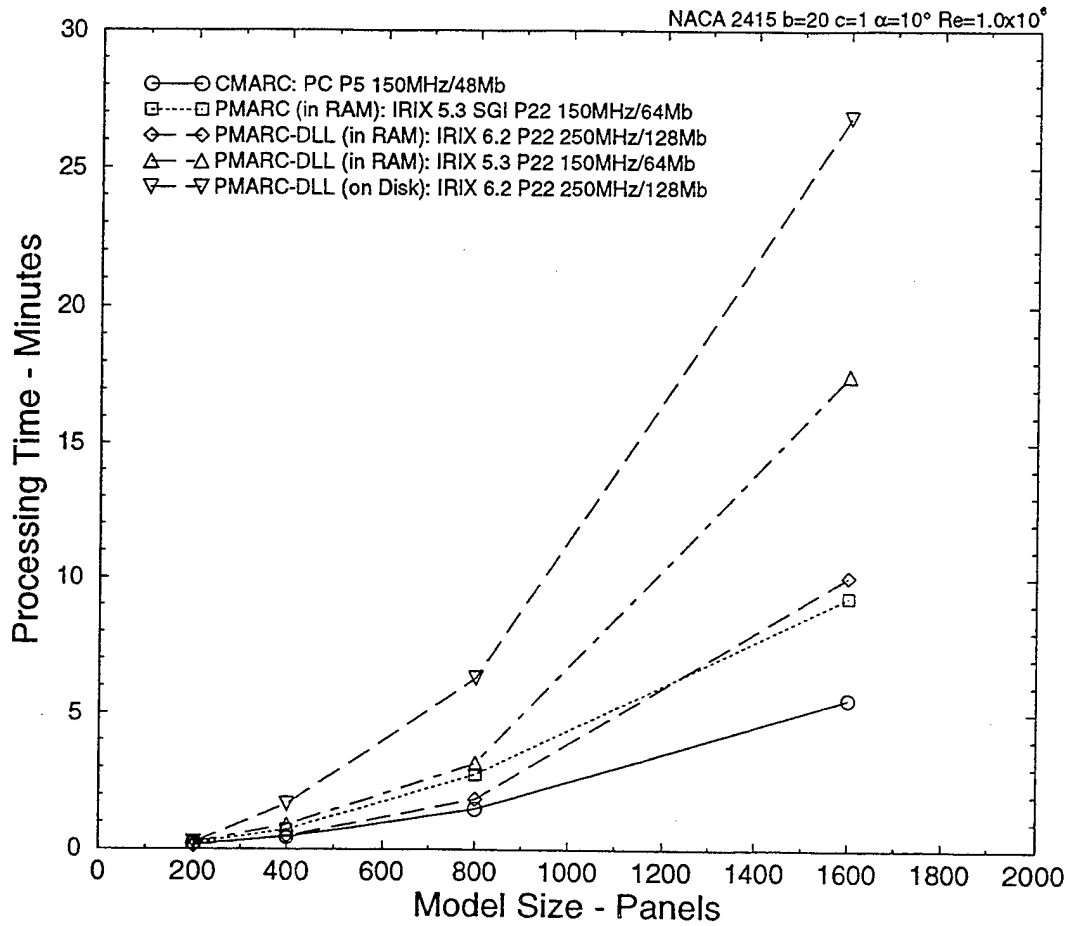


**Figure 4.5 Comparison of CMARC and PMARC Processing Times for Similar Finite Wing Models Ranging from 200 to 1600 Panels.**

## C. COMPARISON OF CMARC TO THE UPOT BOUNDARY LAYER CODE

As a first step in investigating CMARC boundary layer calculations and utility, CMARC results are compared to 2D calculations from the NPS Unsteady Potential Flow Code (UPOT). Although the potential flow solution used by CMARC for the boundary layer calculations is strictly a 3D solution, 2D flow can be approximated with the proper choice of geometry. In this case, flow over the inboard portion of a high aspect ratio (AR) wing is selected. A straight NACA 2415 wing with AR=20 is chosen for the comparison. The NACA 2415 is the same section used in the FROG UAV. Boundary layer transition and separation points are compared at angles-of-attack ranging from 0 to 20 degrees. In addition, boundary layer solution sensitivity is investigated over four Reynolds numbers ranging from  $5.0 \times 10^5$  to  $6.0 \times 10^6$ .

### 1. UPOT Boundary Layer Calculations

The NPS UPOT panel code was developed as a tool to assist in unsteady flow visualization over two-dimensional airfoils. It features an excellent interactive graphical user interface and rapid modeling capabilities [Ref. 10]. Unlike the integral momentum equations used by CMARC and PMARC, UPOT implements the Cebeci-Keller finite difference boundary layer code. The algorithm is documented by Nowak [Ref. 11]. The UPOT code has been compared to experimental data for a range of airfoils with favorable results. As such, it is considered to be acceptable to benchmark CMARC results.

### 2. High AR Wing Model

A high aspect ratio NACA 2415 wing is modeled to evaluate the boundary layer over the inboard section to approximate 2D flow. CMARC's built-in modeling capability was used to generate a finite wing with dimensions of 20 ft wingspan (b) and unit chord (c) yielding an aspect ratio of 20. Fifty chordwise panels are distributed over the top and bottom surface in a full cosine distribution and 10 panel sections in a spanwise direction with half cosine distribution. There are 600 panels total, including the enclosed wing tip, over the semi-span. Figure 4.6 displays a semi-planform view of this configuration. Streamlines are placed on the upper and lower surfaces of the inboard root panels. The root area is chosen as the area where the flow is nearly two-dimensional flow.

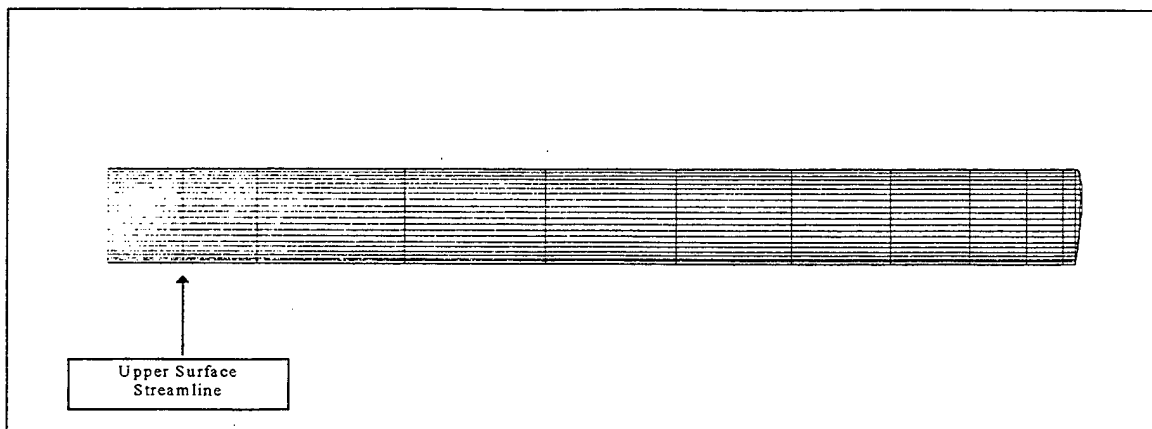


**Figure 4.6 Semi-Span of Finite Wing for the Approximation of Two-Dimensional Flow Near the Root (AR=20). 50 Chordwise x 10 Spanwise Panels.**

### **3. Boundary Layer Results and Analysis (CMARC vs. UPOT)**

CMARC and UPOT boundary layer calculations are compared for the FROG UAV NACA 2415 airfoil. Two angles-of-attack were chosen for comparison. The first,  $-2^\circ$  or zero lift, is used to compare transition models. The second angle-of-attack,  $10^\circ$  is selected for comparison to the  $10^\circ$  incidence of the inclined spheroid discussed in a later section. A comparison for Reynolds numbers ranging from  $0.5 \times 10^6$  to  $6.0 \times 10^6$  is also performed at  $10^\circ$  to investigate boundary layer calculation sensitivity to Reynolds number. In addition, boundary layer transition and separation locations are compared at angles-of-attack ranging from  $0^\circ$  to  $20^\circ$  at  $Re=1.0 \times 10^6$ .

#### ***a. Boundary Layer Transition***

The shortcomings of the point boundary layer transition model coded in CMARC is evident when compared to the more sophisticated transition length model implemented in UPOT. UPOT uses the Michel transition onset and the Chen-Thyison transition length models [Ref. 11]. Figures 4.7 through 4.14 display skin friction coefficient as a function of chordwise location ( $x/c$ ) for the upper and lower surfaces of a NACA 2415 airfoil. Results for four Reynolds numbers ranging from  $0.5 \times 10^6$  to  $6.0 \times 10^6$  are plotted at zero lift ( $-2^\circ$ ) and  $10^\circ$  angle-of-attack. Boundary layer transition will be

discussed first, followed by boundary layer separation. Finally, differences in modeling at the stagnation point will be discussed.

In almost all cases, CMARC predicts an early transition. The transition from laminar to turbulent boundary layer occurs in CMARC as a sudden jump or point transition. The UPOT transition length model provides for a more realistic representation of the boundary layer physics. Combined, early and point transition result in higher total skin friction drag predicted by CMARC. The difference is most pronounced at the lower Reynolds numbers associated with the FROG UAV. At  $Re=0.5 \times 10^6$  and zero lift, CMARC overpredicts skin friction drag by approximately 40% on the upper surface and 20% on the lower surface. Although skin friction drag may be a relatively small portion of the total drag, airframe manufacturers go to great lengths to refine models to accurately predict it. A few percentage points of error can cause the aircraft to meet or miss performance goals.

Despite the differences in transition modeling, CMARC accurately predicts the skin friction coefficient with respect to UPOT. When comparing laminar to laminar and turbulent to turbulent regions in Figures 4.7 through 4.10 (zero lift plots), the skin friction coefficients are a close match. This indicates that an adjustment in the CMARC model delaying transition could provide more accurate results.

As another comparison of boundary layer calculations, displacement thickness ( $\delta^*$ ) is displayed in Figures 4.15 through 4.22 as a function of chord position ( $x/c$ ) for zero lift ( $-2^\circ$ ) and  $10^\circ$  angle-of-attack. In general, CMARC and UPOT predict similar trends in  $\delta^*$ . The final displacement thickness is a good relative indication of total skin friction drag. CMARC always predicts a greater  $\delta^*$  and thus more drag. This is in keeping with the previous observations indicating higher integrated skin friction forces.

### *b. Separation*

Boundary layer separation is indicated in Figures 4.7 through 4.14 by a zero or negative skin friction coefficient. In all cases, CMARC slightly overpredicts the extent of attached flow. Again, the differences are most significant at the lower Reynolds numbers.

Figures 4.23 and 4.24 display transition and separation points for the NACA 2415 as a function of angles-of-attack ranging from  $0^\circ$  to  $20^\circ$ . The data is for  $Re=1.0 \times 10^6$  which is close to the FROG UAV high speed cruise at  $Re=929,000$ . On both

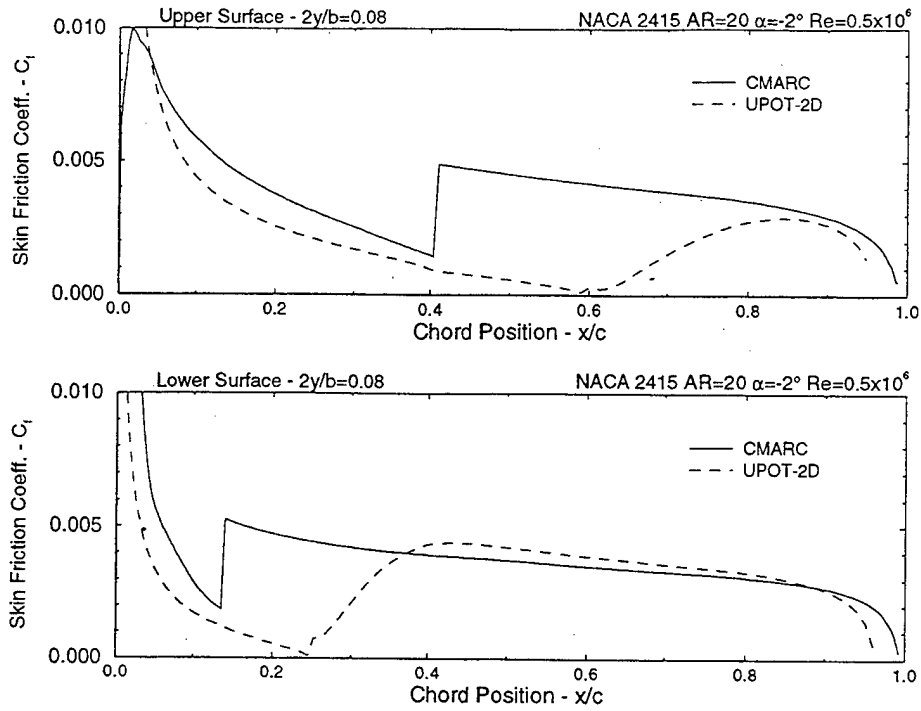


**Figure 4.7 Comparison of CMARC and UPOT Skin Friction Coefficient ( $C_f$ ) for NACA 2415 at zero lift ( $\alpha=-2^\circ$ ) and  $Re=0.5 \times 10^6$ .**

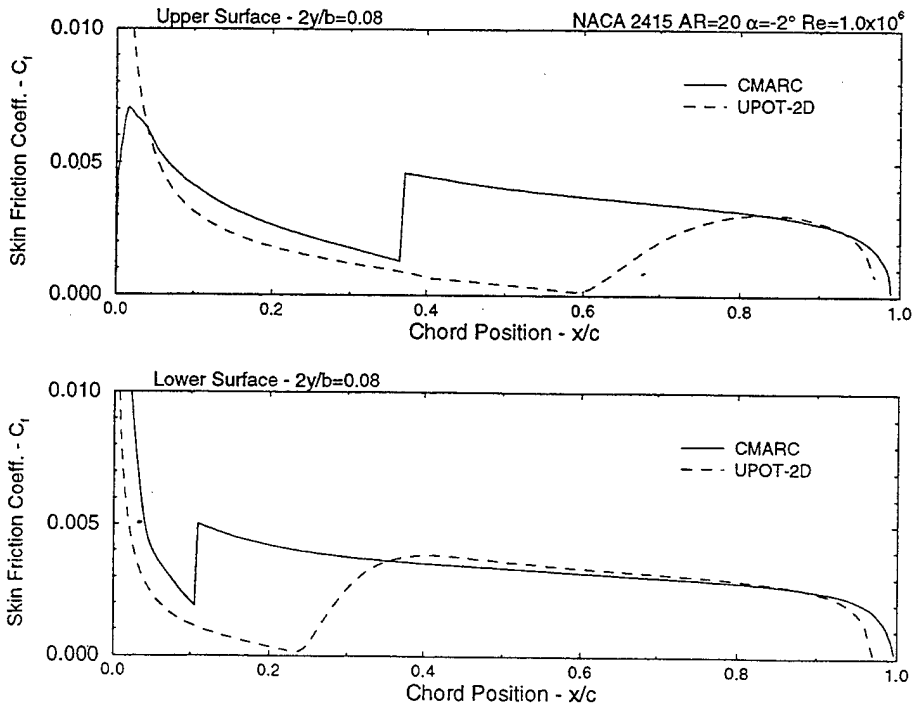


**Figure 4.8 Comparison of CMARC and UPOT Skin Friction Coefficient ( $C_f$ ) for NACA 2415 at zero lift ( $\alpha=-2^\circ$ ) and  $Re=1.0 \times 10^6$ .**

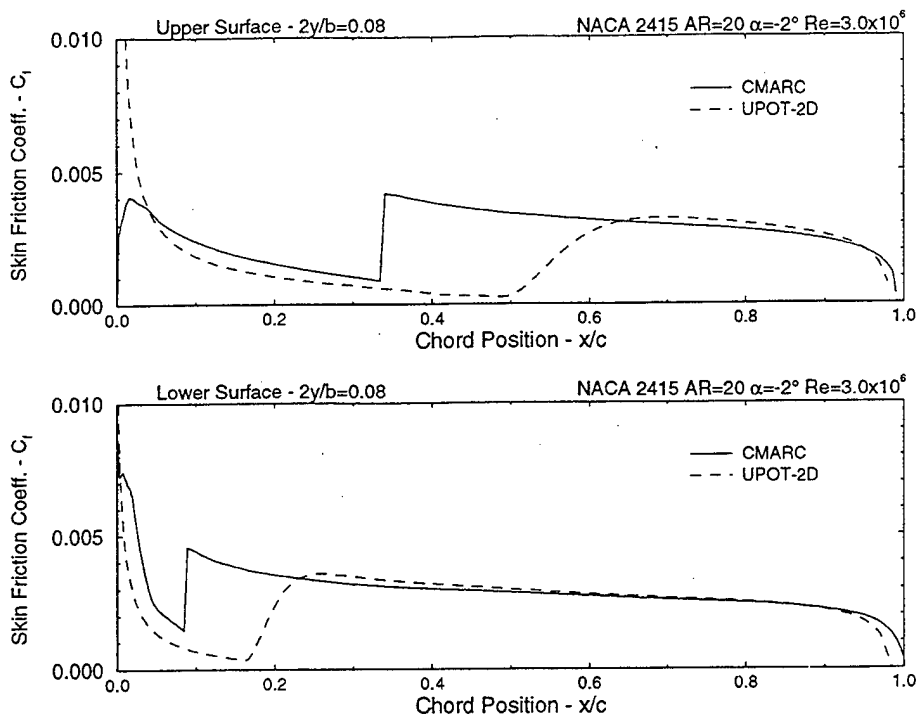


**Figure 4.9 Comparison of CMARC and UPOT Skin Friction Coefficient ( $C_f$ ) for NACA 2415 at zero lift ( $\alpha=-2^\circ$ ) and  $Re=3.0 \times 10^6$ .**

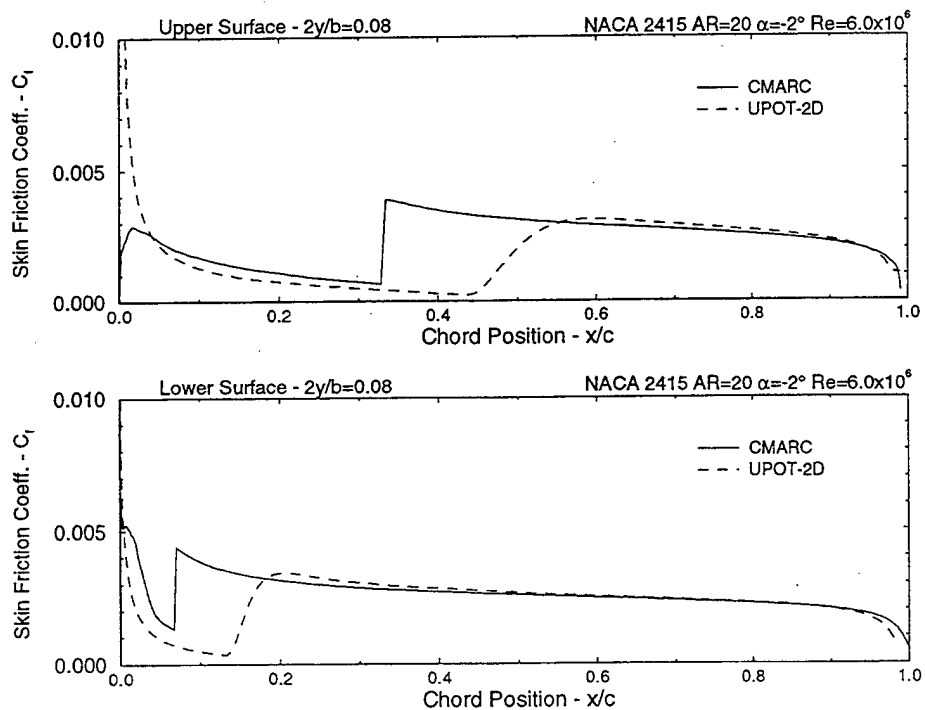


**Figure 4.10 Comparison of CMARC and UPOT Skin Friction Coefficient ( $C_f$ ) for NACA 2415 at zero lift ( $\alpha=-2^\circ$ ) and  $Re=6.0 \times 10^6$ .**

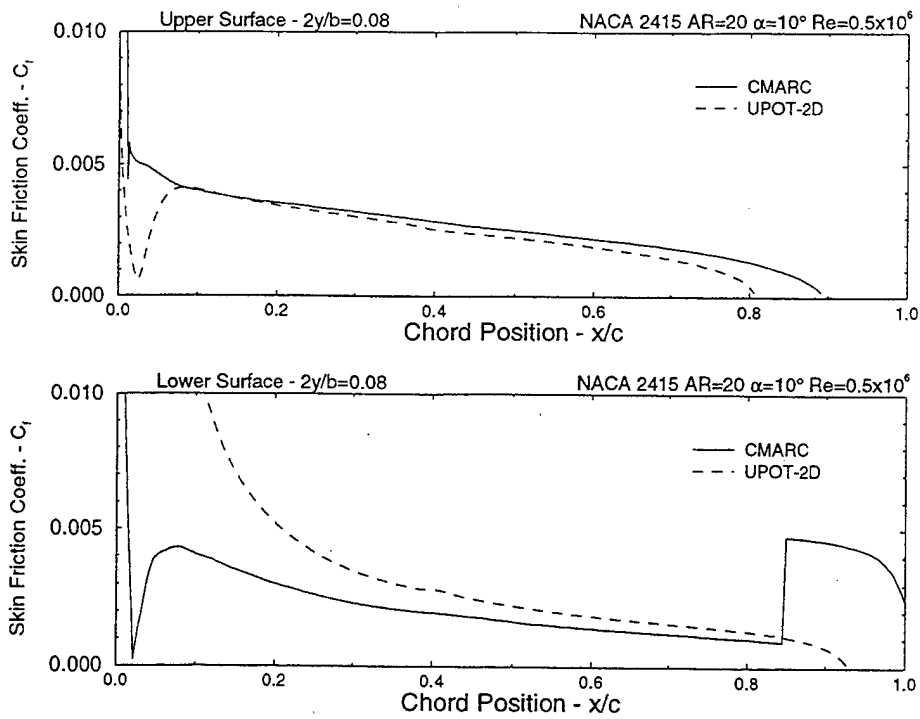


**Figure 4.11 Comparison of CMARC and UPOT Skin Friction Coefficient ( $C_f$ ) for NACA 2415 at  $\alpha=10^\circ$  and  $Re=0.5 \times 10^6$ .**

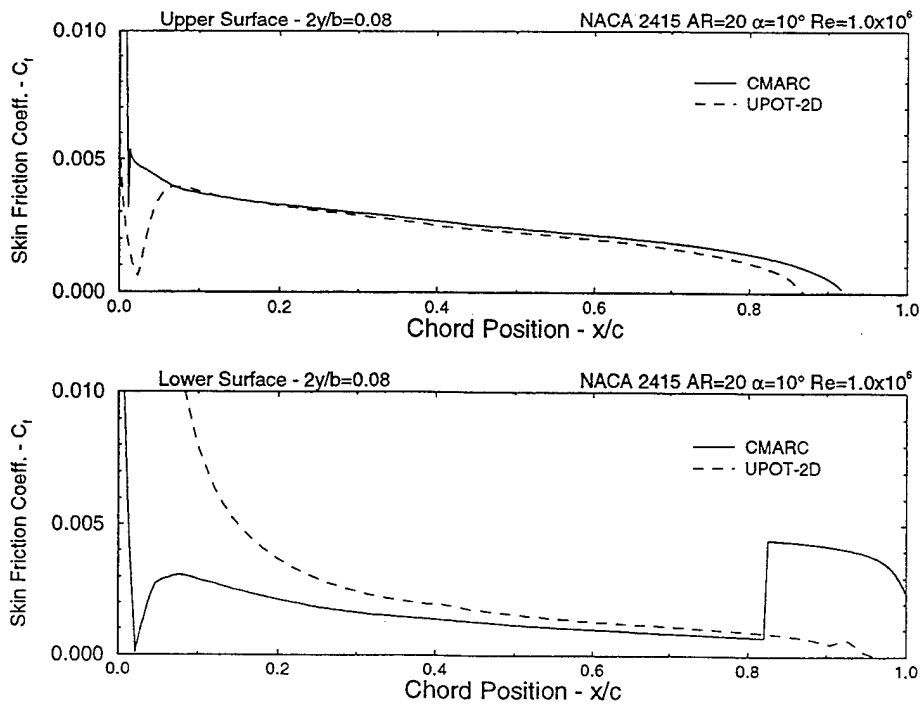


**Figure 4.12 Comparison of CMARC and UPOT Skin Friction Coefficient ( $C_f$ ) for NACA 2415 at  $\alpha=10^\circ$  and  $Re=1.0 \times 10^6$ .**

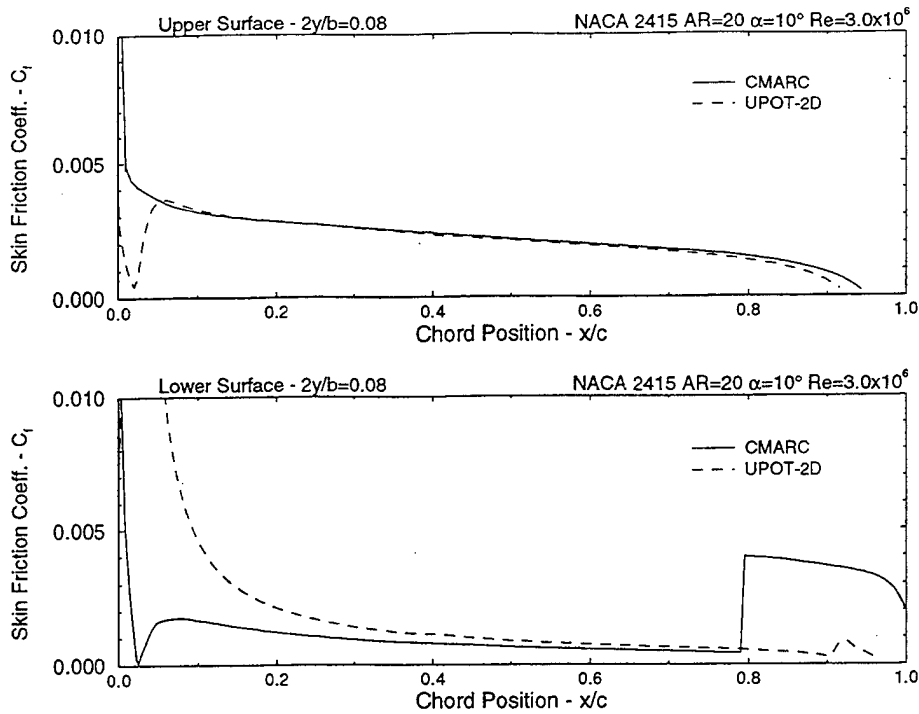


**Figure 4.13 Comparison of CMARC and UPOT Skin Friction Coefficient ( $C_f$ ) for NACA 2415 at  $\alpha=10^\circ$  and  $Re=3.0 \times 10^6$ .**

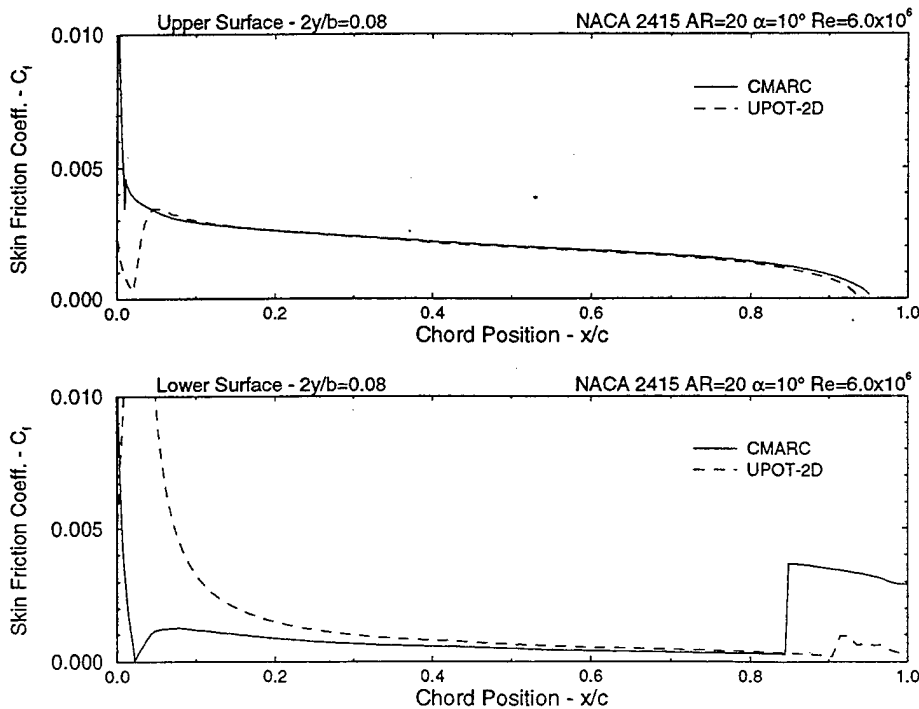


**Figure 4.14 Comparison of CMARC and UPOT Skin Friction Coefficient ( $C_f$ ) for NACA 2415 at  $\alpha=10^\circ$  and  $Re=6.0 \times 10^6$ .**



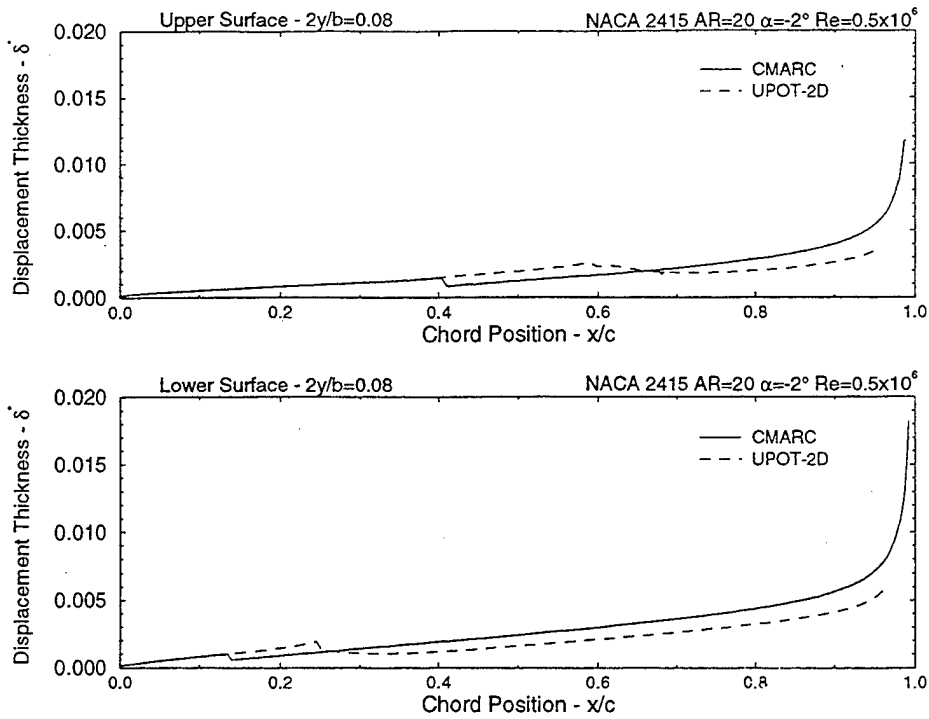


**Figure 4.15 Comparison of CMARC and UPOT Boundary Layer Displacement Thickness ( $\delta^*$ ) for NACA 2415 at zero lift ( $\alpha=-2^\circ$ ) and  $Re=0.5 \times 10^6$ .**

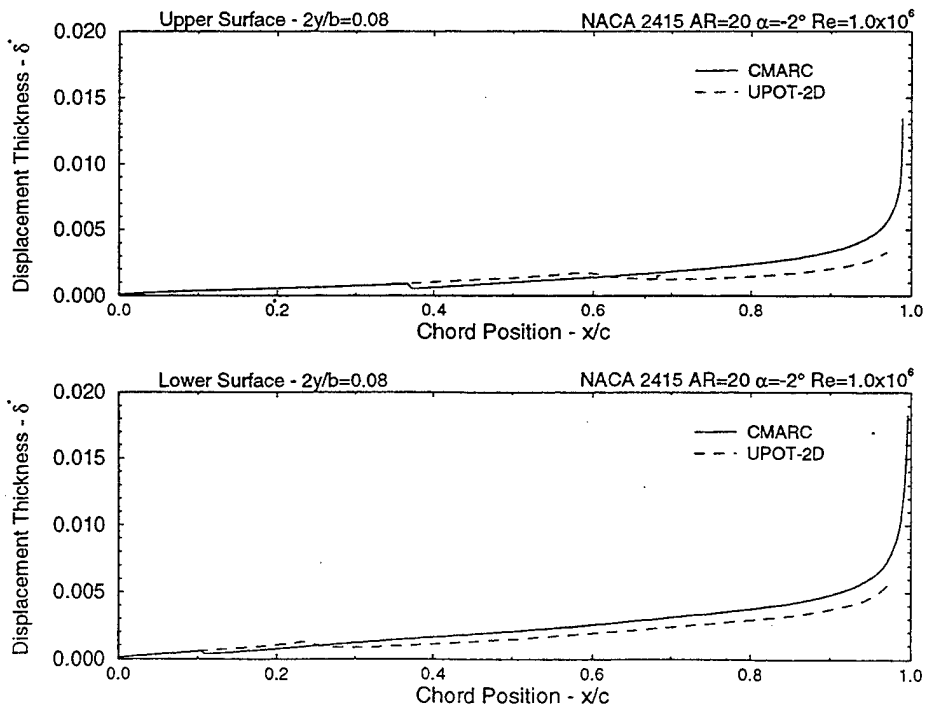


**Figure 4.16 Comparison of CMARC and UPOT Boundary Layer Displacement Thickness ( $\delta^*$ ) for NACA 2415 at zero lift ( $\alpha=-2^\circ$ ) and  $Re=1.0 \times 10^6$ .**

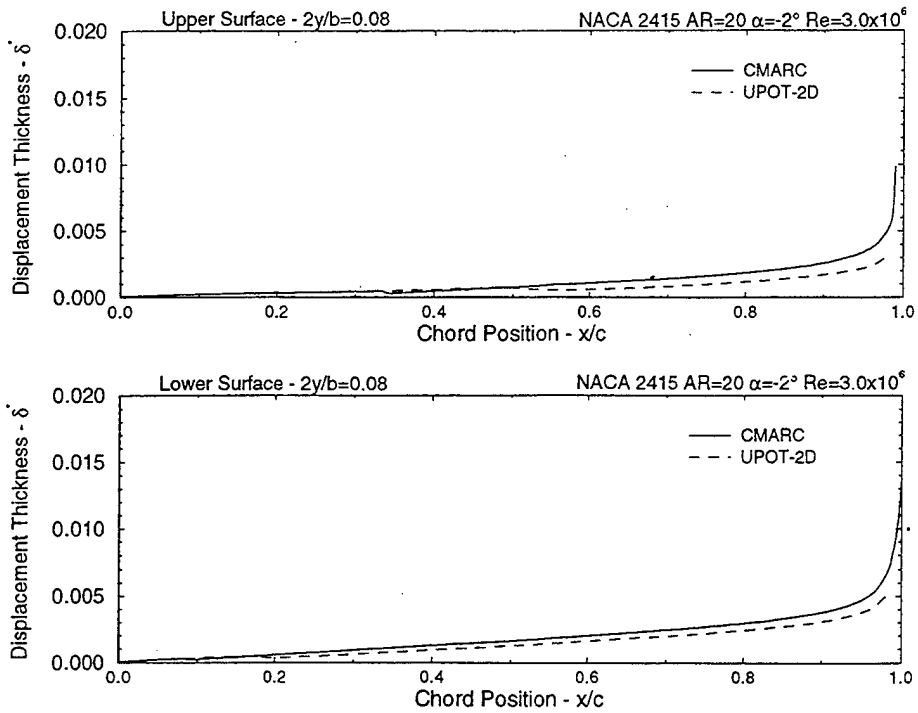


**Figure 4.17 Comparison of CMARC and UPOT Boundary Layer Displacement Thickness ( $\delta^*$ ) for NACA 2415 at zero lift ( $\alpha=-2^\circ$ ) and  $Re=3.0 \times 10^6$ .**

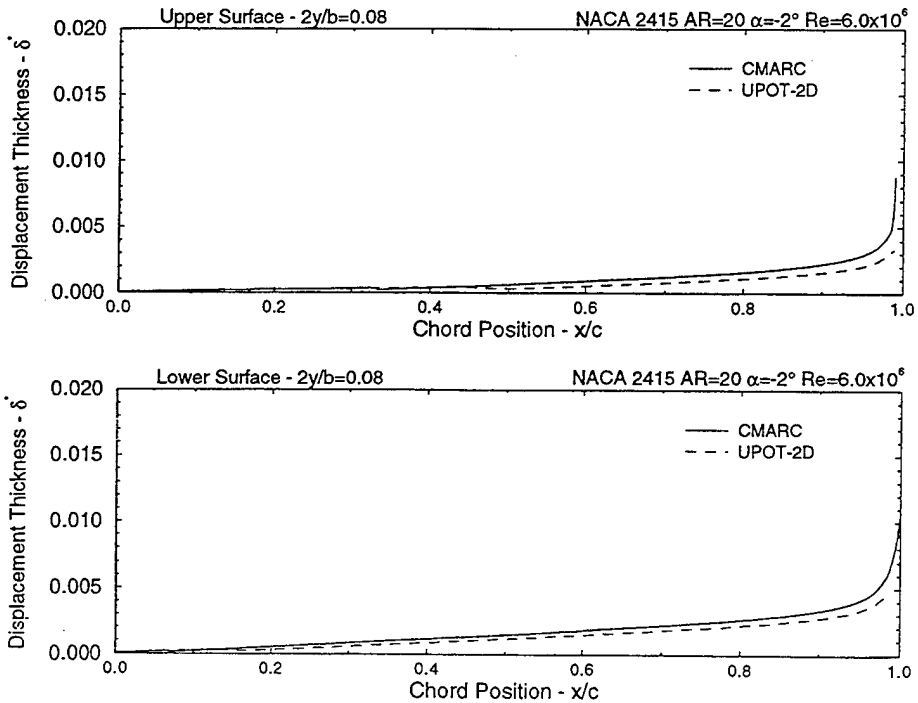


**Figure 4.18 Comparison of CMARC and UPOT Boundary Layer Displacement Thickness ( $\delta^*$ ) for NACA 2415 at zero lift ( $\alpha=-2^\circ$ ) and  $Re=6.0 \times 10^6$ .**

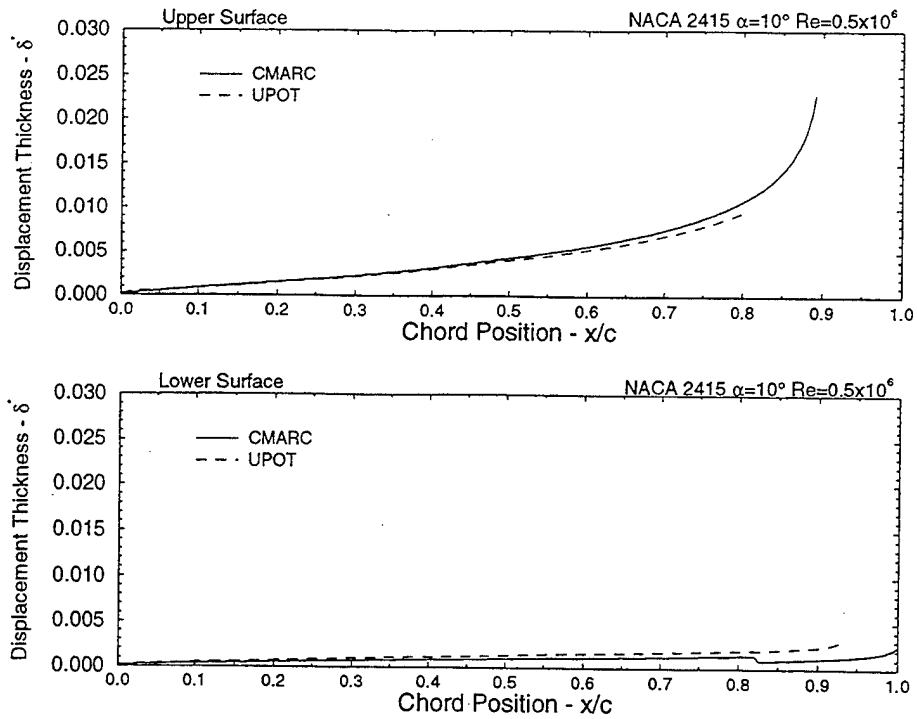


**Figure 4.19 Comparison of CMARC and UPOT Boundary Layer Displacement Thickness ( $\delta^*$ ) for NACA 2415 at  $\alpha=10^\circ$  and  $Re=0.5 \times 10^6$ .**

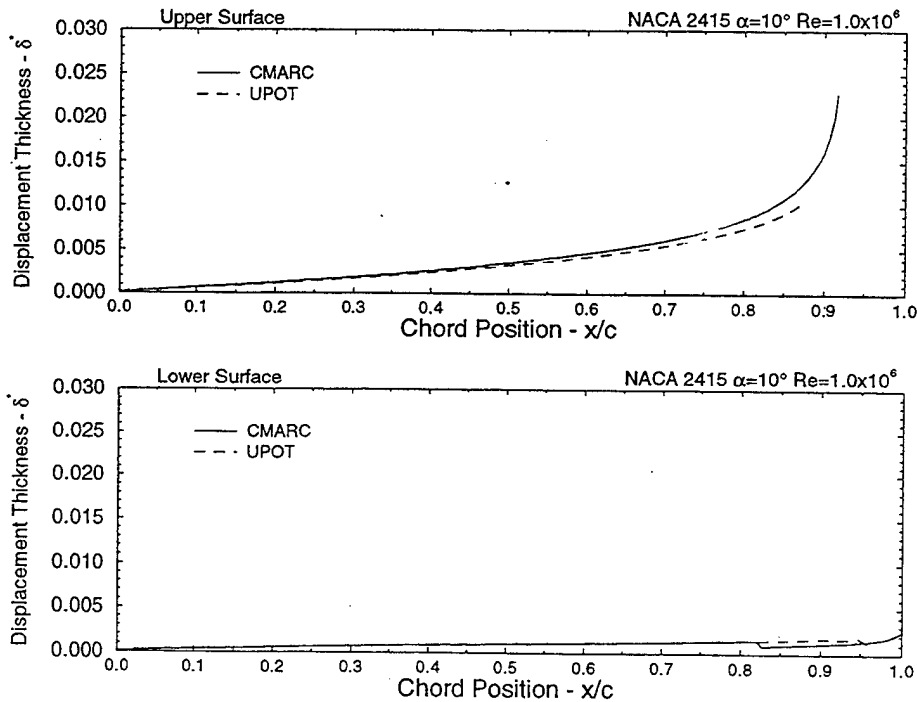


**Figure 4.20 Comparison of CMARC and UPOT Boundary Layer Displacement Thickness ( $\delta^*$ ) for NACA 2415 at  $\alpha=10^\circ$  and  $Re=1.0 \times 10^6$ .**

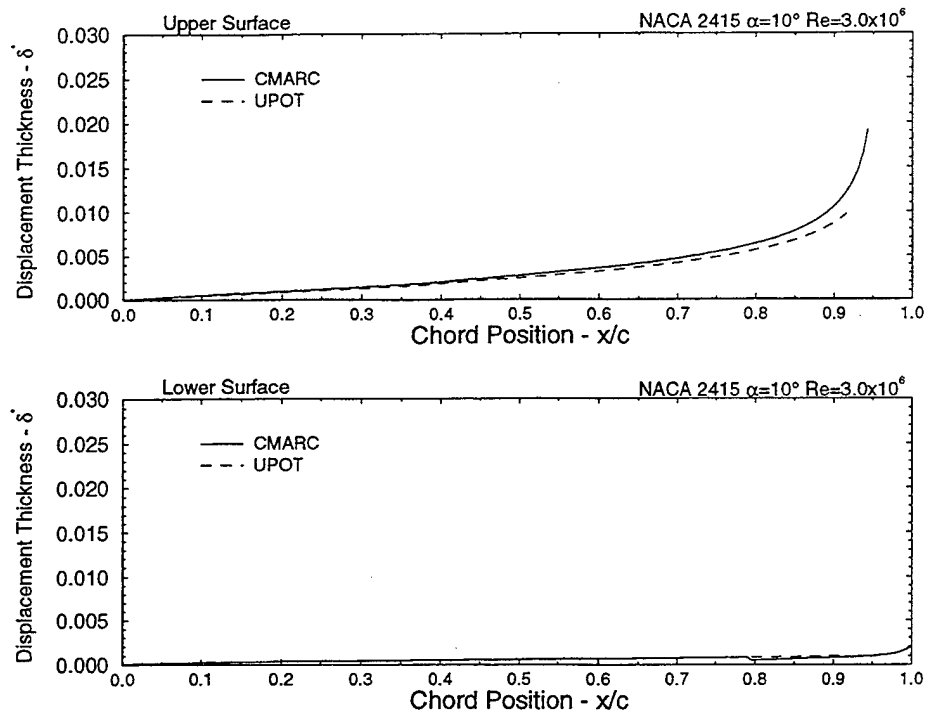


**Figure 4.21 Comparison of CMARC and UPOT Boundary Layer Displacement Thickness ( $\delta^*$ ) for NACA 2415 at  $\alpha=10^\circ$  and  $Re=3.0 \times 10^6$ .**

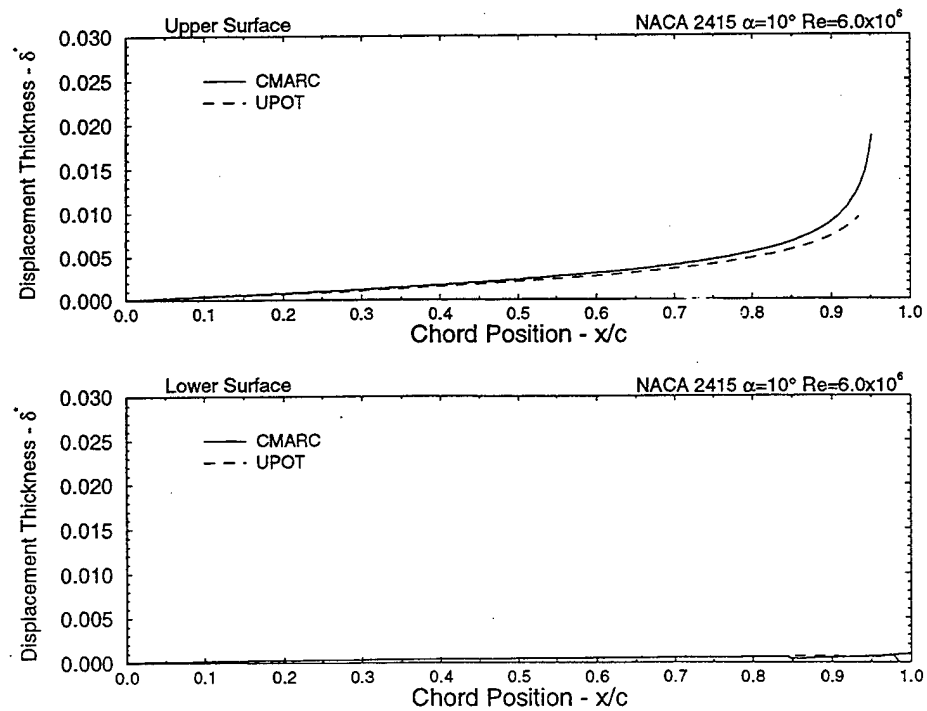


**Figure 4.22 Comparison of CMARC and UPOT Boundary Layer Displacement Thickness ( $\delta^*$ ) for NACA 2415 at  $\alpha=10^\circ$  and  $Re=6.0 \times 10^6$ .**

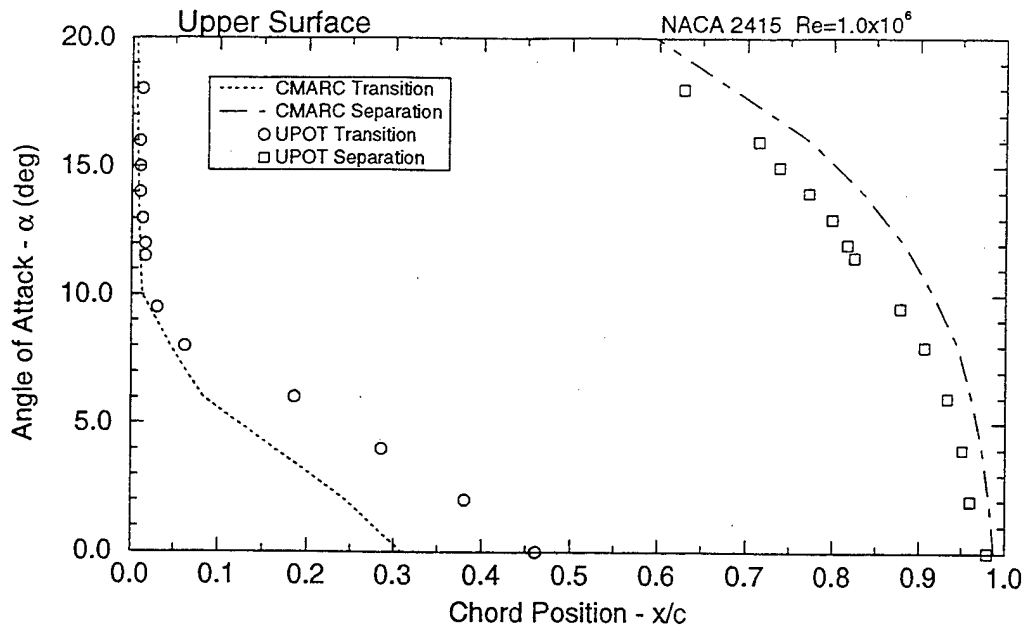


**Figure 4.23 Comparison of CMARC and UPOT Boundary Layer Transition and Separation Points for the Upper Surface of a NACA 2415 Airfoil at  $Re=1.0 \times 10^6$  from  $0^\circ$  to  $20^\circ$  AOA.**

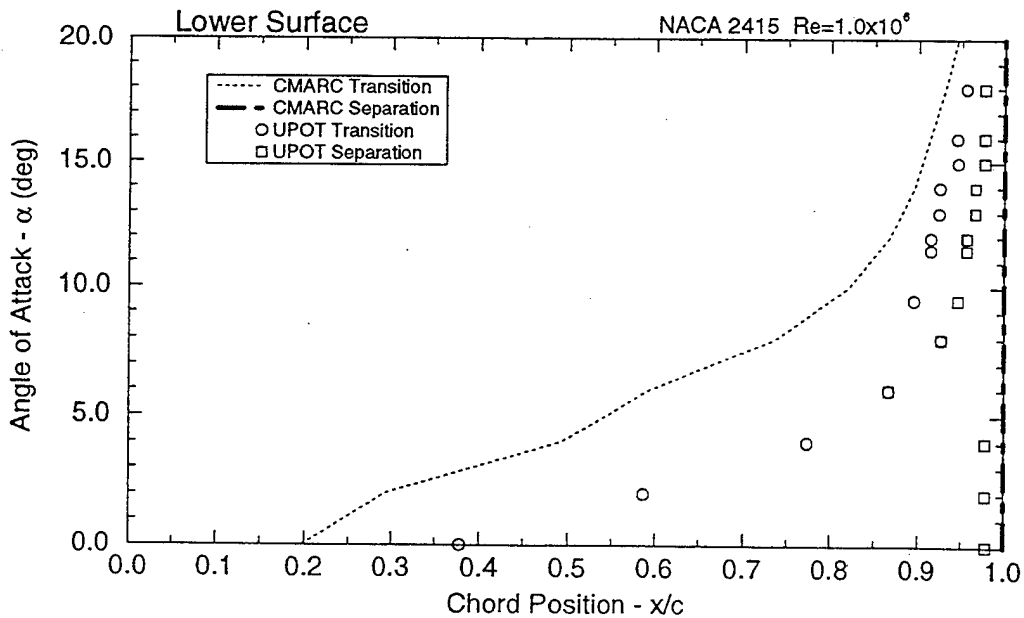


**Figure 4.24 Comparison of CMARC and UPOT Boundary Layer Transition and Separation Points for the Lower Surface of a NACA 2415 Airfoil at  $Re=1.0 \times 10^6$  from  $0^\circ$  to  $20^\circ$  AOA.**

the upper and lower surface, CMARC clearly provides correct trends for both the transition and separation points. However, as seen at zero lift in Figures 4.7 through 4.10, CMARC always predicts an early transition and late separation.

Despite the inaccuracies in transition and separation points, CMARC boundary layer calculations remain useful. A low order panel code is unlikely going to be used for performance calculations. Instead, it is more useful as a design tool. It allows for rapidly visualizing the trend in transition and separation points with minor changes in configuration.

A word of caution is advised when total skin friction drag is integrated. A design change could be implemented that reduces overall skin friction drag but neglects large increases in pressure drag. In other words, one could reduce skin friction drag, but fail to realize earlier separation is taking place. The net result is a small reduction in skin friction drag that is more than offset by a large increase in separation pressure drag. Extending the extent of attached flow should always be considered preferable to reducing overall integrated skin friction drag.

### *c. Skin Friction Coefficient near the Stagnation Point*

Another major difference between the integral boundary layer code in CMARC and the finite difference code in UPOT is highlighted at the stagnation point. In Figure 4.11, both codes locate the stagnation point on the lower surface at  $x/c=0.025$  for the NACA 2415 airfoil at 10 degrees angle-of-attack. However, it is clear that the CMARC skin friction coefficient starts at 0.0002, a small number approaching zero asymptotically, while the UPOT skin friction shoots out of the top of the chart in excess 0.7, a relatively large number approaching  $+\infty$  asymptotically.

From boundary layer theory, it is known that the skin friction coefficient is inversely proportional to the square root of the local Reynolds number or:

$$C_f = \frac{1}{\sqrt{\text{Re}_x}} \quad 4.1$$

At the stagnation point,  $C_f$  approaches  $+\infty$ . The finite difference code in UPOT correctly models this trend. On the other hand, CMARC implements a discrete

integration of the following exact differential laminar skin friction calculation:

$$\theta(\eta)^2 = \frac{0.45\nu}{U(\eta)^6} \int_0^\eta (1 + 2.222g(K, \mu))U(\eta)^5 d\eta + \theta(0)^2 \left( \frac{U(0)}{U(\mu)} \right)^6 \quad 4.2$$

Where: U - velocity at outer edge of boundary layer  
 $\theta$  - momentum thickness  
g - empirical parameter  
 $K = \frac{\theta^2}{\nu} \frac{dU}{d\eta}$   
 $\eta$  - generalized coordinate along a streamline

At  $\eta=0$ , the momentum thickness starts at zero and builds rapidly from the stagnation point. Thus, the momentum integral equation reduces to:

$$\frac{d\theta}{d\eta} = \frac{1}{2} C_f = 0, \quad \text{at the stagnation point.} \quad 4.3$$

The integral solution for  $C_f$  starts at zero and rises quickly until the integral portion of Equation 4.2 dominates.

The incorrect modeling of  $C_f$  near the stagnation point is considered minor due to its local nature at the stagnation point. When skin friction is integrated over the entire surface the differences are bound to be relatively small. In addition, when integrated into a force, the errors in  $C_f$  at the stagnation point tend to cancel out. Close to the stagnation point on either side, skin friction forces are opposite in direction.

#### D. COMPARISON OF CMARC TO INCLINED PROLATE SPHEROID EXPERIMENTAL DATA

In the previous section, model geometry was selected to produce predominantly two-dimensional flow. In this section, CMARC pressure distributions and integral

boundary layer data are investigated for a model geometry that produces largely three-dimensional flow. For comparison, a suitable experimental test case was found in AGARD AR-303: A Selection of Experimental Test Cases for the Validation of CFD Codes [Ref. 12]. Case number C-2, entitled "Three-Dimensional Boundary Layer and Flow Field Data of an Inclined Prolate Spheroid" was selected. A 6:1 prolate spheroid approximates a typical streamlined fuselage. The data set was ordered from AGARD through the NASA Center for Aerospace Information (CASI).

A complete data set for all test cases in AGARD AR-303 was available for a nominal charge of \$59.00 through NASA's CASI publications office. Ordering information inside the rear cover of the publication proved to be accurate and useful. The data arrived on nine PC formatted high density disks. After copying the desired data sets to the hard drive, each file is self extracting through a built-in DOS decompression program. Detailed instructions are printed in the back section of AR-303.

#### **1. Inclined 6:1 Prolate Spheroid - AGARD AR-303 Case C-2**

AGARD AR-303 test case number C-2 contains pressure coefficient and skin friction distributions for a 6:1 prolate spheroid inclined to the flow field. Table 4.2 lists the test conditions for which data are available.

Test case I was chosen for comparison to CMARC output. At 10° angle-of-attack, some separated flow was expected which would provide a good comparison to CMARC integral boundary layer separation points. The only drawback to this test case is the forced transition at  $X/2a = 0.20$ . Natural transition would have been more desirable for comparison to the CMARC transition model. The test cases at 30° angle-of-attack are deemed to have too much separated flow to provide a meaningful comparison to a CMARC potential flow solution.

##### ***a. Wind Tunnel Experimental Set-up***

Figure 4.25 contains a diagram of the experimental set-up for the 6:1 prolate spheroid performed by Kreplin in the DLR Göttingen three meter Low Speed Wind Tunnel (NWG). Of note, the wind tunnel test section is of the Göttingen type with closed return and open test section. No corrections are applied to the data.



PARAMETER	CASE I	CASE II	CASE III
Mach Number	0.16	0.13	0.23
Reynolds Number	$7.7 \times 10^6$	$6.5 \times 10^6$	$43.0 \times 10^6$
Incidence	$10.0^\circ$	$29.7^\circ$	$30.0^\circ$
Transition	tripped at $X/2a = 0.20$	free	free

**Table 4.2 AGARD AR-303 Test Conditions, from Ref. [12].**

Figure 4.26 shows the configuration for the 6:1 prolate spheroid wind tunnel model. The 2.4 meter long model contains 42 pressure taps located along an axial meridian. The model can be rotated axially in 50 steps through just over 180 degrees providing in excess of 2000 pressure readings over half the surface. With yaw angle set to zero, symmetry is assumed for the other half. In addition to pressure ports, surface hot film sensors are located at 12 axial positions for the measurement of wall shear stress. Wall shear stress is normalized by dynamic pressure to provide skin friction coefficient ( $C_f$ ). Once again, the measurements are provided for approximately 50 rotation angles, providing coverage of half the surface.

In addition to pressure and skin friction coefficients, boundary layer velocity profiles and flow field mean velocity vectors are available at several axial locations. Although not used in this investigation, the data would prove useful for more detailed studies.

Unfortunately, the wind tunnel set-up was not instrumented for loads. As will be discussed in the next section, the number of pressure and skin friction measurements was deemed to be sufficient to allow the integration of local forces to provide a reasonable calculation of lift, drag and pitching moments.

#### *b. Experimental Data*

Two data files from test case C-2 at  $\alpha = 10.0^\circ$  are used for comparison to CMARC data. The first file, "cp10nwg.dat," contains pressure coefficient listed as a function of axial location ( $X/2a$ ) and circumferential angle ( $\phi$ ). For each circumferential

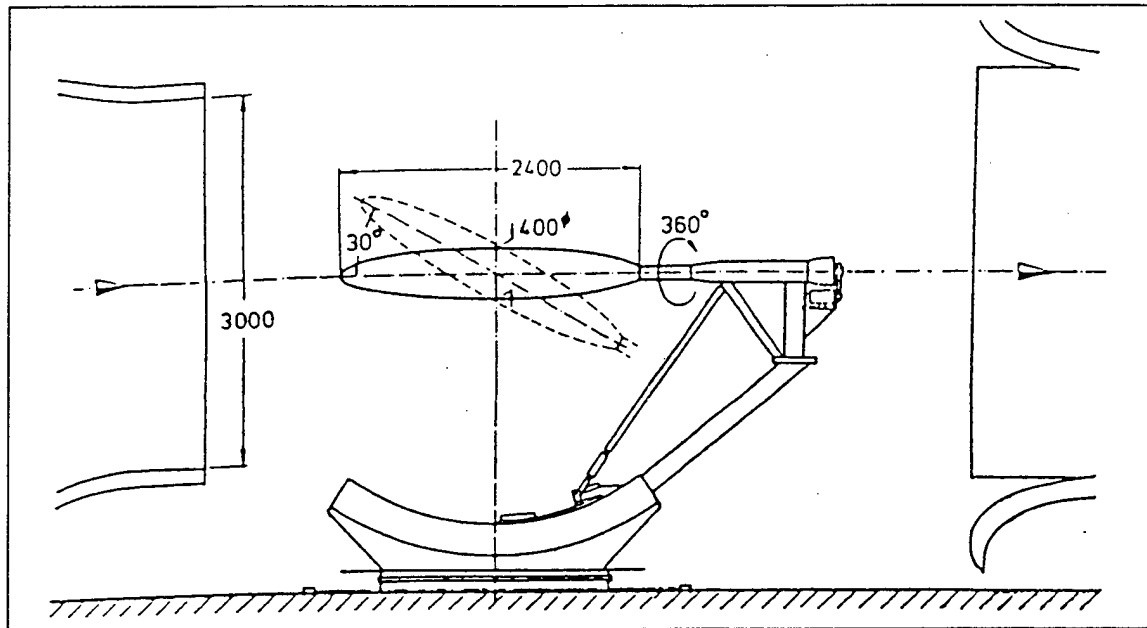


**Figure 4.25** Inclined 6:1 Prolate Spheroid Model in the DLR Göttingen Three Meter Low Speed Wind Tunnel (NWG) , from Ref. [12].

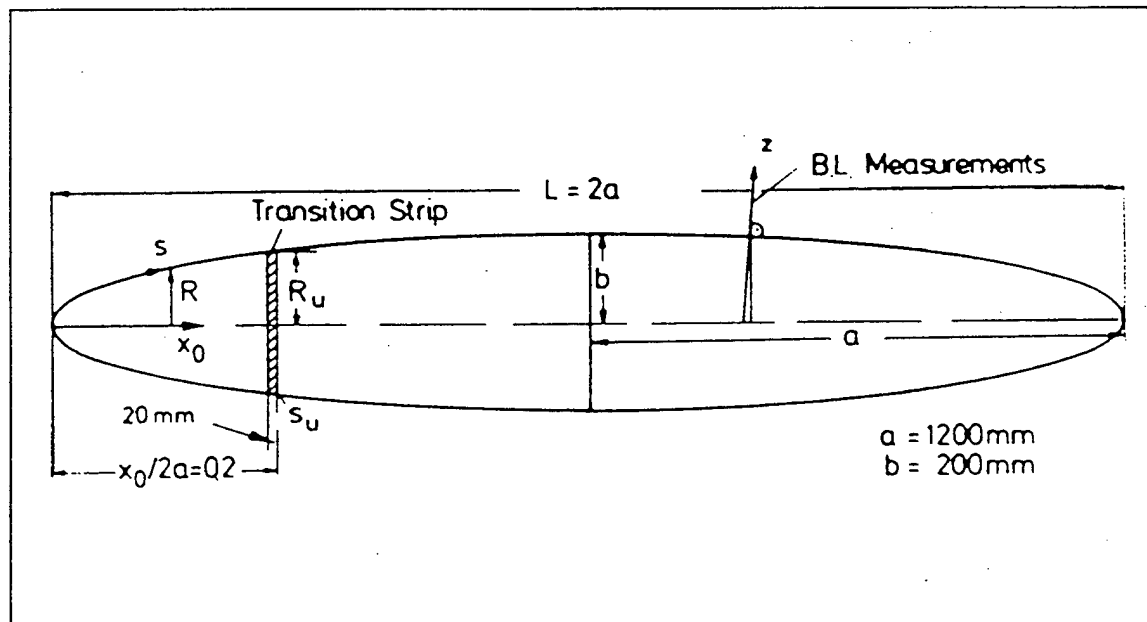


**Figure 4.26** Prolate Spheroid Wind Tunnel Model Configuration, from Ref. [12].

angle all the successive axial location pressure coefficients were listed. It is more common to plot pressure distribution as a function of circumferential angle at a given axial station. The data file was rearranged using the MATLAB M-file listed in Appendix E.

The second data file, "cf10nwg.dat," contains skin friction listed as a function of axial location ( $X/2a$ ) and circumferential angle ( $\phi$ ). The data, listed in two columns, were reordered to one column for ease of plotting.

**c. Integration of Local Forces to Provide Lift Drag and Pitching Moment**

The experimental set-up did not include balance measurement of forces. However, it was deemed that the 2000+ pressure and 500+ skin friction measurements would be sufficient to allow the integration of measurements over the surface of the prolate spheroid for an approximation of total force and moment coefficients. The following equations were developed to provide integrated pressure and friction force coefficients. Symmetry is assumed. Appendix B outlines the development of these relations. Appendix C lists the MATLAB program which implements the discrete integration.

The pressure force coefficients normalized by  $S = \pi b^2$  and  $\bar{c} = 2b$  are yielded by discretely integrating the following equations in a cylindrical coordinate system:

$$C_{N_P} = \frac{N_P}{q_\infty S}, \quad N_P = 2 \sum_{i=1}^m \sum_{j=1}^n - (q_\infty C_P r \bar{n}) \cdot \bar{k} \Delta \phi_j \Delta x_i / 2a \quad 4.3$$

$$C_{A_P} = \frac{A_P}{q_\infty S}, \quad A_P = 2 \sum_{i=1}^m \sum_{j=1}^n - (q_\infty C_P r \bar{n}) \cdot \bar{i} \Delta \phi_j \Delta x_i / 2a \quad 4.4$$

$$C_{M_P} = \frac{M_P}{q_\infty S \bar{c}}, \quad M_P = 2 \sum_{i=1}^m \sum_{j=1}^n [(q_\infty C_P r \bar{n}) \cdot (x_i / 2a \cdot \bar{k} - z_i / 2a \cdot \bar{i})] \Delta \phi_j \Delta x_i / 2a \quad 4.5$$

Where the surface unit normal is given by:

$$\text{Unit Normal: } \bar{n} = -\frac{m}{\sqrt{m^2 + 1}} \bar{i} + \frac{\sin(\phi)}{\sqrt{m^2 + 1}} \bar{j} - \frac{\cos(\phi)}{\sqrt{m^2 + 1}} \bar{k} \quad 4.6$$

The skin friction coefficients normalized by  $S = \pi b^2$  and  $\bar{c} = 2b$  are yielded by discretely integrating the following equations in a cylindrical coordinate system:

$$C_{N_{SF}} = \frac{N_{SF}}{q_{\infty} S}, \quad N_{SF} = 2 \sum_{i=1}^m \sum_{j=1}^n (q_{\infty} C_f r \bar{v}) \cdot \bar{k} \Delta \phi_j \Delta x_i / 2a \quad 4.7$$

$$C_{A_{SF}} = \frac{A_{SF}}{q_{\infty} S}, \quad A_{SF} = 2 \sum_{i=1}^m \sum_{j=1}^n (q_{\infty} C_f r \bar{v}) \cdot \bar{i} \Delta \phi_j \Delta x_i / 2a \quad 4.8$$

$$C_{M_{SF}} = \frac{M_{SF}}{q_{\infty} S \bar{c}}, \quad M_{SF} = 2 \sum_{i=1}^m \sum_{j=1}^n [(q_{\infty} C_f r \bar{v}) \cdot (-x_i / 2a \cdot \bar{k} + z_i / 2a \cdot \bar{i})] \Delta \phi_j \Delta x_i / 2a \quad 4.9$$

Where the unit surface velocity vector is given by:

$$\bar{v} = \frac{\cos(\gamma)}{\sqrt{m^2 + 1}} \bar{i} + \left[ \frac{m \sin(\phi) \cos(\gamma)}{\sqrt{m^2 + 1}} + \cos(\phi) \sin(\gamma) \right] \bar{j} + \left[ -\frac{m \cos(\phi) \cos(\gamma)}{\sqrt{m^2 + 1}} + \sin(\phi) \sin(\gamma) \right] \bar{k} \quad 4.10$$

The surface and local slope of a prolate spheroid comes from the following relations:

$$\text{Prolate Spheroid: } \frac{x^2}{a^2} + \frac{r^2}{b^2} = 1 \quad \Rightarrow \quad \text{slope } m = \frac{dr}{dx} = -\frac{bx}{a^2 \sqrt{1 - \frac{x^2}{a^2}}} \quad 4.11$$

Note: The forces are summed over half the spheroid,  $\phi = 0 \rightarrow 180^\circ$ , and doubled.

The y-direction forces and the roll and yaw moments are neglected zero due to symmetry.

## 2. CMARC Model of 6:1 Prolate Spheroid

A 40x20 panel model of the 2.4 meter 6:1 prolate spheroid wind tunnel model was created with LOFTSMAN. The right half surface was modeled with symmetry around the  $y=0$  plane. Appendix F contains a printout of the LOFTSMAN input file which includes a fore/aft wake. The patch was created with 40 axial and 20 semi-circumferential panels. Full cosine compression was used to bunch panels at the leading and trailing edge.

After creating the patch in LOFTSMAN, it was decided that a doubling of circumferential panel count would increase wake placement flexibility. The CMARC input file was modified to create 40 circumferential panels by setting TNPC=40 in the break point input field for each cross section.

Figure 4.27 is a POSTMARC rendering of the final 1600 (40x40) panel configuration. The input file takes advantage of the plane of symmetry capability built into CMARC. It calculates just half a model symmetric around the  $y=0$  plane of symmetry provided there is zero side slip.

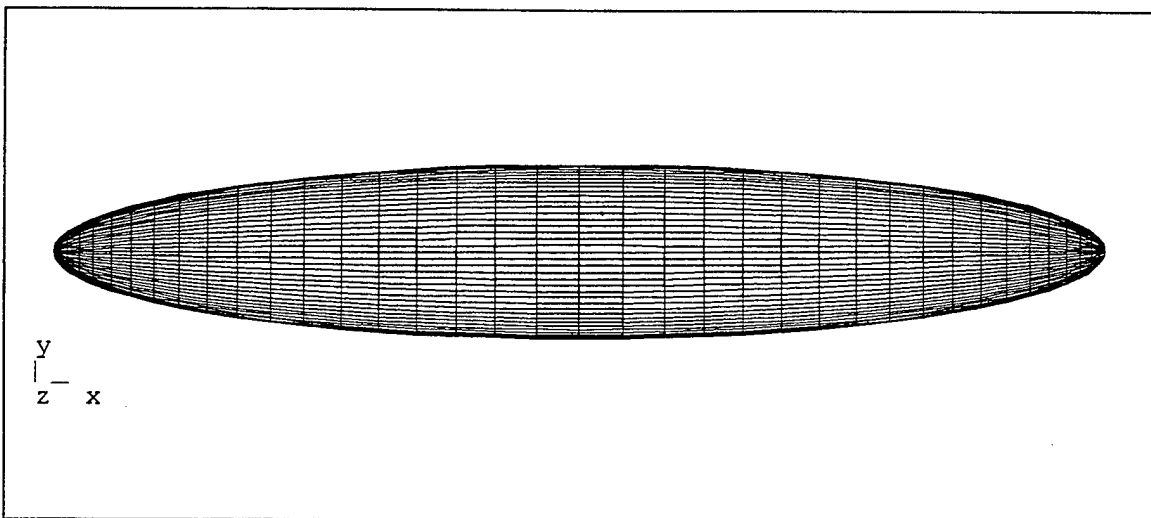


**Figure 4.27 CMARC 40x40 Prolate Spheroid Model Rendered with POSTMARC.**

### **3. Data Extraction**

Pressure coefficient data are extracted using the "postprolate.exe" FORTRAN file listed in Appendix G. This program extracts data from a CMARC or PMARC output file (DATA6) for a range of panel numbers and places them in a separate plot input file. CMARC output files are transferred to the SGI workstations for data extraction using the Windows 3.1 FTP program. Results are then plotted against experimental data with any x-y plotting program (xmgr).

#### 4. Prolate Spheroid Pressure Distribution

CMARC and experimental pressure coefficients are compared at 10 degrees angle-of-attack and  $Re=7.7 \times 10^6$ . Results are displayed as a function of axial station,  $x/2a$ , and circumferential angle,  $\phi$ , in Figure 4.28. Circumferential angle is measured starting from the lower centerline of the model. CMARC generated potential flow pressure coefficients over the forward 60% of the prolate spheroid closely match experimental results. Of note, there is a constant bias between the two sets of data.

The divergence between CMARC and experimental results aft of  $x/2a=0.60$  indicates flow separation over the top portion of the prolate spheroid. It is clear that a potential flow solution without wakes does a poor job of predicting pressure distribution over regions with separated flow.

To model the flow separation, wakes were added to the CMARC model. Tuncer and Platzer's research [Ref. 7] indicates that proper wake placement can produce a close match between panel code and experimental results for slender bodies of revolution for angles-of-attack up to 20 degrees. They concluded that a circumferential wake placement angle of 144 degrees on an ogive cylinder body provides the closest match for force and moment coefficients.

A series of wakes were placed at several circumferential angles ranging from 117 to 162 degrees. The wakes run fore-aft from  $x/2a=0.50$  to a wake separation ring at  $x/2a=0.99$ . Results are plotted in Figure 4.29. A wake angle of 117 degrees produced the closest average match to the experimental results. Figure 4.30 shows the final wake configuration.

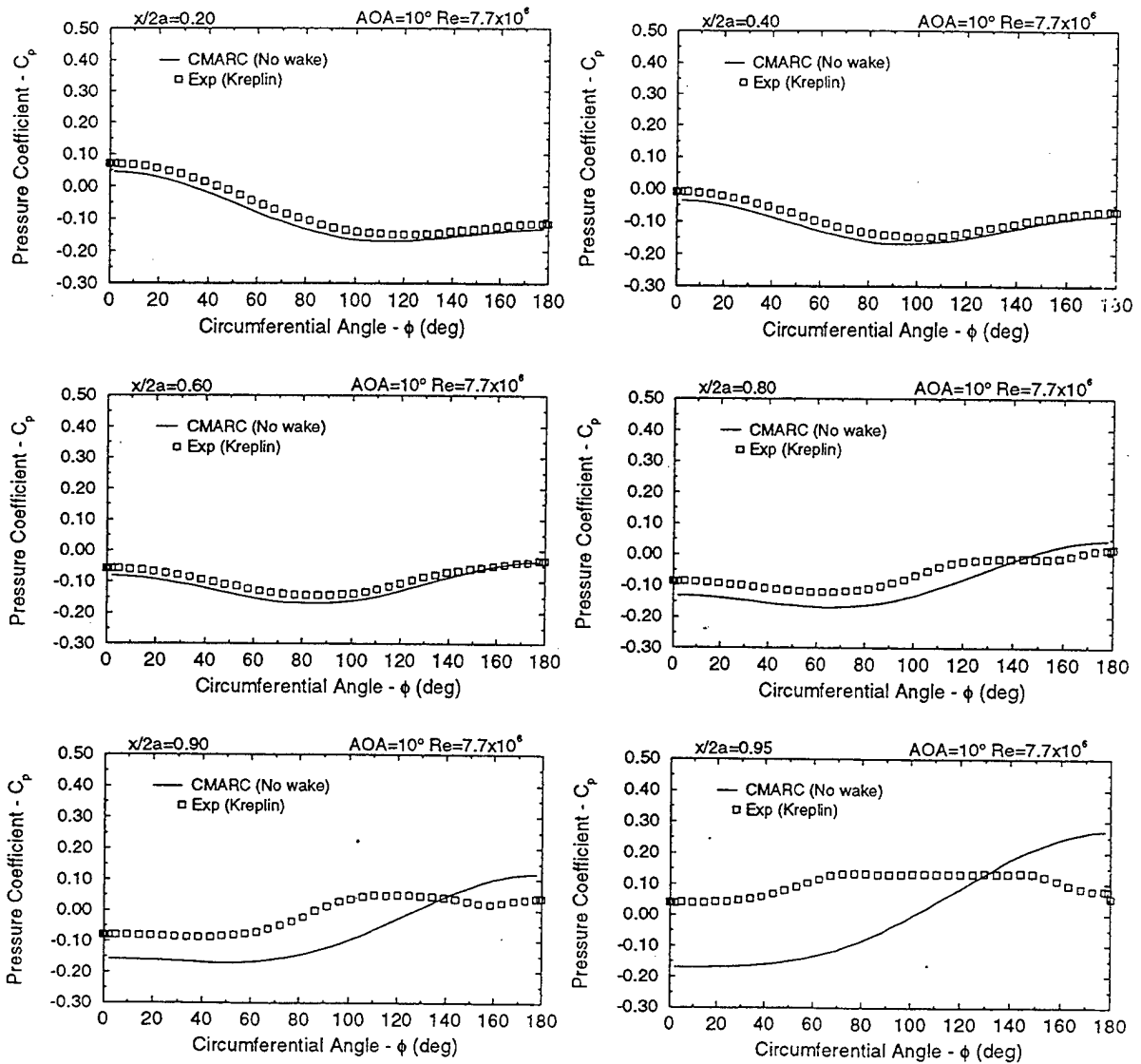


**Figure 4.28 CMARC Potential Flow (No Wakes) Pressure Distribution Compared to Experimental Data, after Ref. [12].**

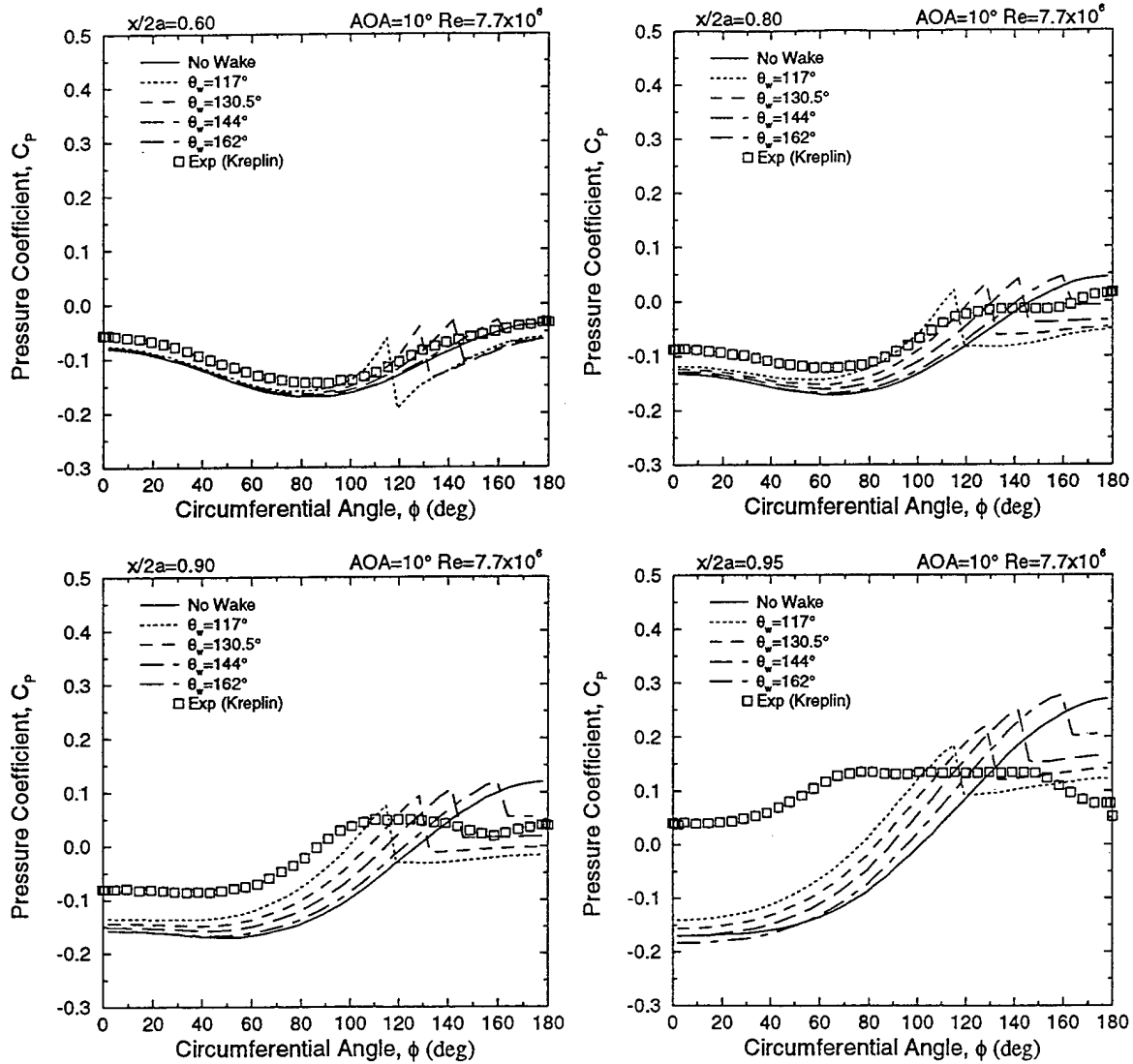
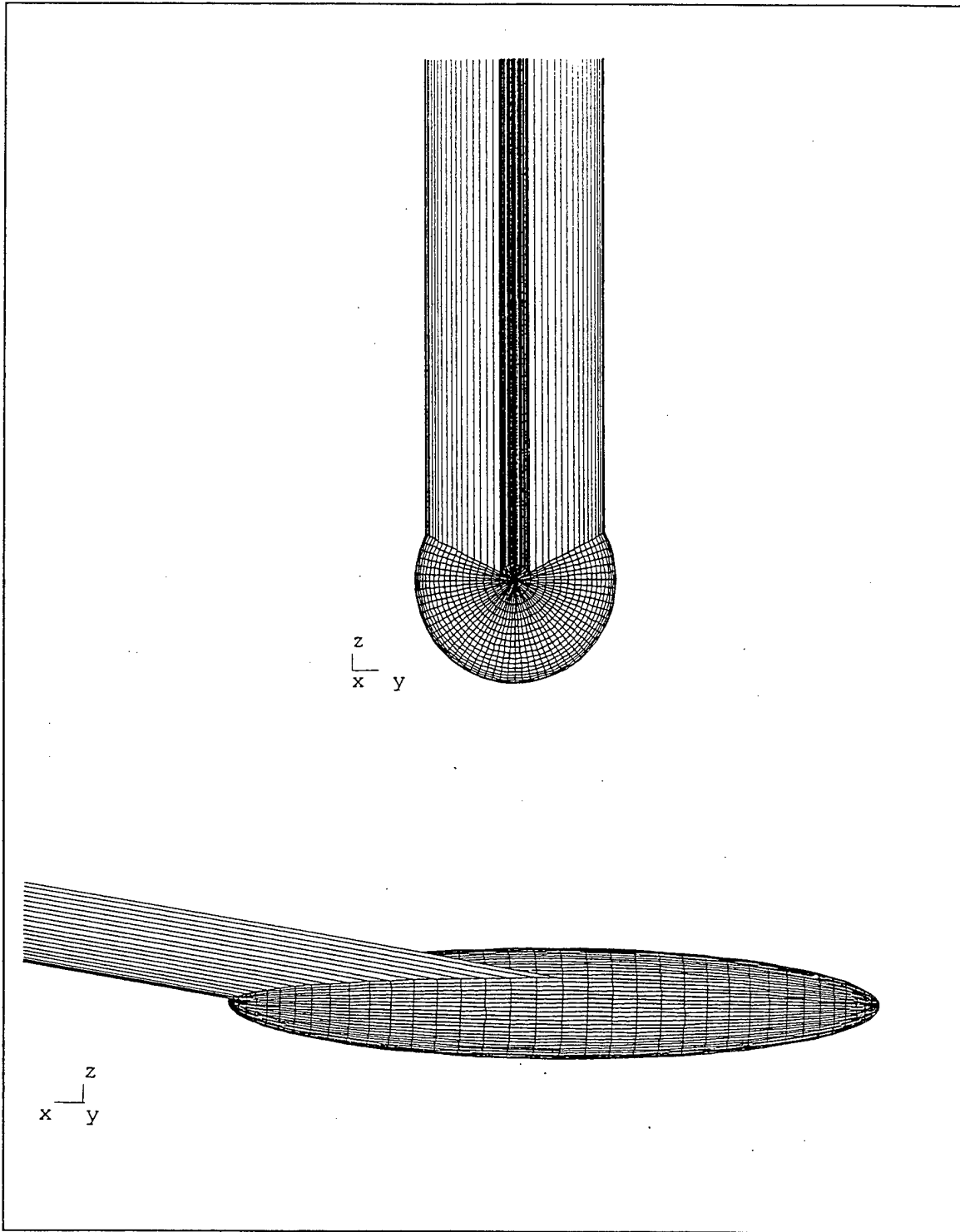


Figure 4.29 CMARC Pressure Distribution with Wake Angles Ranging from  $117^\circ$  to  $162^\circ$  Compared to Experimental Data, after Ref. [12].





**Figure 4.30** POSTMARC Views of CMARC Model with  $117^\circ$  Wake Separation  
Line Running Aft from  $x/2a=0.5$  to  $x/2a=0.99$ .

Coefficients for normal ( $C_N$ ), axial ( $C_A$ ), lift ( $C_L$ ), drag ( $C_D$ ), and pitching moment ( $C_m$ ) are compared to experimental forces in Table 4.3 for a circumferential wake angle of 117 degrees. CMARC automatically outputs the pressure load coefficients in both wind and body axes. Skin friction forces are calculated using POSTMARC and will be discussed in a later section. The experimental results are from integrated pressure forces using the method outlined in Appendix B. The coefficients are normalized by maximum diameter and cross sectional area. A wake angle of 117 degrees produces a close match to experimental results for  $C_N$ ,  $C_L$  and  $C_m$ . As expected, the axial and drag coefficients are off considerably from experimental data.

Force Origin	Force/Moment Coefficient	Experimental AGARD 303-Kreplin	CMARC $\theta_w=117^\circ$	% Difference (CMARC-exp)/exp
Pressure Forces	$C_N$	0.1924	0.1816	-5.6%
	$C_A$	0.0026	0.0411	1480.8%
	$C_L$	0.1890	0.1717	-9.2%
	$C_D$	0.0359	0.0720	100.6%
	$C_m$	0.9009	0.9003	-0.1%

**Table 4.3 Comparison of Integrated Experimental Pressure Forces to the CMARC Model with 117° Wake Placement Angle, after Ref. [12].**

It is concluded that a pure potential flow solution over a streamlined body at 10° angle-off-attack will fail to predict substantial regions of flow separation. However, pressure distributions over bodies with substantial flow separation can be approximated by proper wake distribution. As outlined by Tuncer and Platzer [Ref. 7], a wake separation angle of 144° is a good starting point.

## 5. Boundary Layer Separation Locations

Next, CMARC boundary layer calculations were visualized to see how well CMARC predicted separation points for the inclined prolate spheroid. As reported in the section on the NACA 2415 finite wing, predicted boundary layer separation points from CMARC matched those predicted by the NPS UPOT code fairly well, especially at higher

Reynolds numbers. In this case, the boundary layer points are compared to experimental data at the same  $10^\circ$  angle-of-attack over the three-dimensional prolate spheroid.

Sixty-six streamlines for boundary layer calculations were placed on the CMARC model at locations corresponding to experimental data points. Appendix F contains the input file. CMARC only predicted separation over the very aft end of the body. A separation point is best visualized with POSTMARC by selecting the on-body streamline boundary layer thickness or shape factor functions. The separation point is indicated at the last downstream point on the streamline. It is important to note that if one visualizes streamline pressure coefficient, velocity or Mach number, the streamline will travel all the way to the aft stagnation point. In other words, to visualize a separation point, phenomena derived from the boundary layer calculations and not the streamline calculations must be selected for visualization.

Figure 4.31 displays the streamline separation points on the aft end of the prolate spheroid. CMARC boundary layer separation points are compared to experimental data as a function of axial location and circumferential angle in Figure 4.32. It is to be expected that the 2D code implemented in CMARC fails to accurately predict separation regions over streamlined bodies of revolution with large cross flow velocities. Nevertheless, these results help to quantify the differences.

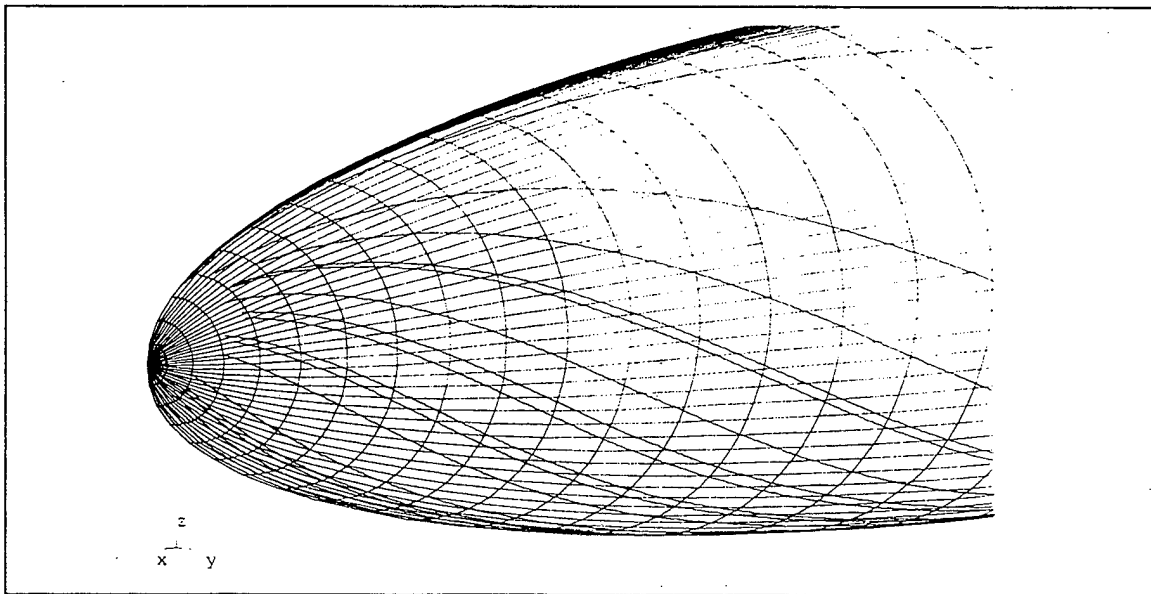


**Figure 4.31 POSTMARC Visualization of CMARC Predicted Separation Points on the Aft End of the Prolate Spheroid Model (No Wakes).**

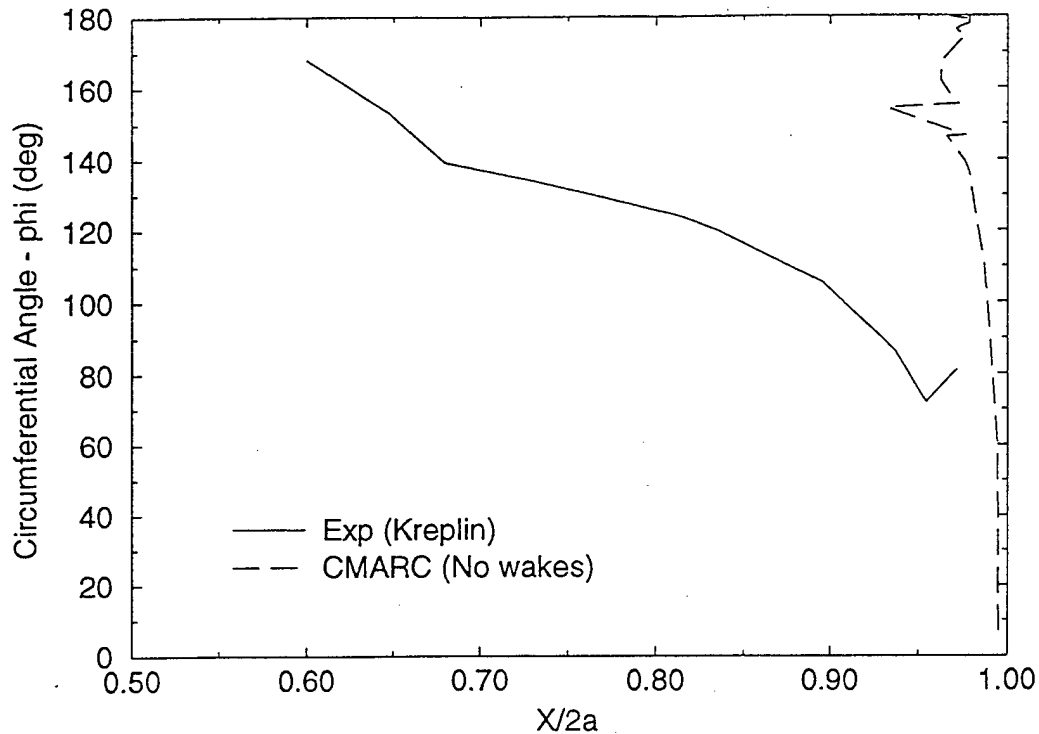


**Figure 4.32 Comparison of CMARC Predicted Separation Line to Experimental Data, after Ref. [12].**

## 6. Boundary Layer Skin Friction Coefficient

CMARC-computed skin friction coefficients were compared to experimental data obtained from hot film sensors [Ref. 12]. Sixty-six streamlines were placed through panels on the CMARC model corresponding to skin friction data pints. Data were extracted manually from the CMARC output file. Data are plotted at six axial locations as a function of circumferential angle in Figure 4.33. The wind tunnel model has a transition strip located at  $x/2a=0.20$ . All CMARC boundary layer calculations are based on a built-in transition model. There are no provisions for specifying the transition location in CMARC.

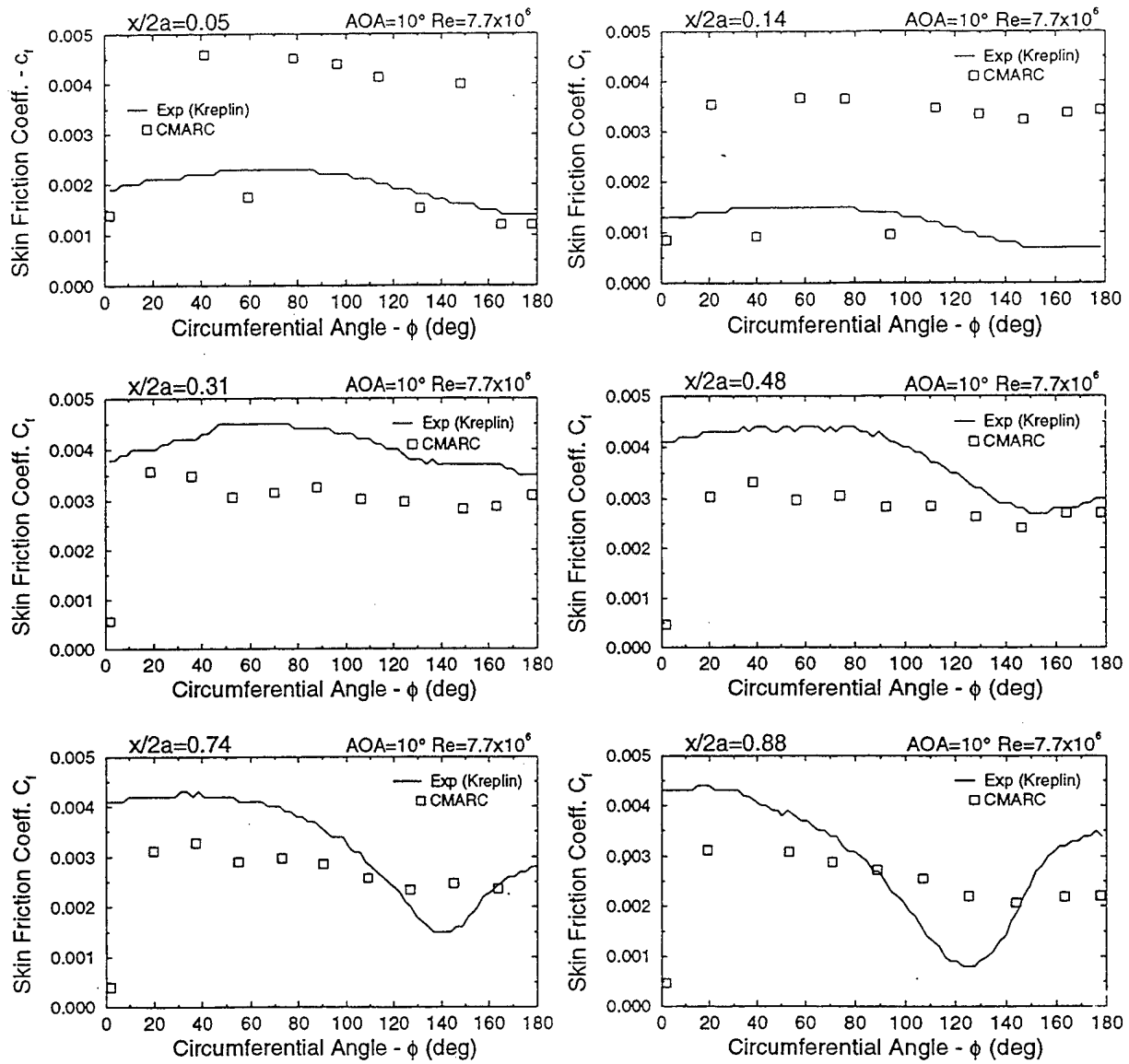


**Figure 4.33 Comparison of CMARC Predicted Skin Friction Coefficient to Experimental Data, after Ref. [12].**

For the two axial locations in front of the transition strip,  $x/2a=0.05$  and  $0.14$ , CMARC predicts a mix of laminar and turbulent flow. A laminar boundary layer is indicated by the data points where  $C_f < 0.002$ . Experimental data indicate strictly laminar flow for these axial locations. CMARC streamlines passing through each circumferential location travel a unique path across different panel geometry from the forward stagnation point to the point of interest. Being an integral two-dimensional boundary layer method, CMARC's empirical transition formula predicts separation for some of the streamlines and laminar flow for the others. In general, CMARC over-predicts skin friction drag in this region due to the mixed flow. If CMARC correctly predicted all laminar flow, the results would be close to experimental results.

Aft of the transition strip at  $x/2a=0.20$ , experimental data indicate fully turbulent flow as expected. CMARC predicts turbulent flow for all but the lower streamline which has a low adverse pressure gradient. At  $x/2a=0.31$  and  $0.48$ , computed skin friction is accurate to within 25%. Aft of  $x/2a=0.48$ , CMARC results are less meaningful due to the large region of separated flow.

## **7. Integrated Skin Friction Forces**

POSTMARC version 1.17.3 contains functionality for performing integrated skin friction calculations. When a CMARC model is processed with the "-p" command line switch, a file with a ".pm" extension is created with the information necessary for POSTMARC to perform boundary layer calculations. POSTMARC then places streamlines on every panel, performs boundary layer calculations and integrates the skin friction loads. Experimental data is integrated as outlined in Appendix B.

Integrated skin friction forces for the prolate spheroid model without wakes are compared to experimental data in Table 4.4. Normal, axial, drag and pitching moment coefficients were all within 40% of the rough estimate provided by integrating the experimental data. This is in keeping with the observations from Figure 4.33. The lift coefficient produced due to skin friction is so small that comparisons between experimental and CMARC data are meaningless.

Force Origin	Force/Moment Coefficient	Experimental AGARD 303-Kreplin	CMARC $\theta_w=117^\circ$	% Difference (CMARC-exp)/exp
Skin Friction Forces	$C_N$	0.0102	0.0071	-30.6%
	$C_A$	0.0610	0.0376	-38.4%
	$C_L$	-0.0006	0.0004	-166.7%
	$C_D$	0.0618	0.0376	-39.2%
	$C_m$	0.0022	0.0019	-12.4%

**Table 4.4 Comparison of Integrated Experimental Skin Friction Forces to the CMARC Model without Wakes, after Ref. [13].**

### 8. Total Integrated Forces

As a final comparison of CMARC results to experimental data, the summed pressure and skin friction force coefficients are presented in Table 4.5. A simple fore/aft wake running from  $x/2a=0.5$  to a partial ring wake at  $x/2a=0.99$  provides good results for all but the axial and drag coefficients. It is concluded that CMARC, with proper wake selection, will provide meaningful force and moment coefficients for the development of stability derivative data. Results for drag coefficient are less meaningful and should be avoided for performance calculations.

Force Origin	Force/Moment Coefficient	Experimental AGARD 303-Kreplin	CMARC $\theta_w=117^\circ$	% Difference (CMARC-exp)/exp
Pressure Forces	$C_N$	0.1924	0.1816	-5.6%
	$C_A$	0.0026	0.0411	1480.8%
	$C_L$	0.1890	0.1717	-9.2%
	$C_D$	0.0359	0.0720	100.6%
	$C_m$	0.9009	0.9003	-0.1%
Skin Friction Forces	$C_N$	0.0102	0.0060	-41.2%
	$C_A$	0.0610	0.0379	-37.9%
	$C_L$	-0.0006	-0.0017	180.0%
	$C_D$	0.0618	0.0388	-37.2%
	$C_m$	0.0022	0.0017	-23.5%
Total Forces	$C_N$	0.2026	0.1876	-7.4%
	$C_A$	0.0635	0.0790	24.4%
	$C_L$	0.1884	0.1700	-9.8%
	$C_D$	0.0977	0.1108	13.4%
	$C_m$	0.9031	0.9020	-0.1%

**Table 4.5 Comparison of Integrated Experimental Forces to the CMARC Model with  $117^\circ$  Wake Placement Angle, after Ref. [12].**





## V. AERODYNAMIC MODEL OF THE FROG UAV

### A. BACKGROUND

The Naval Postgraduate School Aeronautics Department is integrating UAV hardware and software to demonstrate autonomous flight, trajectory tracking and automatic landing. A core requirement for flight control law development is a valid aerodynamic truth model for the UAV airframe. A panel code model of the FROG UAV is one method for estimating many of the stability derivatives required for an aerodynamic truth model. This development effort concentrates on finding the  $C_{L\alpha}$  and  $C_{m\alpha}$  longitudinal stability derivatives followed by the  $C_{Y\beta}$ ,  $C_{l\beta}$  and  $C_{n\beta}$  lateral-directional stability derivatives. A future study will continue the development for rate damping and control effectiveness derivatives.

Panel code modeling utility goes beyond the development of aerodynamic coefficients. Flight control systems require accurate pitot-static and angle-of-attack sensor inputs. CMARC accurately solves on-body static pressure distributions and off-body flow velocities over the predominately attached flow fields of fuselage fore bodies. In this study, correction curves are generated for static-pressure source and angle-of-attack probe position errors.

### B. FROG UAV DESCRIPTION

The FROG UAV is a small single engine flight test vehicle used for autonomous flight research by the Naval Postgraduate School Aeronautics Department. The aircraft was originally designated the FOG-R by the U. S. Army. It was designed as a small lightweight, battlefield observation platform that could be guided by a fiber optic data link. Table 5.1 presents the basic aircraft specifications.

The aircraft is somewhat unconventional in that the engine is mounted in a nacelle tractor style above the fuselage and wing. The aft fuselage consists of a 1.75 in. diameter aluminum tube which connects the tail surfaces to the main fuselage. Figure 5.1 displays a three view drawing of the FROG UAV.

PARAMETER	MEASUREMENT/UNITS	
Length	8.125 ft	97.5 in
Height	1.75 ft	21 in
Weight	67.7 lbs	
Power Plant	12 Hp / 2 Cycle	
Wing Airfoil	NACA 2415	
Horiz. Stab. Airfoil	NACA 0006 (Approx.)	
$S_w (S_{ref})$	17.57 ft <sup>2</sup>	2530 in <sup>2</sup>
$S_t$	3.174 ft <sup>2</sup>	457.1 in <sup>2</sup>
$S_v$	0.9818 ft <sup>2</sup>	141.4 in <sup>2</sup>
c	1.66 ft	20 in
$c_t$	0.958 ft	11.5 in
$b_w$	10.54 ft	126.5 in
$b_t$	3.313 ft	39.75 in
$b_v$	1.25 ft	15.0 in
$l_t$	4.44 ft	53.25 in
$l_v$	4.44 ft	53.25 in
$AR_w$	6.32	
$AR_t$	3.46	
$AR_v$	1.59	
$V_H$	0.49	
$V_v$	0.02	

Table 5.1 FROG UAV Characteristics, after Ref. [1].

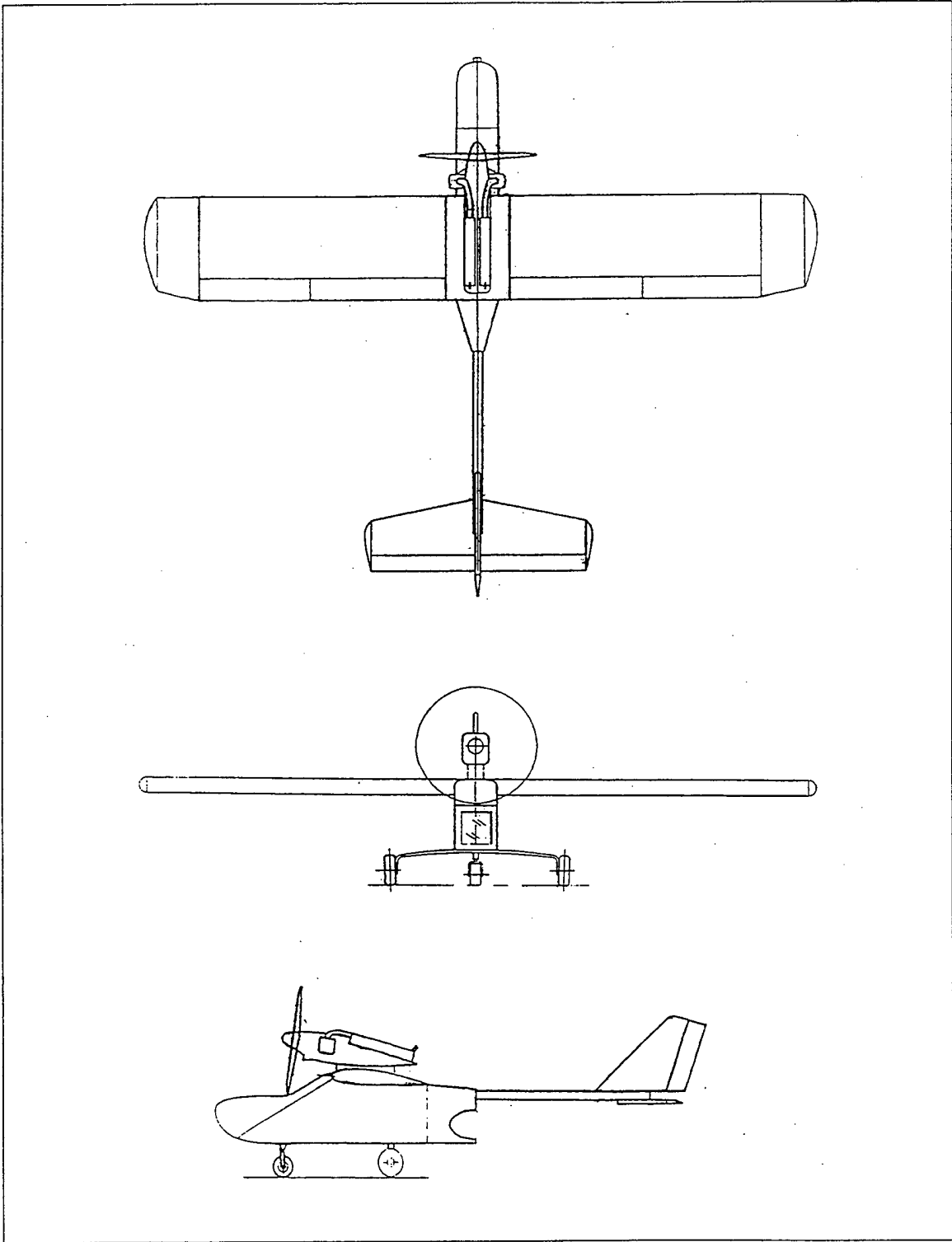


Figure 5.1 FROG UAV Three-View Drawing.

The FROG UAV, as operated by NPS, is equipped with airspeed, angle-of-attack, altitude and control surface sensors. In addition, a miniature Inertial Measurement Unit (IMU) captures aircraft attitude, acceleration and body rates. Data is down linked to a mobile SGI workstation through a spread spectrum modem. Onboard GPS provides differential GPS navigation capability with the ground station used as a reference. The aircraft can be flown by conventional radio control or by up-linking flight control commands from the computer workstation.

Current flight control development revolves around the cruise trim point of 60 m.p.h. or 88 ft/s. This flight condition is selected for the development of stability derivative data. Table 5.2 lists the aircraft parameters for the trim flight condition.

PARAMETER	MEASUREMENT	UNITS
Weight	67.73	lbs
IXX	12.52	slug-ft <sup>2</sup>
IYY	8.43	slug-ft <sup>2</sup>
IZZ	18.55	slug-ft <sup>2</sup>
Airspeed	60/88	mph and ft/s
Altitude	800	ft MSL
Air Density	0.002327	slug/ft <sup>3</sup>
Center of Gravity	34.5%	M.A.C
$C_{L \text{ trim}}$	0.4295	n/a
$\alpha_{\text{trim (est)}}$	-1.3	degrees
$\delta_{E \text{ trim}}$	5.1	degrees

Table 5.2 FROG UAV Trim Flight Condition, after Ref.[1].

## C. FROG UAV MODELING

### 1. General

LOFTSMAN is utilized for the creation of all CMARC input file patches except for wing tips. In some cases, CMARC's more efficient built-in capability to model standard NACA 4-digit wing surfaces could have been used. However, future studies will

require flight control surface patches meshed with LOFTSMAN. Therefore, with growth provisions in mind, all patches were created with LOFTSMAN from the start. Figure 5.2 displays the complete FROG UAV model with all patches and wakes activated.

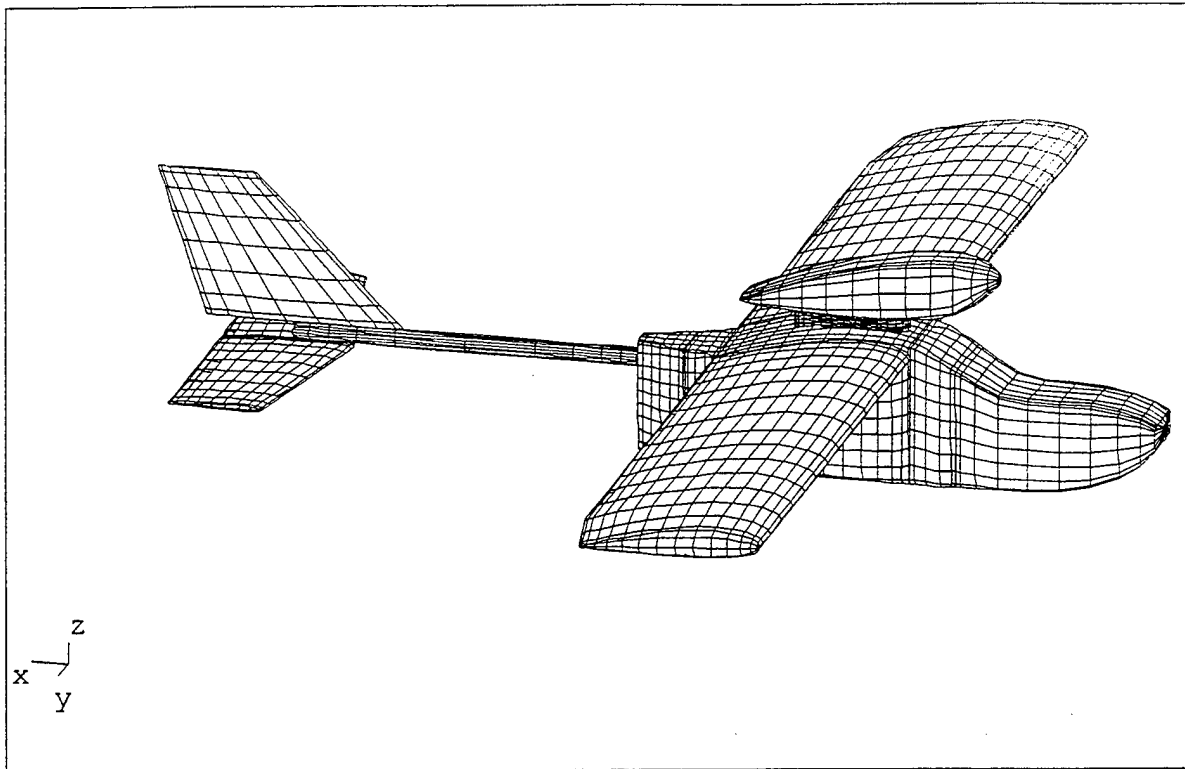


**Figure 5.2 FROG UAV Panel Code Model.**

Some assumptions are made to simplify the modeling process. First, the horizontal and vertical stabilizers are modeled with a NACA 0006 section. The actual surfaces are constructed with a flat section, rounded at the nose and tapered starting at the control surface hinge line to a sharp trailing edge. The NACA 0006 provides a close approximation and allows the use of LOFTSMAN's built-in wing lofting capability. For a potential flow solution, this simplification is considered minor.

A second simplification is made regarding the vertical stabilizer's tip rib orientation. The actual rib is canted down  $5^\circ$  with respect to the longitudinal waterline.

LOFTSMAN will only model a chord line that is parallel to the waterline (constant BL). The vertical tail tip rib is modeled with a constant BL, but the span is adjusted to maintain the same overall surface area.

Finally, there is no attempt to model the tricycle landing gear struts or wheel assemblies. The landing gear components do not contribute significantly to the aerodynamic stability derivatives. However, they certainly need to be taken into account when measuring moments of inertia for a dynamic model.

## **2. Modeling Coordinate System**

The model is developed using a coordinate system selected to simplify fuselage measurements. The +x-axis starts even with the nose and runs aft along the bottom of the fuselage, parallel with the tail boom. The bottom of the fuselage is used as the waterline with +z-axis in the up direction. This allows for easy vertical measurements when the aircraft is placed flat on a horizontal surface. The +y-axis runs from centerline outboard parallel to the right wing. Figure 5.3, which displays static-pressure source and alpha vane locations, also shows the location and origin of the modeling coordinate system.

## **3. LOFTSMAN Patches**

LOFTSMAN is used to generate all the model patches except for wing tips. CMARC's built-in capability is used to create wing tip patches. Appendix H contains listings of all the LOFTSMAN input files. Once a surface is meshed, the mesh is saved to a file as a CMARC/PMARC patch. The resulting text file is then opened, and the text is copied and pasted with any text editor into the patch definition section of the CMARC input file. LOFTSMAN patch files are not listed because they are redundant with the patches in the final CMARC input file listed in Appendix I.

When saving a patch, LOFTSMAN automatically takes care of all CMARC input file formatting except for the TNODS patch continuation or final patch toggle. A patch, as formatted by LOFTSMAN, assumes additional patches will follow in the CMARC input file. Therefore, the last segment's TNODS variable is set TNODS=3. When the patch is the last patch in the input file, the TNODS variable must be manually set to TNODS=5. If CMARC hangs up while reading in geometry information, most likely TNODS=5 is missing on the last patch.

### *a. Fuselage Model*

The fuselage is lofted as a B-type body. A B-type body is used when major portions of the fuselage have a circular or oval cross section. The input file is listed in Appendix H. Only the right side is meshed, with a symmetric left side created by toggling the IPATSYM variable to IPATSYM=1. LOFTSMAN assumes that B-type bodies converge to a specific point at the fore and aft ends. The flat aft fuselage face does not provide this single point. A slight modification was made to the aft face to allow automatic meshing as a B-type body. The center of the aft face is extended very slightly, approximately 1/8 inch, to provide a convergence point for the final rear triangular panels. This small deviation is assumed not affect the aerodynamic fidelity of the model for a potential flow solution.

The right side was originally meshed separately from the wing as a 20 x 20 panel patch. This created a low order fit when the wing patch was butted to the side of the fuselage, resulting in overlapping panels. A final mesh was created that flowed around the wing root and fuselage intersection for a high order fit. All the fuselage panels at the wing root join with the adjacent wing panels. This mesh requires that the fuselage be broken up into six separate panels per side. They are the nose patch, the forward transition patch, the top and bottom wing root patches, the aft transition patch and finally the rear fuselage patch. Some manual editing is required to straighten out panels on the upper fuselage patch. When the six patches are added together, the final configuration is modeled with a 44x15 panel patch.

### *b. Main Wing Patch*

The NACA 2415 wing is created with four separate patches to allow the addition of an aileron mesh at a later date. CMARC comes with a broad selection of "\*.SD" airfoil template files that are automatically loaded during installation. The "NACA2415.SD" file is used for this model. The inboard patch runs from the wing root, past the flaps, to the start of the aileron. The mid patch covers the portion of the wing spanned by the aileron. The outboard patch creates the tapered wing extension. Finally, a semi-circular wing tip patch is added in the input file using CMARC's built-in wing tip functionality. The wing is set to a 4.5° incidence in the LOFTSMAN input file. Alternatively, the patch could be created with zero incidence and then the patch



coordinate system could be rotated in the CMARC input file. Together, the four wing patches add to make a 20 x 30 panel wing model.

*c. Horizontal Stabilizer Patch*

The horizontal stabilizer patch is created with a single 10 x 22 mesh using the "NACA0006.SD" airfoil template. No special modifications are required. A tip patch is not added because some of the resulting panels would be too small. In particular, the triangular panels closing out the aft end of the tip are too small in proportion to the other panels. An attempt was made to model horizontal and vertical stabilizer wing tips, but the model will not converge with them. Leaving off tip patches will not significantly influence results according to the CMARC User's Guide [Ref. 2].

*d. Vertical Stabilizer Patch*

The vertical stabilizer patch is created with a single 8 x 18 mesh using the "NACA0006.SD" airfoil template. The LOFTSMAN input file is different in that a vertical wing surface requires a modification to the rib axis. The rib axis must be specified with an x-axis rotation of 90°, a y-axis rotation of 0° and an unspecified (999.0) z-axis rotation. No symmetry is selected for the vertical stabilizer because the patch is already symmetric about the y=0 plane. As with the horizontal stabilizer, a tip patch is not added because some of the resulting panels would be too small.

*e. Tail Boom Patch*

The tail boom patch is created as a single 12 x 10 mesh using a B-type body. Again, only the right side is meshed due to symmetry. The LOFTSMAN input file requires modifications at both ends in a similar fashion to the aft fuselage. A single point is added to allow convergence of the triangular panels at either end. With this point, the tail boom has the appearance of being tapered at both ends. The point is then manually edited out in the CMARC input file by replacing the "x" coordinate of the beginning and ending section panels with the correct value. In most cases, the tail boom is left out of solution to aid in convergence. This is due to the small overlapping panels at the fuselage tail boom junction. Being a slender, round tube directly in the fuselage slip stream, the tail boom should have little influence on the stability derivatives.

#### *f. Engine Pod Patch*

The engine pod patch, or nacelle, is created as a single 15 x 10 mesh using a B-type body. Only the right side is meshed due to symmetry. The prop spinner is an integral part of the patch. No attempt is made to model the prop, engine heads or exhaust system.

#### *g. Engine Pylon Patch*

The engine pylon patch is modeled with a single 15 x 10 mesh using an A-type body. A-type bodies are used to model surfaces similar to boat hulls with cornered surfaces or sharp chines. In addition, A-type bodies do not require the body to be completely enclosed. As a result, an A-body was selected to model just the sides of the pylon. Only the right side is meshed due to symmetry. A low order fit is achieved with the adjacent fuselage and engine pod panels. This results in questionable pressure distributions. As a result, the pylon patch was turned off for most configurations. A future attempt will be made to create a high order fit between the other patches. This will probably require manual editing of the intersecting patches.

### **4. Common CMARC Input File Errors**

The patches created in LOFTSMAN are assembled into a single CMARC input file with any text editor. A default minimum input file comes with CMARC or any old file may be modified. There are many errors that will cause CMARC to hang up without an error message. The two most common errors are forgetting to designate the last patch and incorrectly numbering the wake patches.

The last patch must be designated by including a TNODS=5 setting in the last section of the last patch. If it is not included, CMARC hangs up when reading in the geometry. In a similar manner, the last wake must be designated with a NODEW=5 setting. If the last wake is not designated, CMARC hangs up while reading in the wake information.

Another common error involves incorrect wake to patch number association. Patch numbering changes whenever patches are disabled or reordered. The KWPACH field for each wake definition must be checked to make sure it reflects the current patch numbering.

## **D. STATIC-PRESSURE SOURCE AND YAW VANE CORRECTIONS THROUGH OFF-BODY FLOW ANALYSIS**

CMARC is ideally suited for off-body flow analysis. Off-body streamlines may be placed through a point anywhere in the flow field. CMARC will then follow the streamline up and downstream the distance designated in the input file. This is particularly useful for flow visualization. In addition, CMARC calculates pressure coefficient and velocity at each point along the streamline. For this study, two streamlines are placed through the locations of the static-pressure source and alpha probe locations. Pressure coefficient is used to quantify static source position error and velocity is used to calculate alpha probe position error as a function of FROG UAV angle-of-attack. Both static pressure and AOA are digitized for down link to the ground station allowing the values to be easily corrected. Either a look-up table or curve fit correction can be applied subsequent to being passed to the flight control routines.

### **1. Description of the FROG UAV Pitot-Static and AOA Systems**

The pitot-static system and angle-of-attack probe share a common flight test boom extending from the nose of the UAV. The boom contains both the total and static pressure ports. Figure 5.3 depicts the general dimensions of the flight test boom installation and the modeling coordinate system.

### **2. Modeling Off-Body Streamlines**

Streamlines are placed at the two locations indicated in Figure 5.3 which correspond to the static source and alpha probe locations. Two off body streamlines were activated in CMARC by setting NSTLIN=2 in the &SLIN1 line. Only a short distance of 2 inches is selected up and downstream in the SU and SD fields to reduce the size of the output file. Figure 5.4 is a POSTMARC rendering of the two off-body streamlines used for sensor corrections. With the model at  $\alpha_i=0^\circ$ , notice that the streamline is curving up at the angle-of-attack vane location 6.5 inches in front of the aircraft nose.

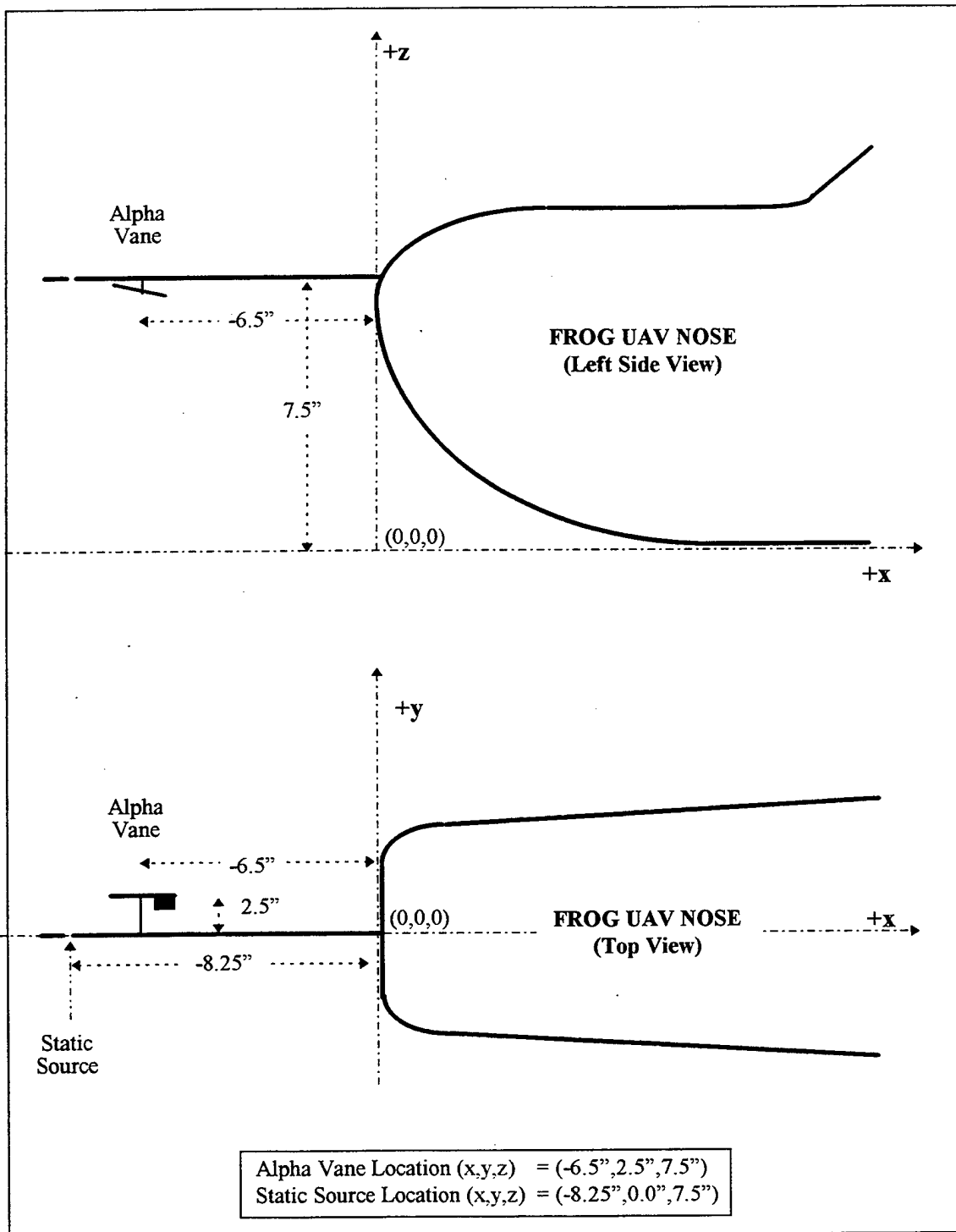


**Figure 5.3** Diagram of the FROG UAV Pitot-Static and AOA Systems.

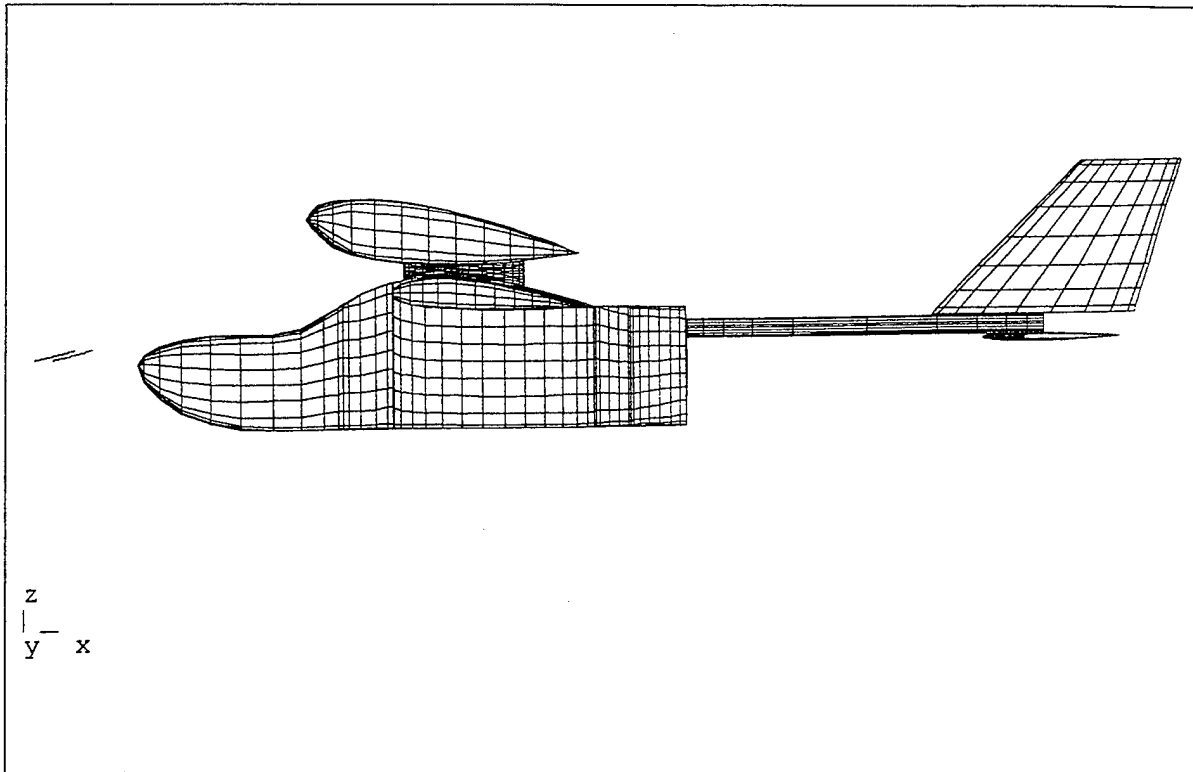


**Figure 5.4 FROG UAV Off-Body Streamline visualization with POSTMARC ( $\alpha_t=10^\circ$ ).**

### 3. Analysis of Static Source Position Errors

In general, the position error pressure coefficient,  $\Delta C_{p_{pe}}$  or  $\Delta P_p/q_e$ , is a function of freestream Mach number and angle-of-attack provided that the static source is located outside of a thick boundary layer and sideslip is minimized [Ref. 13]. In the case of the FROG UAV with incompressible flow,  $\Delta P_p/q_e$  becomes a function of angle-of-attack only. As a result, the corrections can be simply defined as a function of measured angle-of-attack.

A DOS batch file was executed to step the CMARC model through angles-of-attack ranging from  $-8^\circ$  to  $20^\circ$ . The batch file incremented the angle-of-attack using CMARC's command line override feature. In addition, a new output file name was designated for each angle-of-attack. Position error pressure coefficient is then read from the off-body streamline listing of the output file at the location corresponding to the static

source. Table 5.3 lists the values of  $\Delta P_p/q_c$  calculated from CMARC data. Figure 5.5 displays  $\Delta C_{p\ pc}$  as a function of indicated angle-of-attack. The second order influence of angle-of-attack is clear with the second order curve fitting tightly through the data points. Of note, the error is relatively constant for a  $\pm 8^\circ$  band around trim angle-of-attack. For incompressible flow, position error pressure coefficient is independent of airspeed and altitude.

Position error pressure coefficient can be turned into position corrections for airspeed and altitude. The following relations were developed which assume small errors and incompressible flow:

$$\Delta V_{pc} = \frac{V_i \Delta C_p}{2} \quad \text{and} \quad \Delta V_{pc} = V_c - V_i \quad 5.1$$

$$\Delta H_{pc} = \frac{\Delta V_{pc} V_i}{\sigma_{std} g_0} \quad \text{and} \quad \Delta H_{pc} = H_c - H_i \quad 5.2$$

Where:

$\Delta H_{pc}$  is the altitude position correction.

$\Delta V_{pc}$  is the velocity position correction.

$\Delta C_p = \frac{\Delta P_p}{q_c}$  or position error pressure coefficient.

$\sigma_{std}$  is standard day density ratio.

$g_0$  is the gravitational constant.

Table 5.3 displays corrections calculated for both airspeed and altitude at the FROG UAV trim condition of 88 ft/s and 800 ft MSL. The corrections are added to the indicated value to obtain the corrected value. Figures 5.6 and 5.7 display the corrections as a function of indicated angle-of-attack. Again, a second order curve fits nicely through the data points. Equations 5.1 and 5.2 can be used to implement a correction algorithm based on airspeed and altitude.

UAV AOA $\alpha_T$ (deg)	$\Delta C_{p_{pc}}$ $\Delta P/q_c$	V Correction $\Delta V_{pc}=V_c-V_i$ (ft/s)	H Correction $\Delta H_{pc}=H_c-H_i$ (ft)
-8	0.1092	4.8	13.5
-6	0.1120	4.9	13.8
-3	0.1141	5.0	14.1
-2	0.1140	5.0	14.1
-1	0.1137	5.0	14.1
0	0.1132	5.0	14.0
1	0.1123	5.0	13.9
2	0.1111	4.9	13.7
3	0.1096	4.8	13.5
4	0.1078	4.8	13.3
5	0.1057	4.7	13.1
6	0.1034	4.6	12.8
8	0.0977	4.3	12.1
10	0.0909	4.0	11.2
12	0.0831	3.7	10.3
14	0.0741	3.3	9.2
16	0.0641	2.8	7.9
18	0.0530	2.3	6.6
20	0.0410	1.8	5.1

**Table 5.3 Position Error Corrections for the NPS FROG UAV at V=88 ft/s and H=800 ft MSL. Derived from CMARC Panel Code Off-Body Flow Field Analysis.**

Source: CMARC Panel Code  
 Trim Condition: V=88 ft/s H=800 ft MSL  
 Flight Test Boom Static Source (8.25" forward of nose)

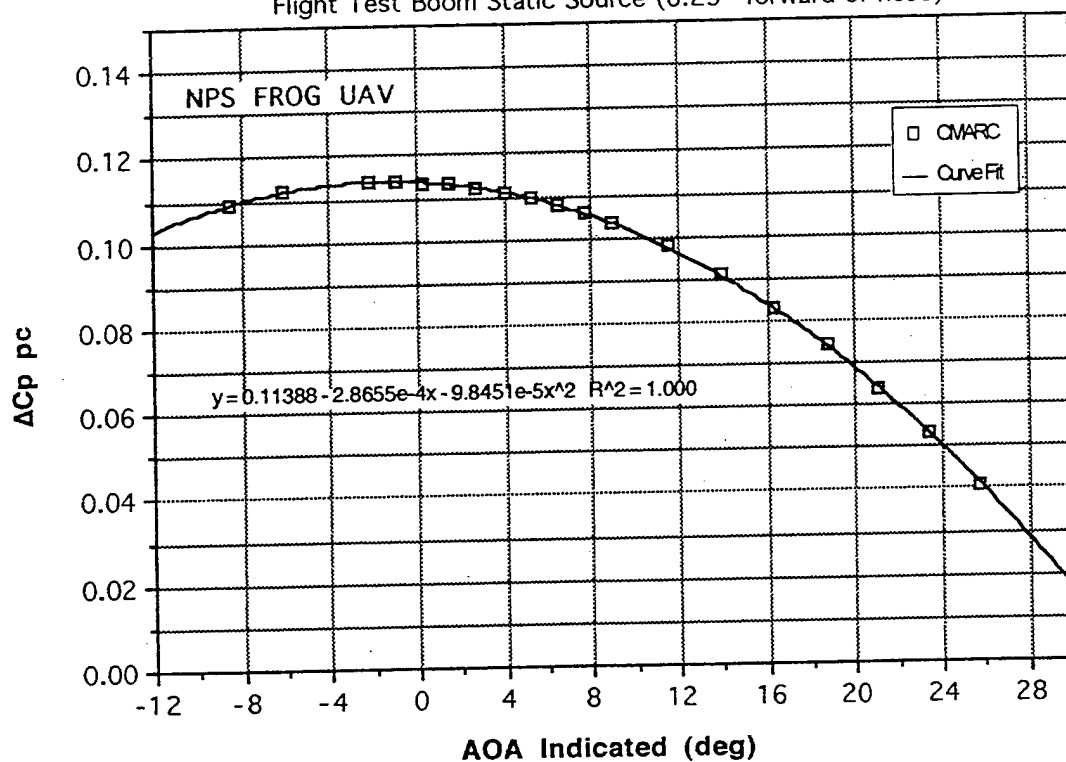
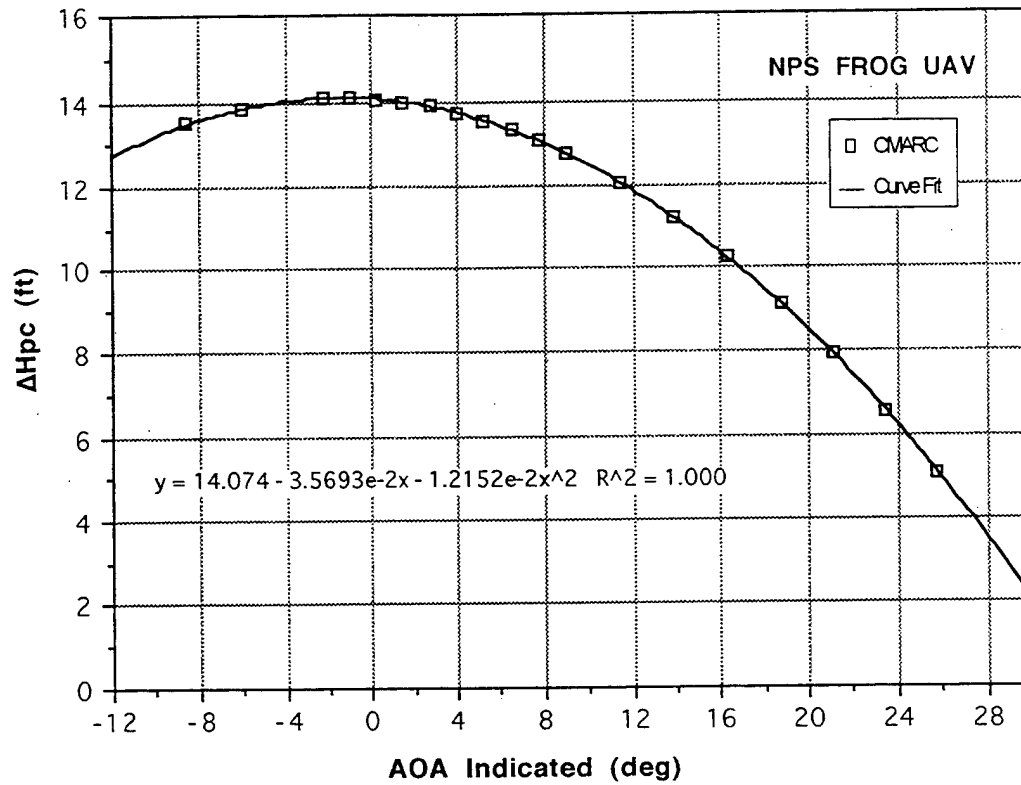


Figure 5.5 Position Error Pressure Coefficient,  $\Delta C_{P_{pc}}$ , for the NPS FROG UAV. Derived from CMARC Panel Code Off-Body Flow Field Analysis.



Source: CMARC Panel Code  
 Trim Condition: V=88 ft/s H=800 ft MSL  
 Flight Test Boom Static Source (8.25" forward of nose)



**Figure 5.6** Altitude Position Error,  $\Delta H_{pc}$ , for the NPS FROG UAV at V=88 ft/s and H=800 ft MSL. Derived from CMARC Panel Code Off-Body Flow Field Analysis.

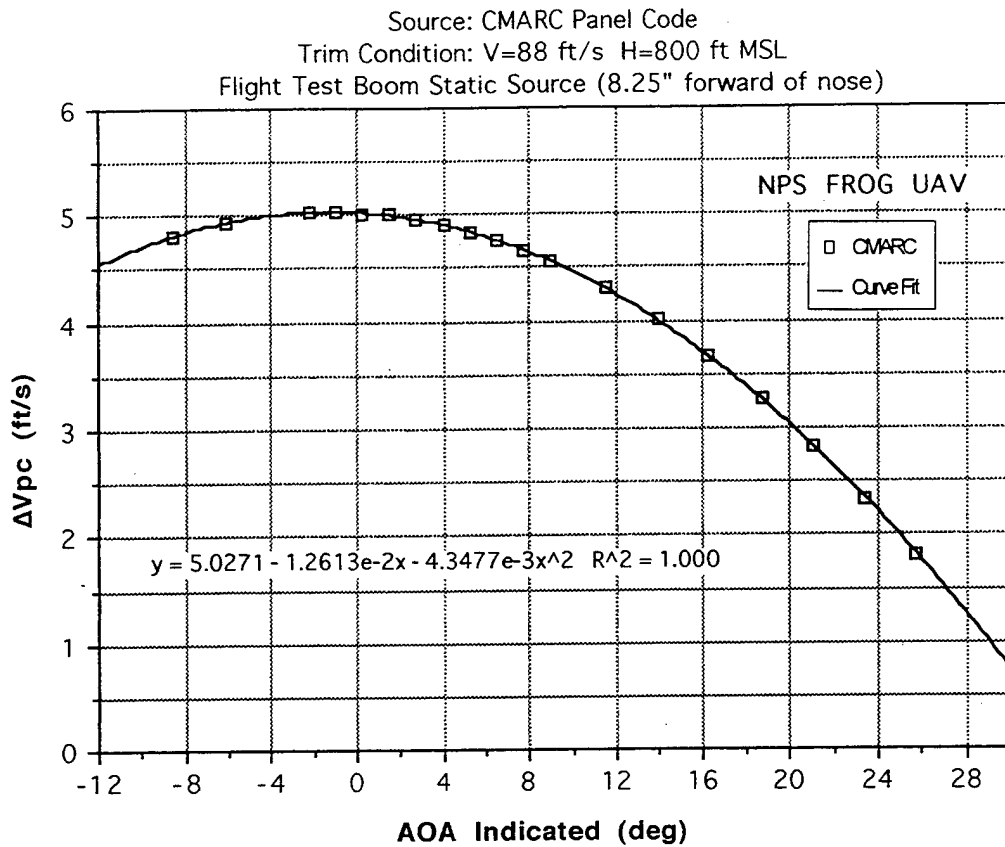


**Figure 5.7** Airspeed Position Error,  $\Delta V_{pc}$ , for the NPS FROG UAV at V=88 ft/s and H=800 ft MSL. Derived from CMARC Panel Code Off-Body Flow Field Analysis.

#### 4. Analysis of Alpha Vane Position Error

Local flow field velocity is extracted from the off-body streamline listing to obtain local angle-of-attack. The alpha vane is assumed to capture the x-z component of the local velocity field and ignore cross flow in the y direction. Flow field velocity is turned into indicated angle-of-attack and angle-of-attack position correction with the following equations:

$$\alpha_i^\circ = a \tan\left(\frac{V_z}{V_x}\right) * \frac{180}{\pi} \text{ degrees} \quad 5.3$$

$$\Delta\alpha_{pc}^\circ = \alpha_t - \alpha_i \text{ degrees} \quad 5.4$$

A DOS batch file is executed to step the CMARC model, with an off-body streamline located at the vane position, through angles-of-attack ranging from  $-8^\circ$  to  $20^\circ$ . Local velocity components are then read from the location corresponding to the alpha vane. Table 5.4 lists the values of  $\Delta\alpha_{pc}$  calculated from CMARC data. Figure 5.8 displays  $\Delta\alpha_{pc}$  as a function of indicated angle-of-attack. Linear and second order curve fit equations are also indicated on Figure 5.8. Angle-of-attack correction is fairly linear through the FROG operating envelope, with approximately  $-1.25$  degrees of position error at the FROG cruise trim condition. The corrections apply at all incompressible airspeeds and all altitudes.

#### 5. Summary of Off-Body Flow Field Analysis

CMARC proved useful for both static-pressure source and alpha vane position corrections. Measured data may be corrected using look-up tables with the values in Table 5.3 and 5.4 or by using the curve fits in Figures 5.5 through 5.8. Flight testing is recommended for validation of sensor corrections obtained from this CMARC off-body flow field analysis.

UAV AOA $\alpha_T$ (deg)	Velocity at Alpha Vane			AOA <sub>Correction</sub>	AOA <sub>Indicated</sub>
	$V_x$ (ft/s)	$V_y$ (ft/s)	$V_z$ (ft/s)	$\Delta\alpha = \alpha_T - \alpha_i$ (deg)	$\alpha_i$ (deg)
-8	80.92	1.66	-12.23	0.60	-8.60
-6	81.27	1.65	-8.65	0.08	-6.08
-3	81.60	1.64	-3.21	-0.75	-2.25
-2	81.67	1.63	-1.47	-0.97	-1.03
-1	81.71	1.63	0.28	-1.20	0.20
0	81.73	1.62	2.13	-1.49	1.49
1	81.73	1.61	3.93	-1.75	2.75
2	81.70	1.60	5.72	-2.00	4.00
3	81.66	1.59	7.51	-2.25	5.25
4	81.58	1.58	9.30	-2.50	6.50
5	81.48	1.57	11.08	-2.75	7.75
6	81.37	1.56	12.88	-2.99	8.99
8	81.07	1.53	16.43	-3.46	11.46
10	80.67	1.51	19.98	-3.91	13.91
12	80.17	1.48	23.50	-4.34	16.34
14	79.61	1.46	26.99	-4.73	18.73
16	78.93	1.43	30.47	-5.11	21.11
18	78.18	1.39	33.90	-5.44	23.44
20	77.34	1.36	37.31	-5.75	25.75

**Table 5.4 Angle-of Attack Vane Position Error Corrections for the NPS FROG UAV. Derived from CMARC Panel Code Off-Body Flow Field Analysis.**

Source: CMARC Panel Code  
 Trim Condition: V=88 ft/s H=800 ft MSL  
 Flight Test Boom Alpha Vane (6.5" forward of nose)

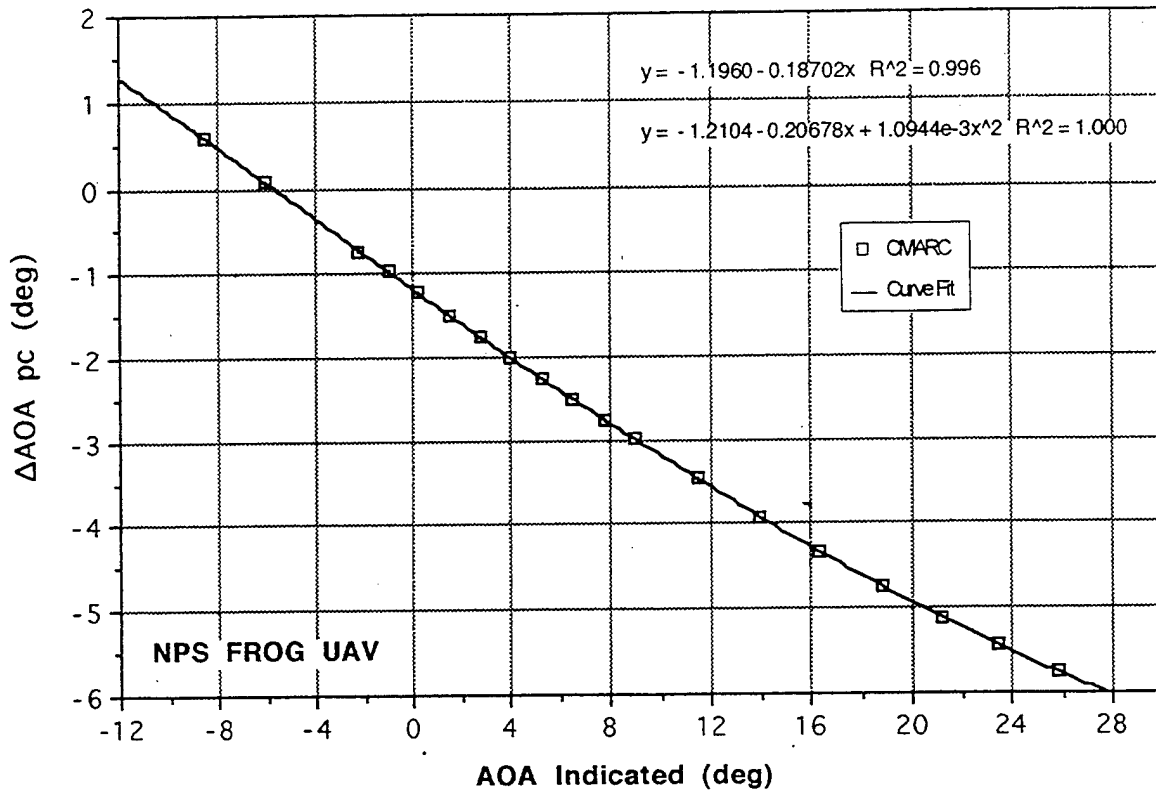


**Figure 5.8** Angle-of-Attack Vane Position Error,  $\Delta\alpha_{pc}$ , for the NPS FROG UAV. Derived from CMARC Panel Code Off-Body Flow Field Analysis.

## E. DEVELOPMENT OF BASIC STABILITY DERIVATIVES

In this section, CMARC is used to develop some of the basic longitudinal and lateral-directional stability derivatives for the FROG UAV. The development effort focuses on finding the  $C_{L\alpha}$  and  $C_{m\alpha}$  longitudinal stability derivatives followed by the  $C_{Y\beta}$ ,  $C_{l\beta}$  and  $C_{n\beta}$  lateral-directional stability derivatives. Control power and rate damping derivatives will be the focus of ongoing research.

CMARC contains built-in functionality to integrate forces and moments in all axes over the surface of a body. Forces and moments are automatically normalized into non-dimensional coefficients based on the mean aerodynamic chord, reference wing area, semi-span and center of gravity location in the CMARC BINP9 input line. Coefficients are presented in both wind and body axes. The CMARC model is run at two different angles-of-attack and one sideslip angle. The slope of the force and moment coefficients is then taken to produce the  $C_{L\alpha}$  and  $C_{m\alpha}$  longitudinal derivatives and the  $C_{Y\beta}$ ,  $C_{l\beta}$  and  $C_{n\beta}$  lateral-directional derivatives.

The CMARC model must be analyzed in the linear slope regions of  $\alpha$  and  $\beta$  for valid results. A potential flow solution will not produce satisfactory results for bodies with significant areas of flow separation.

### 1. Longitudinal Stability Derivatives

#### a. Longitudinal Stability Derivative Methods

Three basic longitudinal stability derivatives can be measured with just two runs of the CMARC model. The model is first analyzed at an angle-of-attack corresponding to the estimated trim condition. In this case,  $\alpha_t=0^\circ$  is selected for the first run. A second CMARC run is conducted with angle-of attack incremented one or two degrees.  $C_L$  and  $C_m$  are then extracted manually from the data files. The slope of  $C_L$  and  $C_m$  versus angle-of-attack provide the  $C_{L\alpha}$  and  $C_{m\alpha}$  longitudinal derivatives. For this study, several angles-of-attack were analyzed to check consistency of the slope. In addition,  $\alpha_{trim}$  is calculated from the lift curve slope and trim lift coefficient. Equations 5.5 through 5.7 are used for these calculations. For the longitudinal analysis, only half the model is analyzed. The symmetric calculation mode is selected by setting both  $RSYM=0.0$  and  $IPATSYM=0$  in the CMARC input file.

$$C_{L\alpha} = \frac{(C_{L2} - C_{L1})}{(\alpha_2 - \alpha_1)} * \frac{180}{\pi} \text{ per radian} \quad 5.5$$

$$C_{m\alpha} = \frac{(C_{m2} - C_{m1})}{(\alpha_2 - \alpha_1)} * \frac{180}{\pi} \text{ per radian} \quad 5.6$$

$$\alpha^{\circ}_{\text{trim}} = \alpha^{\circ}_1 + \frac{(C_{L_{\text{trim}}} - C_{L1})}{C_{L\alpha}} * \frac{180}{\pi} \text{ degrees} \quad 5.7$$

Several FROG UAV model configurations were analyzed in a build-up approach to check results against classical calculations and flight test data. Figure 5.9 shows the simplified CMARC models. First, just the wing and horizontal tail were considered. The patches for all other surfaces and wakes were turned off and the wing root was extended to centerline. The FROG fuselage was then analyzed separately and the results were added to the simplified wing and horizontal tail combination. Next, the original butted (low order fit) wing/fuselage and horizontal tail were considered. Finally, the blended wing/fuselage and horizontal tail were analyzed. Values of  $C_{L\alpha}$  and  $C_{m\alpha}$  for these four configurations are presented in Table 5.5.

Classical design calculations are also performed to estimate  $C_{m\alpha}$  for comparison to CMARC results. Equation 5.8 is used for the calculation of  $C_{m\alpha}$ . In classical design, the horizontal tail downwash derivative,  $d\varepsilon/d\alpha$ , is generally selected from empirical data. Using a taper ratio of TR=1:1 and aspect ratio of AR=6,  $d\varepsilon/d\alpha=0.4$  is selected from empirical charts in Ref. [14] for the FROG UAV configuration. A few other values of the horizontal tail downwash derivative,  $d\varepsilon/d\alpha$ , are selected to see how well CMARC models downwash effects. Classical design estimates of  $C_{m\alpha}$  for values of  $d\varepsilon/d\alpha$  ranging from 0 to 0.4 are presented in Table 5.5 for comparison with CMARC results.

$$C_{m\alpha} = a_w \left[ (h - h_{ac}) - V_H \frac{a_t}{a_w} \left( 1 - \frac{d\varepsilon}{d\alpha} \right) \right] \quad 5.8$$

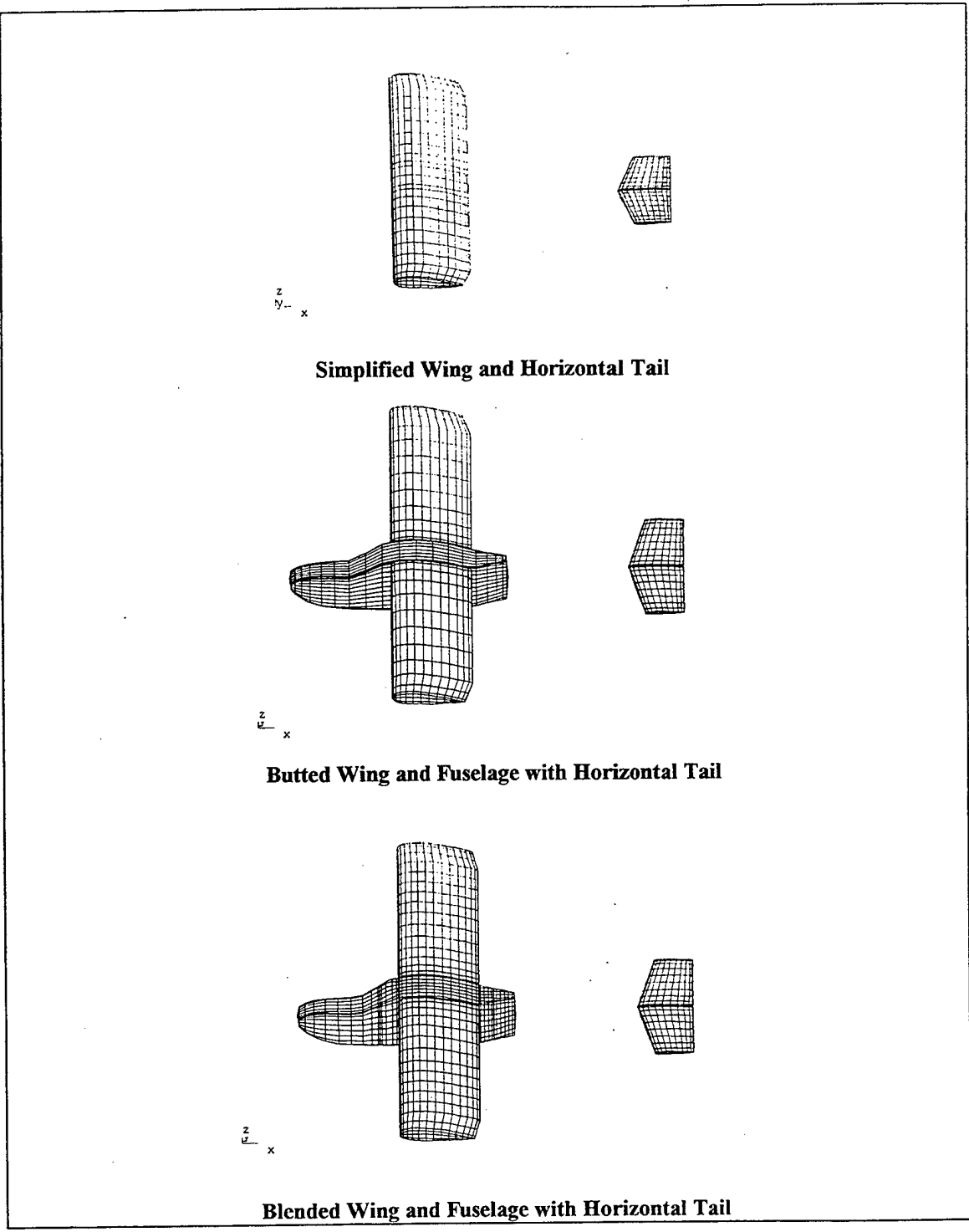


**Figure 5.9 Simplified CMARC Models of the FROG UAV for the Determination of Longitudinal Stability Derivatives.**



Flight test data for the short period and phugoid modes were used for longitudinal parameter estimation. Values for  $C_{L\alpha}$  and  $C_{m\alpha}$  based on preliminary parameter estimation work by Engdahl [pending publication] are presented in Table 5.5. Caution is advised against making definitive comparisons until the work is published.

METHOD	CONFIGURATION <sup>1</sup>	LONGITUDINAL PARAMETERS		
		$\alpha_{trim}^2$ (deg)	$C_{L\alpha}$ (per rad)	$C_{m\alpha}$ (per rad)
CMARC Panel Code	Wing/Horiz Tail	-0.87	4.86	-0.835
	Wing/Horiz Tail + Fuselage	-0.86	4.78	-0.608
	Blended Wing-Fuselage/Horiz Tail	-0.01	4.72	-1.105
	Butted Wing-Fuselage/Horiz Tail	-0.8	5.37	-1.348
Classical Design <sup>3</sup>	Wing/Horiz Tail - $\delta\epsilon/\delta\alpha=0$	-0.78	4.89	-1.50
	Wing/Horiz Tail - $\delta\epsilon/\delta\alpha=0.25$	-0.81	4.85	-1.00
	Wing/Horiz Tail - $\delta\epsilon/\delta\alpha=0.35$	-0.82	4.83	-0.80
	Wing/Horiz Tail - $\delta\epsilon/\delta\alpha=0.40$	-0.82	4.82	-0.70
Parameter Estimation <sup>4</sup>	Flying Aircraft	n/a	4.09	-0.42

NOTES: 1)  $CG_x=34.5\%$  M.A.C. /  $CG_z=8.6"$  from bottom of fuselage.

2) Zero lift wing incidence is  $+6.5^\circ$  from the longitudinal reference line.

3) Classical Design after Ref. [14].

4) Unpublished parameter estimation from flight test data by Engdahl.

**Table 5.5 Comparison of FROG UAV Longitudinal Stability Derivatives.**

***b. Analysis of Longitudinal Stability Data***

The first three configurations in Table 5.5 produce good results for  $C_{L\alpha}$  and reasonable values for  $C_{m\alpha}$ . However, the fourth configuration, the butted wing root and fuselage, produces excessively large values of both  $C_{L\alpha}$  and  $C_{m\alpha}$ . This configuration should be avoided in future models. It is recommended that CMARC model developers spend the time up front to produce the higher fidelity model from the start.

The values produced for  $C_{m\alpha}$  from CMARC are somewhat high when compared with to the classical design calculations. Clearly, some downwash is sensed by the horizontal tail in the CMARC analysis because all values for  $C_{m\alpha}$  are considerably less

than the classical calculation with  $d\varepsilon/d\alpha=0$ . Still, high values compared to flight test data indicates that CMARC has a difficult time capturing the complete  $d\varepsilon/d\alpha$  downwash effect. This could be due to the requirement to select rigid wakes to prevent the wing wake from impacting the horizontal tail. A more careful wake definition may help capture the tail downwash derivative with more fidelity. A study by Walden et al. [Ref. 15] studied wake turbulence by modeling an aircraft flying in trail of a wake generating wing. A horizontal tail trailing the main wing is a similar configuration. The study found that a streamline-based wake is the best method for modeling downwash effects. This wake definition should be investigated for modeling the  $C_{m\alpha}$  derivative. Of note, the wake diffusion process is neglected in a potential flow analysis.

In summary, CMARC produced accurate values for  $C_{L\alpha}$  and slightly high values of  $C_{m\alpha}$ . Difficulties were encountered trying to model the horizontal tail downwash derivative. A more careful study of the effects of wing wake placement on the downwash derivative is recommended.

## 2. Lateral Directional Stability Derivatives

### *a. Lateral-Directional Stability Derivative Methods*

Development of the lateral-directional stability derivatives is more straight forward than for the longitudinal derivatives because the vertical tail sidewash angle plays a lesser role. However, both sides must be modeled by setting both  $RSYM=1.0$  and  $IPATSYM=1$ . This creates symmetric patches around the  $y=0$  plane allowing CMARC to perform asymmetric calculations around the entire body and significantly increases processing times.

For the lateral-directional axis, the aircraft is modeled with the blended wing and fuselage in combination with the vertical and horizontal stabilizers as shown in Figure 5.10. The engine nacelle and pylon are left off because their wakes impact the vertical tail. In addition, the pylon/fuselage and pylon/nacelle junctions were meshed with a low order, butted fit. This type of junction was found to produce poor results during the longitudinal stability study.

The model is first checked for lateral directional balance at zero yaw angle. The side force, rolling and yawing coefficients should be zero when a trial run is

performed at zero yaw angle. If lateral-directional forces or moments are present, the model and wake geometry should be checked for symmetry.

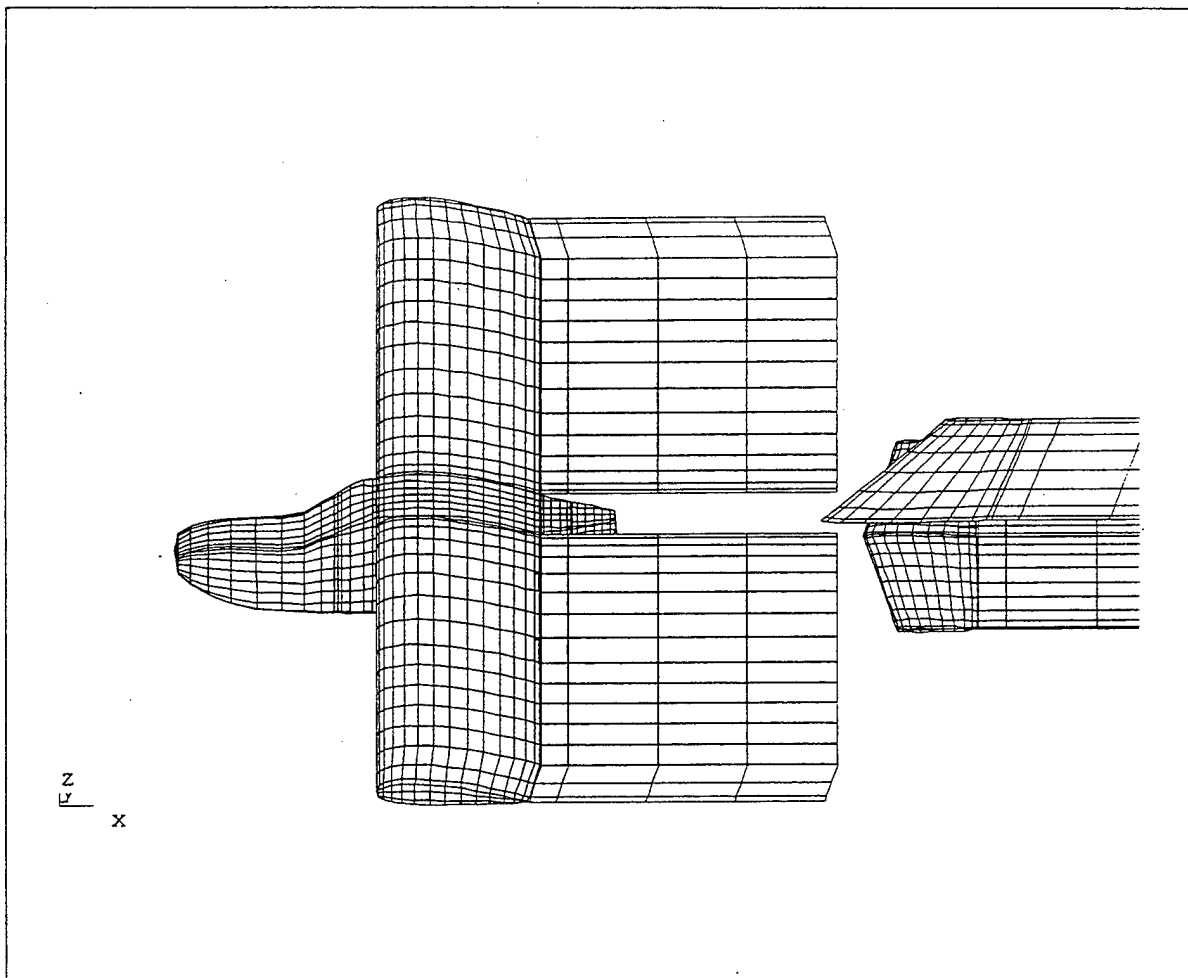


**Figure 5.10 Simplified CMARC Model of the FROG UAV for the Determination of Lateral-Directional Stability Derivatives.**

Next, a single CMARC run is performed with  $\alpha = \alpha_{trim}$  and yaw angle set to one degree. The lateral-directional derivatives,  $C_{Y\beta}$ ,  $C_{l\beta}$  and  $C_{n\beta}$ , are then obtained directly with equations 5.9 through 5.11:

$$C_{Y\beta} = \frac{C_Y}{\Delta\beta^\circ} * \frac{180}{\pi} \text{ per radian} \quad 5.9$$

$$C_{l\beta} = \frac{C_l}{\Delta\beta^\circ} * \frac{180}{\pi} \text{ per radian} \quad 5.10$$

$$C_{n\beta} = \frac{C_n}{\Delta\beta^\circ} * \frac{180}{\pi} \text{ per radian} \quad 5.11$$

It should be noted that the stability axis as modeled (x-aft and z-up) differs from the standard flight dynamics stability axis. Care must be taken to reverse the signs of the appropriate coefficients to convert from a CMARC model's stability axis into the flight dynamics stability axes

### ***b. Analysis of Lateral-Directional Stability Data***

Lateral-directional stability derivatives obtained from CMARC are presented in Table 5.6. For comparison three other sets of data are also presented. The first comes from the classical analysis presented by Papageorgiou in Ref. [1]. The second set comes from estimates based on data recorded from flight test static sideslip maneuvers, also published in Ref. [1]. The third set comes from parameter estimation by Engdahl based on dynamic flight test data. It is unpublished and should be considered preliminary. In all cases, the CMARC lateral-directional stability derivatives produce a closer match to flight test data than those derived from classical methods. It is concluded that CMARC is a good tool for lateral-directional stability analysis.

### **3. Summary of CMARC Stability Derivative Analysis**

In summary, for the longitudinal axis, CMARC produces accurate values for  $\alpha_{trim}$  and  $C_{L\alpha}$  and slightly high values of  $C_{m\alpha}$ . Difficulties may be encountered while trying to model the horizontal tail downwash derivative. A more careful study of the effects wing wake placement on the downwash derivative is recommended. Specifically, modeling should include streamline-based wake placement techniques [Ref. 15]. Analysis of the lateral-directional axis proves more straightforward. Lateral-directional derivatives from CMARC for  $C_{Y\beta}$ ,  $C_{l\beta}$  and  $C_{n\beta}$  provide a closer match to flight test data than the classical estimates. The engine nacelle and pylon should be re-meshed and included in future studies.

Overall, CMARC derived stability derivatives are sufficiently accurate for entry into an initial aerodynamic model. Adjustments through analysis of flight test data will still be required. Future CMARC studies should concentrate on developing the rate damping and control power derivatives.

METHOD	CONFIGURATION <sup>1</sup>	LAT-DIR PARAMETERS		
		$C_{Y\beta}$ (per rad)	$C_{l\beta}$ (per rad)	$C_{n\beta}$ (per rad)
CMARC Panel Code	Blended Wing-Fuselage/Horz/Vert Tails	-0.573	-0.063	0.120
Classical Design <sup>2</sup>	Wing/Fuselage/Vert Tail	-0.310	-0.051	0.058
Flight Test <sup>3</sup>	Flying Aircraft	-0.700	-0.053	0.057
Parameter Estimation <sup>4</sup>	Flying Aircraft	-0.987	-0.094	0.176

- NOTES: 1)  $CG_x=34.5\%$  M.A.C. /  $CG_z=8.6''$  from bottom of fuselage.  
 2) Classical Design calculations by Papageorgio, from Ref. [1].  
 3) Flight test results from Steady Heading Sideslip, from Ref. [1]  
 4) Unpublished parameter estimation from flight test data by Engdahl.

**Table 5.6 Comparison of FROG UAV Lateral-Directional Stability Derivatives.**

## VI. CONCLUSIONS AND RECOMMENDATIONS

CMARC is a DOS personal computer hosted panel code adopted from the NASA Ames PMARC code. AeroLogic, Inc., created CMARC by converting PMARC FORTRAN 77 source code into the C language. Significant memory management and command line enhancements were also added. CMARC solves for inviscid, incompressible flow over complex three-dimensional bodies. Emphasis in this study is first placed on verifying CMARC against the PMARC and Naval Postgraduate School Unsteady Potential Flow (UPOT) panel codes. CMARC pressure distributions and boundary layer calculations are then compared to experimental data for an inclined prolate spheroid. Finally, a complex three-dimensional panel model of the Naval Postgraduate School FROG UAV is developed which successfully generates static-pressure source position corrections, alpha vane correction curves and basic stability derivatives.

CMARC results are found to be equivalent to the NASA-Ames PMARC panel code. As expected, pressure distribution and boundary layer calculations from CMARC match exactly those obtained with PMARC. The following enhancements are noteworthy. CMARC, hosted on a Pentium class PC, processes input files significantly faster than PMARC hosted on a networked SGI Indigo<sup>2</sup> UNIX workstation. CMARC's extensive command line functionality greatly enhances batch file processing capabilities. On the other side, CMARC's poor error flagging capability leaves the user frequently spending much time searching for input file mistakes. Improved input file error checking should be incorporated into CMARC functionality.

CMARC integral boundary layer calculations are compared to the two-dimensional finite difference methods implemented in the UPOT code. In general, CMARC provides correct trends for both the transition and separation points. However, in all cases, CMARC predicts early transition and late flow separation. As expected, the differences are greatest at lower Reynolds numbers where boundary layer thickness is larger. An adjustment of the empirical transition and separation models contained in CMARC may prove useful.

CMARC calculations are also compared to wind tunnel data for a 6:1 inclined prolate spheroid model at 10 degrees angle-of-attack. With proper wake placement, CMARC can produce accurate normal force and pitching moment coefficients. Over the three dimensional body, CMARC boundary layer calculations also predict early transition

and late flow separation. Despite inaccuracies, CMARC boundary layer calculations remain useful when used as a design tool for visualizing the trend in transition and separation points with configuration changes.

CMARC integrated skin friction forces are compared to prolate spheroid wind tunnel data. Normal, axial, and pitching moment coefficients for skin friction forces are underpredicted by CMARC, but remain within 40% of integrated experimental data.

The LOFTSMAN and POSTMARC portions of the Personal Simulation Works software suite are used exclusively for the pre-process modeling and post-process visualization of CMARC files. The LOFTSMAN capability to automatically format and generate CMARC input patches is an enhancing characteristic. Functionality should be added to allow the modeling of wing tip ribs that are not parallel to the aircraft butt line.

POSTMARC is an excellent tool for visualizing CMARC output files. The capability to create streamlines and perform boundary layer calculations external to CMARC is extremely useful. However, much time could be saved if POSTMARC maintained previous settings and selections following translations, rotations and re-scaling. Additionally, a capability to overlay multiple data types is desired.

CMARC off-body flow field analysis is useful for both static-pressure source and alpha vane position corrections. Measured data may be corrected using look-up tables or through curve fits of CMARC derived data. Flight testing is recommended for validation of sensor corrections obtained from the CMARC off-body analysis.

For the longitudinal analysis, CMARC produces accurate values for  $\alpha_{trim}$  and  $C_{L\alpha}$  and slightly high values of  $C_{m\alpha}$ . Some difficulties are encountered trying to model the horizontal tail downwash derivative. A more careful study of the effects of wing wake placement on the downwash derivative is recommended.

Analysis of the lateral-directional axis proves more straightforward. Lateral-directional derivatives from CMARC for  $C_{Y\beta}$ ,  $C_{l\beta}$  and  $C_{n\beta}$  provide a closer match to flight test data than classical design calculations. Adjustments through analysis of flight test data may still be required. The engine nacelle and pylon should be re-meshed and included in future studies.

Overall, the CMARC panel code is found to be suitable for aerodynamic modeling of the Naval Postgraduate School FROG UAV. CMARC derived stability derivatives are sufficiently accurate for incorporation into an initial aerodynamic model. Future CMARC studies should concentrate on the development of the rate damping and control power derivatives.

## APPENDIX A.

### DEVELOPMENT OF THE MOMENTUM INTEGRAL EQUATION

The CMARC and PMARC User's Guides contain the development of the implemented boundary layer equations starting from the two-dimensional momentum integral equation. For completeness, the momentum integral equation is developed here to provide continuity.

The development of the momentum boundary layer equations is outlined by Young in Ref. [9]. In 1904 Prandtl first presented his *Boundary Layer Theory* based on the following observations:

- 1) However small the viscosity of a fluid, it cannot be ignored. At the surface, the fluid is at rest compared to the body (no slip condition).
- 2) Shear stresses are directly proportional to the rates of strain.
- 3) The ratio of inertial forces to viscous forces, or Reynolds number, is important in characterizing flow phenomena.
- 4) The full non-linear viscous Navier-Stokes equations are difficult to solve directly. Prandtl observed that simplifications could be made when assuming a thin boundary layer. Viscosity can be ignored outside the boundary layer allowing the use of classical inviscid methods.

Thin boundary layer theory also assumes that the pressure distribution outside the thin boundary layer is transmitted normally through the boundary layer to the surface without loss. CMARC takes advantage of this assumption by neglecting the thickness of the boundary layer and imposes a potential flow solution over the surface.

The momentum integral equation for two-dimensional incompressible flow is the starting point for the boundary layer analysis outlined in References [2] and [4]. It is obtained through the following total energy integral analysis as outlined by Young in Ref. [9].



Figure A.1 depicts an incremental portion of a two-dimensional boundary layer.

The mass flow rate ( $\dot{m}$ ) across each side is given by:

$$\dot{m}_{AD} = 0$$

$$\dot{m}_{DC} - \dot{m}_{AB} = \frac{d}{dx} \left[ \int_0^h \rho u dz \right] \Delta x + O(\Delta x^2)$$

$$\dot{m}_{BC} = \rho_e w_h \Delta x \quad \text{and} \quad \dot{m}_{DC} - \dot{m}_{AB} = \dot{m}_{BC} \quad \text{from continuity.} \quad \text{A.1}$$

$$\therefore \rho_e w_h = \frac{d}{dx} \left[ \int_0^h \rho u dz \right] + O(\Delta x)$$

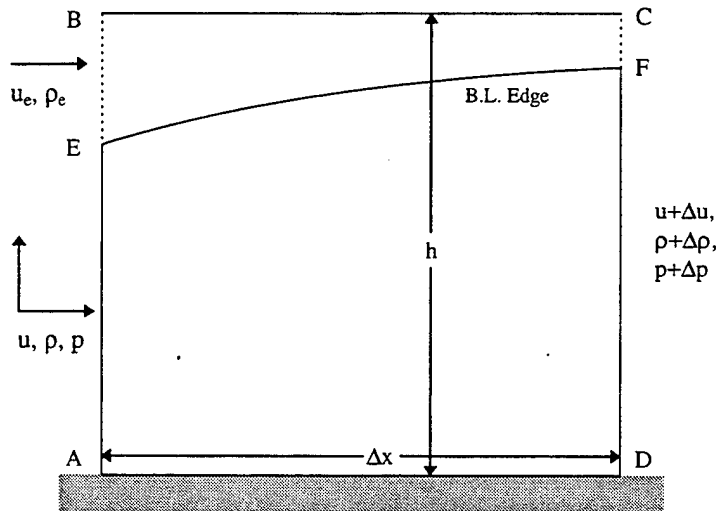


Figure A.1 Elementary boundary layer section for deriving the momentum integral equation for two-dimensional flow, after Ref. [9].

Similarly, the rate of momentum transport across each boundary is given by:

$$\begin{aligned}
 AD: &= 0 \\
 DC - AB: &= \frac{d}{dx} \left[ \int_0^h \rho u^2 dz \right] + O(\Delta x^2) \\
 BC: &= \rho w_h \cdot u_e \Delta x = u_e \frac{d}{dx} \left[ \int_0^h \rho u dz \right] \Delta x + O(\Delta x^2)
 \end{aligned} \tag{A.2}$$

The force due to pressure on the sectional boundary layer element is given by:

$$= -h \Delta p = -h \left( \frac{dp}{dx} \right) \Delta x + O(\Delta x^2) \tag{A.3}$$

And, the friction force exerted by the wall is:

$$= -\tau_w \cdot \Delta x \tag{A.4}$$

Summing the momentum terms and equating them to the forces while taking the limit as  $\Delta x \rightarrow 0$  yields the momentum integral equation:

$$\frac{d}{dx} \left( \int_0^h \rho u dz \right) = -h \frac{dp}{dx} - \tau_w \tag{A.5}$$

It is more convenient to express the relation in terms of displacement and momentum thickness by substituting the following:

$$-\frac{dp}{dx} = \rho_e u_e \frac{du_e}{dx} \tag{A.6}$$

The momentum integral is then reduced to:

$$\begin{aligned}
 \frac{d}{dx} \left[ \int_0^h \rho u (u - u_e) dz \right] + \frac{du_e}{dx} \left[ \int_0^h \rho u dz \right] &= h \rho_e u_e \frac{du_e}{dx} - \tau_w \rightarrow \frac{d}{dx} \left[ \int_0^h \rho u (u - u_e) dz \right] + \frac{du_e}{dx} \left[ \int_0^h (\rho u - \rho u_e) dz \right] = -\tau_w \\
 \text{or } \frac{d}{dx} (\rho_e u_e^2 \theta) + \frac{du_e}{dx} \rho_e u_e \delta^* &= \tau_w
 \end{aligned} \tag{A.7}$$

$$\text{Where } d^* = \int_0^h \left(1 - \frac{ru}{r_e u_e}\right) dz \quad \text{and} \quad q = \int_0^h \frac{ru}{r_e u_e} \left(1 - \frac{u}{u_e}\right) dz \quad \text{A.8}$$

Substituting  $H = \delta^*/\theta_e$ , where H is the boundary layer shape factor, and rearranging after the chain rule, the momentum integral can be written in as:

$$\frac{d\theta}{dx} + \frac{1}{u_e} \frac{du_e}{dx} \theta(H+2) + \frac{\theta}{\rho_e} \frac{dp_e}{dx} = \frac{\tau_w}{\rho_e u_e^2} \quad \text{A.9}$$

And finally, by substituting  $C_f = \frac{\tau_w}{\frac{1}{2} \rho_e q_\infty} = \frac{2\tau_w}{\rho_e u_e^2}$ , one obtains Equation 16 in References [2]

and [4]:

$$\frac{d\theta}{dx} + \frac{1}{u_e} \frac{du_e}{dx} \theta(H+2) + \frac{\theta}{\rho_e} \frac{dp_e}{dx} = \frac{C_f}{2} \quad \text{A.10}$$

From here, the CMARC or PMARC guides provide a detailed development of the implemented boundary layer models.

## APPENDIX B.

### INTEGRATION OF AERODYNAMIC FORCES OVER THE SURFACE OF A PROLATE SPHEROID

The experimental set-up in Ref. [12] did not include measurement of forces. However, it was deemed that the 2000+ pressure and 500+ skin friction measurements would be sufficient to allow the integration of measurements over the surface of the prolate spheroid for a good approximation of total force and moment coefficients. The following technique is developed to provide an estimate of integrated pressure and friction forces. Symmetry is assumed. Appendix C lists the entire MATLAB program which implements the technique that follows.

In general the pressure force is given by:

$$\bar{F}_p = \iint_S P \bar{n} dS, \quad \bar{n} \text{ is a unit surface normal} \quad \text{B.1}$$

However, the test data is provided discretely in cylindrical coordinates, resulting in the following discrete double summation:

$$\bar{F}_p = \sum_{x/2a} \sum_{\phi} P \bar{n} r \Delta \phi \Delta x / 2a, \quad \text{where } dS = r \Delta \phi \Delta x / 2a \quad \text{B.2}$$

Figure B.1 shows a diagram of the pressure and skin friction acting over the incremental surface areas,  $\Delta S$ . The pressure and skin friction coefficients, scalars, are assumed to be constant over the incremental surface.

$$\Delta \bar{F}_p = P \bar{n} r \Delta \phi \Delta x / 2a = (q C_p + p_\infty) \bar{n} \Delta S, \quad \text{B.3}$$

$$\text{where } C_p = \frac{P - P_\infty}{q} \Rightarrow P = C_p \cdot q + P_\infty \quad \text{B.4}$$

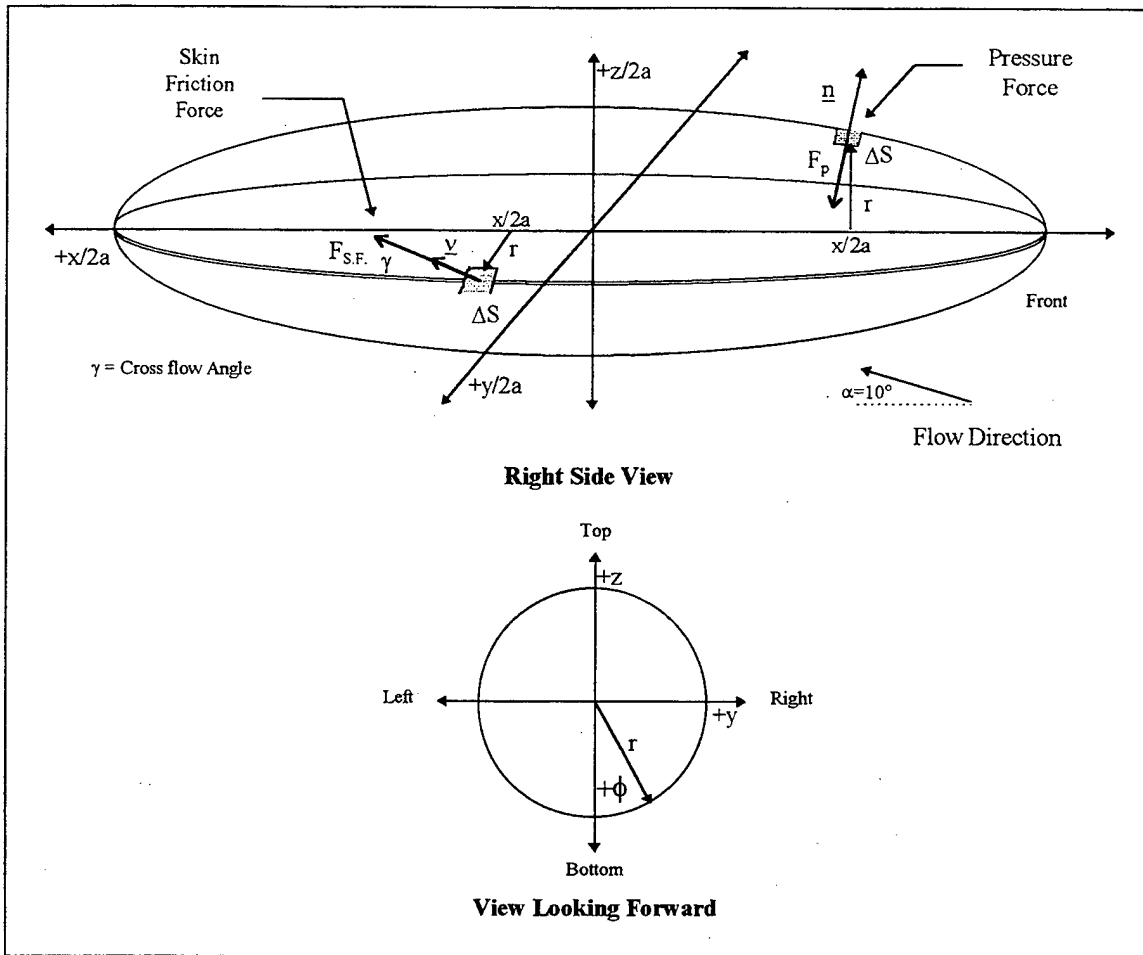


**Figure B.1 Prolate Spheroid Geometry and Forces**

Free stream pressure ( $P_\infty$ ), assumed to be constant, can be dropped from the integration due to symmetry. This leaves the following relation:

$$F_p = \sum_{x/2a=0}^1 \sum_{\phi=0}^{360} q C_p \bar{n} r \Delta \phi \Delta x / 2a \quad \text{B.5}$$

Likewise, skin friction can also be integrated using the following relations:

$$\Delta F_{SF} = q C_f \bar{v} \Delta S = q C_f \bar{v} r \Delta \phi \Delta x / 2a, \quad \text{where } \bar{v} \text{ is a unit velocity vector} \quad \text{B.6}$$

$$F_{SF} = \sum_{x/2a=0}^1 \sum_{\phi=0}^{360} q C_f r \bar{v} \Delta \phi \Delta x / 2a$$

B.7

The pressure force coefficients, normalized by  $S = \pi b^2$  and  $\bar{c} = 2b$ , are yielded by discretely integrating the following equations in a cylindrical coordinate system:

$$C_{N_p} = \frac{N_p}{q_\infty S}, \quad N_p = 2 \sum_{i=1}^m \sum_{j=1}^n - (q_\infty C_p r \bar{n}) \cdot \bar{k} \Delta \phi_j \Delta x_i / 2a$$

B.8

$$C_{A_p} = \frac{A_p}{q_\infty S}, \quad A_p = 2 \sum_{i=1}^m \sum_{j=1}^n - (q_\infty C_p r \bar{n}) \cdot \bar{i} \Delta \phi_j \Delta x_i / 2a$$

B.9

$$C_{M_p} = \frac{M_p}{q_\infty S \bar{c}}, \quad M_p = 2 \sum_{i=1}^m \sum_{j=1}^n [(q_\infty C_p r \bar{n}) \cdot (x_i / 2a \cdot \bar{k} - z_i / 2a \cdot \bar{i})] \Delta \phi_j \Delta x_i / 2a$$

B.10

Where the surface unit normal is given by:

$$\text{Unit Normal: } \bar{n} = -\frac{m}{\sqrt{m^2 + 1}} \bar{i} + \frac{\sin(\phi)}{\sqrt{m^2 + 1}} \bar{j} - \frac{\cos(\phi)}{\sqrt{m^2 + 1}} \bar{k}$$

B.11

The skin friction coefficients, normalized by  $S = \pi b^2$  and  $\bar{c} = 2b$ , are yielded by discretely integrating the following equations in a cylindrical coordinate system:

$$C_{N_{SF}} = \frac{N_{SF}}{q_\infty S}, \quad N_{SF} = 2 \sum_{i=1}^m \sum_{j=1}^n (q_\infty C_f r \bar{v}) \cdot \bar{k} \Delta \phi_j \Delta x_i / 2a$$

B.12

$$C_{A_{SF}} = \frac{A_{SF}}{q_\infty S}, \quad A_{SF} = 2 \sum_{i=1}^m \sum_{j=1}^n (q_\infty C_f r \bar{v}) \cdot \bar{i} \Delta \phi_j \Delta x_i / 2a$$

B.13

$$C_{M_{SF}} = \frac{M_{SF}}{q_\infty S \bar{c}}, \quad M_{SF} = 2 \sum_{i=1}^m \sum_{j=1}^n [(q_\infty C_f r \bar{v}) \cdot (-x_i / 2a \cdot \bar{k} + z_i / 2a \cdot \bar{i})] \Delta \phi_j \Delta x_i / 2a$$

B.14

Where the unit surface velocity vector is given by:

$$\bar{v} = \frac{\cos(\gamma)}{\sqrt{m^2 + 1}} \bar{i} + \left[ \frac{m \sin(\phi) \cos(\gamma)}{\sqrt{m^2 + 1}} + \cos(\phi) \sin(\gamma) \right] \bar{j} + \left[ -\frac{m \cos(\phi) \cos(\gamma)}{\sqrt{m^2 + 1}} + \sin(\phi) \sin(\gamma) \right] \bar{k}$$

B.15

The surface and local slope of a prolate spheroid comes from the following relations:

$$\text{Prolate Spheroid: } \frac{x^2}{a^2} + \frac{r^2}{b^2} = 1 \quad \Rightarrow \quad \text{slope } m = \frac{dr}{dx} = -\frac{bx}{a^2 \sqrt{1 - \frac{x^2}{a^2}}} \quad \text{B.16}$$

Note: The forces are summed over half the spheroid,  $\phi = 0 \rightarrow 180^\circ$ , and doubled.

The y-direction forces and the roll and yaw moments are neglected zero due to symmetry.

## APPENDIX C.

# MATLAB PROGRAMS TO INTEGRATE AERODYNAMIC FORCES OVER THE SURFACE OF A PROLATE SPHEROID

```

Jun 4 1997 02:18                                icp_prolate.m                                Page 1
% This Matlab M-file script performs a first order (linear approximation)
% integration of pressure forces over a 6:1 prolate spheroid. Central Differencing
% of location is used for the first order integration routine. Data is input from
% AGARD AR-303 Test C-2 as rotation angle, x/c, and Cp. Data is for two test
% conditions, AOA = 10 and 29.7 degrees.

clear
% Load in experimental data for AOA = 10 degrees, Re = 7.7x10e6, Vinf = 55 m/s:
% M = 0.162
load cpl0data
fid1=fopen('icp10raw','r+'); %open file for prining step data for error checking
fprintf(fid1,'i      j      l      phi      dphi      x      M      r      dx      Cp
nx      ny      nz      ds      dN      dA      dm      \n');
data = [cpl0data(:,2) cpl0data(:,4) cpl0data(:,5)]; % Extract columns 2,4,5
nphi = 40; nxc = 42; %Initialize # of rotation steps and pressure ports
m = 0; N = 0; A = 0; Si=0; % Initialize summed forces to zero
a = 0.5; b = 0.5/6; % a and b for 6:1 Prolate Spheroid
S = pi*b^2; % Reference area - max cross section
for i = 1:nphi
    for j = 1:nxc
        l = (i-1)*nxc+j;
        phi = data(l,1);
        x = data(l,2)-a;
        Cp = data(l,3);
        r = b*sqrt(1-x^2/a^2);
        M = -b*x/(a^2*sqrt(1-x^2/a^2+.000001));
        z = -r*cos(phi);
        nx = -M/sqrt(M^2+1);
        ny = sin(phi/57.296)/sqrt(M^2+1);
        nz = -cos(phi/57.296)/sqrt(M^2+1);
        nt=sqrt(nx^2+ny^2+nz^2);
        if j == 1
            dx = data(l+1,2)/2; % dx at first pressure port
        elseif j == nxc
            dx = (2*a-data(l-1,2))/2; % dx at last pressure port
        else
            dx = (data(l+1,2)-data(l-1,2))/2; % central differencing at interne
diate pressure ports
        end
        if i == 1
            dphi = data((i*nxc+1),1)/2;
        elseif i == nphi
            dphi = (180-data((i-1)*nxc,1))/2;
        else
            dphi = (data((i*nxc+1),1)-data((i-1)*nxc,1))/2;
        end
        ds = r*dphi/57.296*dx*sqrt(M^2+1);
        dN = 2*(-Cp)*ds*nz;
        dA = 2*(-Cp)*ds*nx;
        dm = 2*(-Cp)*ds*(-x*nz+z*nx);
        N = N+dN;
        A = A+dA;
        m = m+dm;
        raw(l,:)=[i j l phi dphi x M r dx Cp nx ny nz ds dN
dA dm];
        Si=Si+2*dS;
    end
end
CN_AOA10 = N/S
CA_AOA10 = A/S
CM_AOA10 = m/(S*2*b)
Si
fprintf(fid1,'%3.0f %3.0f %5.0f %5.2f %6.4f %4.3f %5.2f %6.3f %6.4f %4.3f
%4.3f %4.3f %4.3f %8.7f %8.7f %8.7f %8.7f\n ',raw');
fprintf(fid1,'i      j      l      phi      dphi      x      M      r      dx      Cp
nx      ny      nz      ds      dN      dA      dm      \n');
fclose('all');

```



```

% This Matlab M-file script performs a first order (linear approximation)
% integration of skin friction over a 6:1 prolate spheroid. Central Differencing
% of location is used for the first order integration routine. Data is input from
% AGARD AR-303 Test C-2 as rotation angle, x/c, Cf and gamma (crossflow angle). Dat
a is for two test
% conditions, AOA = 10
clear
% Load in experimental data for AOA = 10 degrees, Re = 7.7x10e6, Vinf = 55 m/s:
% M = 0.162
load cf10reorder
%fidl=fopen('icf10raw','r+');
%fprintf(fidl,'i      j      l      phi      dphi      x      r      m      dx      Cf
gamma      vx      vy      vz      dS      dN      dA      dm \n');

data = [cf10reorder(:,2) cf10reorder(:,1) cf10reorder(:,3) cf10reorder(:,4)]; % Extr
act columns 2,4,5
nphi = 74; nxc = 12; %Initialize # of rotation steps and pressure ports
Nsf=0; Asf=0; msf=0;
m = 0; N = 0; A = 0; Si=0; % Initialize summed forces to zero
a = 0.5; b = 0.5/6; % a and b for 6:1 Prolate Spheroid
S = pi*b^2; % Reference area - max cross section
for i = 1:nxc
    for j = 1:nphi
        l = (i-1)*nphi+j;
        phi = data(l,1);
        x = data(l,2)-a;
        Cf = data(l,3);
        gamma = data(l,4);
        r = b*sqrt(1-x^2/a^2);
        M = -b*x/(a^2*sqrt(1-x^2/a^2+.000001));
        z = -r*cos(phi);
        vx = cos(gamma/57.3)/sqrt(M^2+1);
        vy = M*sin(phi/57.296)*cos(gamma/57.3)/sqrt(M^2+1)+cos(phi/57.3)*sin(gamma/
57.3);
        vz = -M*cos(phi/57.296)*cos(gamma/57.3)/sqrt(M^2+1)+sin(phi/57.3)*sin(gamma
/57.3);
        nt=sqrt(vx^2+vy^2+vz^2);
        if i == 1
            dx = data(nphi+1,2)/2; % dx at first hot film sensor
        elseif i == nxc
            dx = (2*a-data(((i-1)*nphi),2))/2; % dx at last hot film
sensor
        else
            dx = (data((i*nphi+1),2)-data(((i-1)*nphi),2))/2;
        end
        if j == 1
            dphi = data((l+1),1)/2;
        elseif j == nphi
            dphi = (180-data(l-1,1))/2;
        else
            dphi = (data(l+1,1)-data(l-1,1))/2;
        end
        dS = r*dphi/57.296*dx*sqrt(M^2+1);
        dN = 2*(Cf)*dS*vz;
        dA = 2*(Cf)*dS*vx;
        dm = 2*(Cf)*dS*(-x*vz+z*vx);
        Nsf = Nsf+dN;
        Asf = Asf+dA;
        msf = msf+dm;
        raw(l,:)=[i j l phi dphi x M r dx Cf gamma vx vy vz
        dS dN dA dm];
    end
end
CNsf_AOA10 = Nsf/S
CAsf_AOA10 = Asf/S
CMSf_AOA10 = msf/(S*2*b)
%fprintf(fidl,'%3.0f %3.0f %5.0f %5.2f %6.4f %4.3f %5.2f %6.3f %6.4f %6.5f
%4.1f %4.3f %4.3f %4.3f %8.7f %8.7f %8.7f %8.7f\n ',raw');
%fclose('all');

```

# APPENDIX D. REPRESENTATIVE CMARC/PMARC SPEED TEST FILE

Printed by pollard from hawkkeye

Jun.20.1997 04:39 Page 2  
24p1600.in

```

6V63 X1= -0.1000, V1= 1.5000, Z1= 0.1000, NPT1= 0, &END
6V64 X2= -0.1000, V2= 1.5000, Z2= 0.1000, NPT2= 20, &END
6V65 X3= 1.1000, V3= 1.5000, Z3= -0.1000, NPT3= 25, &END
6V66 XR0= 2.0000, VR0= 2.0000, ZR0= 0.0000, INTVSC= 1, &END
6V67 XR1= 4.0000, VR1= 2.0000, ZR1= 0.0000, &END
6V68 XR2= 2.0000, VR2= 2.0000, ZR2= 1.0000, &END
6V69 R1= 0.1000, RPH1= 0.0, PH12=160.0, &END
6V70 NRAD= 5, NPH1= 12, NLEN= 3, &END
6SLIN1 NSTLIN=0, &END
6SLIN2 SKO= -2.0000, SYO= 1.0000, SZO= -0.5000, &END
SU= 0.0000, SD= 10.0000, DS= 0.2500, INTSL= 1, &END
    
```

Jun.20.1997 04:39 Page 1  
24p1600.in

```

HRC2115 RECTANGULAR WING - 1600 Panels for CHARC/PMARC Time Trials
b720 FT. cbar=1.00 FT, AR = 20 Re = 1,000,000 Vinf = 157.23 FT/S
File purpose: For comparison of CHARC / PHARC processing times.
Created: 5/18 by Steve Pollard
&BHP2 LSTINP=2, LSTOUM=0, LSTFRO=0, LLENRUN=0, LPLITYP=1, &END
&BHP3 LSTWAB=0, LSTWAB=0, LSTWAB=0, &END
&BHP4 LSTWAB=0, LSTWAB=0, LSTWAB=0, &END
&BHP5 HSTWPS=10, DSTSEP=0.5, SOURRES=0.0005, &END
&BHP6 RSPR=0.0, RCPR=0.0, RFF=5.0, RCORES=0.0080, RCOREN=0.0080, &END
&BHP7 VINF=157.23, VSOUND=1116.0, &END
&BHP8 ALDEG=10.00, YANDEG=0.0, PHIDOT=0.0, THEDOT=0.0, PSIDOT=0.0, &END
&BINP8A PHIMAX=0.0, THEMAX=0.0, PSIMAX=0.0, &END
&BINP8B WRM=0.0, WRY=0.0, WRZ=0.0, &END
&BINP8C DTMAX=0.0, DTMX=0.0, WTX=0.0, &END
&BINP8D WTX=0.0, WTY=0.0, WTZ=0.0, &END
&BINP8E SREF=20, SSPAN=10, &END
&BINP8F CGR=1.25, RHPY=0.00, HRCZONE=0, &END
&BINP8G NBCHGE=0, NORSET=0, &END
&BINP8H KCZPCH=0, CZDUB=0.0, VREF=0.0, &END
&BINP8I NORPCH=0, NORF=0, NORL=0, &END
&BINP8J NOCF=0, NOCL=0, VNORM=0.0, &END
&BINP8K KSID=0, NEWSID=0, &END
&BINP8L NBLIT=0, &END
&ASEM1 ASEM1=0.00, ASEM2=0.00, &END
&ASEM2 ASCAL=1.00, ATHET=0.00, &END
&ASEM3 APXX=0.00, APYZ=0.00, &END
&ASEM4 AHXX=0.00, AHYZ=1.00, &END
&COMP1 COMPX=0.0000, COMFY=0.0000, COMFZ=0.0000, &END
&COMP2 CSCAL=1.0000, CSET=0.0000, CODEC=5 &END
&COMP3 CPXX=0.0000, CHY=0.0000, CPZZ=0.0000, &END
&COMP4 CHXX=0.0000, CHY=1.0000, CHZZ=0.0000, &END
&PATCH1 IREV=0, IDPAT=1, MAKE=0, KCOMP=1, KASS=1, IPATSYH=0, &END
IPATCOP=0, &END
&SECT1 WING STX=0.0000, STY=0.0000, STZ=0.0000, SCALE=1.00, &END
WING THETA=0.0, &END
&SECT2 THODE=5, THODES=0, THPS=0, TINTS=3, &END
RTC=0.1500, RMC=0.0200, RPC=0.4000, &END
&SECT3 IPLANE=2, TMFC=40, TINTC=3, &END
STX=0.00, STY=10, STZ=0.0000, SCALE=1.00, &END
&SECT4 ALF=0.0, THETA=0.0, THPS=20, TINTS=3, &END
INMODE=0, THODES=5, &END
&PATCH1 IREV=0, IDPAT=1, MAKE=1, KCOMP=1, KASS=1, IPATSYH=0, &END
IPATCOP=0, &END
&PATCH2 ITYP=2, THODES=5, THPS=4, TINTS=3, &END
&WAKE1 IDWAK=1, IFLW=0, ITRFZ=0, INTRW=0, &END
&WAKE2 KWACH=2, KWACH=4, KWLINE=0, KWPAH=0, &END
&WAKE3 KWPAH=2, KWPAH=0, KWLINE=0, KWPAH=0, &END
&WAKE4 KWACH=1, KWACH=1, KWLINE=0, KWPAH=0, &END
&WAKE5 KWPAH=2, KWPAH=0, KWLINE=0, KWPAH=0, &END
&CONSTRM HOHSL=0, KPSL=1.50, &END
&BLPAPAM RH=1000000, VISC=0.00015723, NSLEL=1.2, &END
&VSI HVOLR=0, HVOLC=0, &END
&VSI X0=-0.1000, Y0=1.5000, Z0=-0.1000, INTVSR=1, &END
&VSI X0=-0.1000, Y0=1.5000, Z0=-0.1000, INTVSR=1, &END
    
```



## APPENDIX E. MATLAB PROGRAM FOR REORDERING AGARD DATA FILE

```
Jun 20 1997 04:42                                reorder.m                                Page 1
% This Matlab M-file transforms AGARD Prolate Spheroid Cp data listed
% in a chordwise direction and converts it into slices for a given x/c location.
% Created by: Steve Pollard

load cwcp10;
load cwcp30;
fid1=fopen('swcp10','r+');
fid2=fopen('swcp30','r+');
fprintf(fid1,'# DPN   PHI I   X0/L   CP   \n');
fprintf(fid2,'# DPN   PHI I   X0/L   CP   \n');
for i=1:42
    for j=1:42
        swcp10((i-1)*42+j,:)=cwcp10((j-1)*42+i,:);
    end
end
for i=1:42
    for j=1:51
        swcp30((i-1)*51+j,:)=cwcp30((j-1)*42+i,:);
    end
end
fprintf(fid1,'%6.0f %7.2f %3.1f %8.5f %8.5f \n',swcp10');
fprintf(fid2,'%6.0f %7.2f %3.1f %8.5f %8.5f \n',swcp30');
fclose('all');
```





```

0.1768 0.0920 0.0495
0.1768 0.0815 0.0628
0.1768 0.0737 0.0739
0.1768 0.0624 0.0837
0.1768 0.0491 0.0922
0.1768 0.0339 0.0988
0.1768 0.0174 0.1030
0.1768 0.0000 0.1045
&BPNODE TNODE=3, TNPC=40, TINTC=3, &END
&SECT1 STV=0.0, STV=0.0, STZ=0.0, SCALE=1.0, ALF=0.0, THETA=0.0, INHODE=4,
TNODES=0, TNPS=0, TINTS=0, &END
0.2292 0.0000 0.1175
0.2292 0.0198 -0.1158
0.2292 0.0385 -0.1110
0.2292 0.0556 -0.1035
0.2292 0.0705 -0.0940
0.2292 0.0831 -0.0831
0.2292 0.0942 -0.0702
0.2292 0.1037 -0.0552
0.2292 0.1111 -0.0382
0.2292 0.1175 -0.0200
0.2292 0.1158 0.0198
0.2292 0.1110 0.0385
0.2292 0.1035 0.0556
0.2292 0.0940 0.0705
0.2292 0.0831 0.0831
0.2292 0.0702 0.0942
0.2292 0.0556 0.1037
0.2292 0.0382 0.1111
0.2292 0.0195 0.1158
0.2292 0.0000 0.1175
&BPNODE TNODE=3, TNPC=40, TINTC=3, &END
&SECT1 STV=0.0, STV=0.0, STZ=0.0, SCALE=1.0, ALF=0.0, THETA=0.0, INHODE=4,
TNODES=0, TNPS=0, TINTS=0, &END
0.2875 0.0000 -0.1298
0.2875 0.0219 0.1280
0.2875 0.0426 0.1227
0.2875 0.0718 0.1184
0.2875 0.0919 0.1017
0.2875 0.1041 0.0776
0.2875 0.1146 0.0611
0.2875 0.1228 0.0422
0.2875 0.1280 0.0216
0.2875 0.1298 0.0000
0.2875 0.1280 0.0219
0.2875 0.1127 0.0426
0.2875 0.1038 0.0780
0.2875 0.0917 0.0919
0.2875 0.0776 0.1041
0.2875 0.0611 0.1146
0.2875 0.0422 0.1228
0.2875 0.0216 0.1280
0.2875 0.0000 0.1298
&BPNODE TNODE=3, TNPC=40, TINTC=3, &END
&SECT1 STV=0.0, STV=0.0, STZ=0.0, SCALE=1.0, ALF=0.0, THETA=0.0, INHODE=4,
TNODES=0, TNPS=0, TINTS=0, &END
0.3515 0.0000 -0.1414
0.3515 0.0239 0.1393
0.3515 0.0464 0.1336
0.3515 0.0669 0.1245
0.3515 0.0850 0.1130
0.3515 0.1001 0.0998
0.3515 0.1217 0.0846
0.3515 0.1337 0.0660
0.3515 0.1394 0.0235
0.3515 0.1414 0.0000
0.3515 0.1393 0.0239
0.3515 0.1336 0.0464
0.3515 0.1245 0.0669
0.3515 0.1130 0.0850
0.3515 0.1001 0.0998
0.3515 0.0846 0.1217
0.3515 0.0660 0.1337
0.3515 0.0235 0.1394
0.3515 0.0000 0.1414

```

```

0.0587 0.0609 -0.0102
0.0587 0.0000 0.0618
0.0587 0.0609 0.0106
0.0587 0.0609 0.0106
0.0587 0.0593 0.0203
0.0587 0.0544 0.0293
0.0587 0.0416 0.0417
0.0587 0.0368 0.0496
0.0587 0.0289 0.0546
0.0587 0.0200 0.0584
0.0587 0.0102 0.0609
0.0587 0.0000 0.0618
&BPNODE TNODE=3, TNPC=40, TINTC=3, &END
&SECT1 STV=0.0, STV=0.0, STZ=0.0, SCALE=1.0, ALF=0.0, THETA=0.0, INHODE=4,
TNODES=0, TNPS=0, TINTS=0, &END
0.0913 0.0000 0.0754
0.0913 0.0130 -0.0754
0.0913 0.0251 -0.0772
0.0913 0.0362 -0.0674
0.0913 0.0459 0.0612
0.0913 0.0541 -0.0541
0.0913 0.0614 -0.0456
0.0913 0.0676 -0.0359
0.0913 0.0724 -0.0248
0.0913 0.0765 0.0000
0.0913 0.0754 0.0130
0.0913 0.0722 0.0251
0.0913 0.0674 0.0362
0.0913 0.0612 0.0459
0.0913 0.0541 0.0541
0.0913 0.0456 0.0614
0.0913 0.0359 0.0676
0.0913 0.0274 0.0724
0.0913 0.0130 0.0754
0.0913 0.0000 0.0765
&BPNODE TNODE=3, TNPC=40, TINTC=3, &END
&SECT1 STV=0.0, STV=0.0, STZ=0.0, SCALE=1.0, ALF=0.0, THETA=0.0, INHODE=4,
TNODES=0, TNPS=0, TINTS=0, &END
0.1308 0.0000 -0.0908
0.1308 0.0154 -0.0894
0.1308 0.0298 -0.0857
0.1308 0.0429 -0.0799
0.1308 0.0546 -0.0746
0.1308 0.0643 -0.0646
0.1308 0.0728 0.0541
0.1308 0.0801 -0.0426
0.1308 0.0858 0.0294
0.1308 0.0895 0.0150
0.1308 0.0908 0.0000
0.1308 0.0894 0.0154
0.1308 0.0799 0.0298
0.1308 0.0726 0.0542
0.1308 0.0641 0.0642
0.1308 0.0541 0.0728
0.1308 0.0426 0.0801
0.1308 0.0294 0.0858
0.1308 0.0150 0.0895
0.1308 0.0000 0.0908
&BPNODE TNODE=3, TNPC=40, TINTC=3, &END
&SECT1 STV=0.0, STV=0.0, STZ=0.0, SCALE=1.0, ALF=0.0, THETA=0.0, INHODE=4,
TNODES=0, TNPS=0, TINTS=0, &END
0.1768 0.0000 -0.1045
0.1768 0.0177 0.1029
0.1768 0.0343 0.0987
0.1768 0.0495 0.0920
0.1768 0.0628 0.0835
0.1768 0.0737 0.0737
0.1768 0.0822 0.0624
0.1768 0.0922 0.0541
0.1768 0.0988 0.0416
0.1768 0.1030 0.0289
0.1768 0.1045 0.0177
0.1768 0.1029 0.0177
0.1768 0.0987 0.0343

```

```

&BPNODE TNODE=3, TNPC=40, TINTC=3, &END
&SECT1 STX=0.0, STY=0.0, STZ=0.0, SCALE=1.0, ALF=0.0, THETA=0.0, INNODE=4,
TNODS=0, TNFS=0, TINTS=0, &END
0.6552 0.0000 -0.1782
0.6552 0.0300 -0.1255
0.6552 0.0600 -0.0728
0.6552 0.0843 -0.1569
0.6552 0.1071 -0.1424
0.6552 0.1261 -0.1258
0.6552 0.1427 -0.1067
0.6552 0.1571 -0.0840
0.6552 0.1685 -0.0580
0.6552 0.1757 -0.0297
0.6552 0.1782 0.0000
0.6552 0.1736 0.0580
0.6552 0.1569 0.0843
0.6552 0.1424 0.1071
0.6552 0.1258 0.1261
0.6552 0.1067 0.1427
0.6552 0.0840 0.1571
0.6552 0.0580 0.1685
0.6552 0.0297 0.1757
0.6552 0.0000 0.1782
&BPNODE TNODE=3, TNPC=40, TINTC=3, &END
&SECT1 STX=0.0, STY=0.0, STZ=0.0, SCALE=1.0, ALF=0.0, THETA=0.0, INNODE=4,
TNODS=0, TNFS=0, TINTS=0, &END
0.7408 0.0000 -0.1848
0.7408 0.0311 -0.1821
0.7408 0.0604 -0.1746
0.7408 0.0873 -0.1628
0.7408 0.1109 -0.1478
0.7408 0.1306 -0.1195
0.7408 0.1530 -0.0870
0.7408 0.1747 -0.0601
0.7408 0.1822 -0.0307
0.7408 0.1848 0.0000
0.7408 0.1821 0.0311
0.7408 0.1746 0.0604
0.7408 0.1628 0.0873
0.7408 0.1478 0.1109
0.7408 0.1306 0.1306
0.7408 0.1109 0.1480
0.7408 0.0870 0.1630
0.7408 0.0601 0.1747
0.7408 0.0307 0.1822
0.7408 0.0000 0.1848
&BPNODE TNODE=3, TNPC=40, TINTC=3, &END
&SECT1 STX=0.0, STY=0.0, STZ=0.0, SCALE=1.0, ALF=0.0, THETA=0.0, INNODE=4,
TNODS=0, TNFS=0, TINTS=0, &END
0.8292 0.0000 -0.1875
0.8292 0.0323 -0.1797
0.8292 0.0623 -0.1675
0.8292 0.0900 -0.1520
0.8292 0.1143 -0.1343
0.8292 0.1346 -0.1139
0.8292 0.1523 -0.1139
0.8292 0.1677 -0.0937
0.8292 0.1778 -0.0717
0.8292 0.1802 0.0000
0.8292 0.1875 0.0320
0.8292 0.1797 0.0623
0.8292 0.1675 0.0900
0.8292 0.1520 0.1143
0.8292 0.1343 0.1346
0.8292 0.1139 0.1523
0.8292 0.0937 0.1677
0.8292 0.0717 0.1778
0.8292 0.0317 0.1875
0.8292 0.0000 0.1902
&BPNODE TNODE=3, TNPC=40, TINTC=3, &END
&SECT1 STX=0.0, STY=0.0, STZ=0.0, SCALE=1.0, ALF=0.0, THETA=0.0, INNODE=4,
TNODS=0, TNFS=0, TINTS=0, &END
0.9199 0.0000 -0.1945

```

```

0.3515 0.0656 0.1247
0.3515 0.0460 0.1137
0.3515 0.0235 0.1194
0.3515 0.0000 0.1414
&BPNODE TNODE=3, TNPC=40, TINTC=3, &END
&SECT1 STX=0.0, STY=0.0, STZ=0.0, SCALE=1.0, ALF=0.0, THETA=0.0, INNODE=4,
TNODS=0, TNFS=0, TINTS=0, &END
0.4207 0.0000 -0.1520
0.4207 0.0257 -0.1492
0.4207 0.0495 -0.1436
0.4207 0.0717 -0.1341
0.4207 0.0914 -0.1215
0.4207 0.1077 -0.1073
0.4207 0.1217 -0.0910
0.4207 0.1341 -0.0717
0.4207 0.1437 -0.0495
0.4207 0.1499 -0.0253
0.4207 0.1520 0.0000
0.4207 0.1432 0.0495
0.4207 0.1339 0.0720
0.4207 0.1215 0.0914
0.4207 0.1073 0.1077
0.4207 0.0910 0.1217
0.4207 0.0717 0.1341
0.4207 0.0495 0.1437
0.4207 0.0253 0.1492
0.4207 0.0000 0.1520
&BPNODE TNODE=3, TNPC=40, TINTC=3, &END
&SECT1 STX=0.0, STY=0.0, STZ=0.0, SCALE=1.0, ALF=0.0, THETA=0.0, INNODE=4,
TNODS=0, TNFS=0, TINTS=0, &END
0.4947 0.0000 -0.1618
0.4947 0.0273 -0.1595
0.4947 0.0530 -0.1528
0.4947 0.0765 -0.1425
0.4947 0.0972 -0.1343
0.4947 0.1192 -0.0958
0.4947 0.1427 -0.0762
0.4947 0.1530 -0.0526
0.4947 0.1595 -0.0269
0.4947 0.1618 0.0000
0.4947 0.1595 0.0273
0.4947 0.1528 0.0530
0.4947 0.1425 0.0765
0.4947 0.1243 0.0972
0.4947 0.1145 0.1192
0.4947 0.0958 0.1296
0.4947 0.0762 0.1427
0.4947 0.0526 0.1530
0.4947 0.0269 0.1595
0.4947 0.0000 0.1618
&BPNODE TNODE=3, TNPC=40, TINTC=3, &END
&SECT1 STX=0.0, STY=0.0, STZ=0.0, SCALE=1.0, ALF=0.0, THETA=0.0, INNODE=4,
TNODS=0, TNFS=0, TINTS=0, &END
0.5730 0.0000 -0.1681
0.5730 0.0287 -0.1661
0.5730 0.0558 -0.1611
0.5730 0.0806 -0.1502
0.5730 0.1023 -0.1364
0.5730 0.1206 -0.1205
0.5730 0.1366 -0.1020
0.5730 0.1504 -0.0824
0.5730 0.1681 -0.0581
0.5730 0.1705 0.0000
0.5730 0.1681 0.0287
0.5730 0.1611 0.0558
0.5730 0.1502 0.0806
0.5730 0.1364 0.1023
0.5730 0.1205 0.1206
0.5730 0.1020 0.1366
0.5730 0.0824 0.1504
0.5730 0.0581 0.1681
0.5730 0.0000 0.1705

```





```

1.7448 0.1569 0.0843
1.7448 0.1424 0.1071
1.7448 0.1258 0.1261
1.7448 0.1067 0.1427
1.7448 0.0840 0.1571
1.7448 0.0580 0.1655
1.7448 0.0297 0.1782
1.7448 0.0000 0.1917
4BPNODE TNODE=3, TNPC=40, TINTC=3, &END
&SECT1 STX=0.0, STY=0.0, STZ=0.0, SCALE=1.0, ALF=0.0, THETA=0.0, INMODE=4,
TNODS=0, TNPS=0, TINTS=0, &END
1.8270 0.0000 0.1705
1.8270 0.0287 -0.1681
1.8270 0.0558 -0.1611
1.8270 0.0806 -0.1502
1.8270 0.1062 -0.1364
1.8270 0.1326 -0.1202
1.8270 0.1594 -0.0802
1.8270 0.1681 -0.0554
1.8270 0.1681 -0.0283
1.8270 0.1705 0.0000
1.8270 0.1681 0.0287
1.8270 0.1511 0.0558
1.8270 0.1324 0.1023
1.8270 0.1205 0.1206
1.8270 0.1020 0.1366
1.8270 0.0802 0.1504
1.8270 0.0554 0.1612
1.8270 0.0283 0.1681
1.8270 0.0000 0.1705
4BPNODE TNODE=3, TNPC=40, TINTC=3, &END
&SECT1 STX=0.0, STY=0.0, STZ=0.0, SCALE=1.0, ALF=0.0, THETA=0.0, INMODE=4,
TNODS=0, TNPS=0, TINTS=0, &END
1.9053 0.0000 0.1618
1.9053 0.0273 -0.1595
1.9053 0.0510 -0.1528
1.9053 0.0765 -0.1425
1.9053 0.0972 -0.1293
1.9053 0.1145 -0.1143
1.9053 0.1296 -0.0968
1.9053 0.1427 -0.0762
1.9053 0.1593 -0.0526
1.9053 0.1618 0.0000
1.9053 0.1595 0.0273
1.9053 0.1528 0.0510
1.9053 0.1425 0.0765
1.9053 0.1293 0.0972
1.9053 0.1143 0.1145
1.9053 0.0968 0.1296
1.9053 0.0762 0.1427
1.9053 0.0526 0.1595
1.9053 0.0000 0.1618
4BPNODE TNODE=3, TNPC=40, TINTC=3, &END
&SECT1 STX=0.0, STY=0.0, STZ=0.0, SCALE=1.0, ALF=0.0, THETA=0.0, INMODE=4,
TNODS=0, TNPS=0, TINTS=0, &END
1.9793 0.0000 0.1520
1.9793 0.0257 -0.1499
1.9793 0.0499 -0.1436
1.9793 0.0720 -0.1332
1.9793 0.0974 -0.1173
1.9793 0.1217 -0.0910
1.9793 0.1341 -0.0717
1.9793 0.1437 -0.0495
1.9793 0.1499 -0.0253
1.9793 0.1520 0.0000
1.9793 0.1499 0.0257
1.9793 0.1436 0.0499
1.9793 0.1332 0.0720
1.9793 0.1212 0.0914
1.9793 0.1073 0.1177
1.9793 0.0910 0.1217

```

```

1.4801 0.1917 -0.0324
1.4801 0.1645 0.0000
1.4801 0.1917 0.0327
1.4801 0.1837 0.0637
1.4801 0.1713 0.0920
1.4801 0.1554 0.1168
1.4801 0.1373 0.1377
1.4801 0.1165 0.1577
1.4801 0.0937 0.1748
1.4801 0.0637 0.1818
1.4801 0.0324 0.1917
1.4801 0.0000 0.1945
4BPNODE TNODE=3, TNPC=40, TINTC=3, &END
&SECT1 STX=0.0, STY=0.0, STZ=0.0, SCALE=1.0, ALF=0.0, THETA=0.0, INMODE=4,
TNODS=0, TNPS=0, TINTS=0, &END
1.5708 0.0000 -0.1902
1.5708 0.0320 -0.1875
1.5708 0.0637 -0.1818
1.5708 0.0963 -0.1475
1.5708 0.1143 -0.1520
1.5708 0.1346 -0.1343
1.5708 0.1523 -0.1139
1.5708 0.1677 -0.0897
1.5708 0.1798 -0.0620
1.5708 0.1875 -0.0317
1.5708 0.1875 0.0000
1.5708 0.1872 0.0320
1.5708 0.1797 0.0623
1.5708 0.1675 0.0900
1.5708 0.1520 0.1143
1.5708 0.1343 0.1346
1.5708 0.1139 0.1523
1.5708 0.0897 0.1677
1.5708 0.0620 0.1798
1.5708 0.0317 0.1872
1.5708 0.0000 0.1902
4BPNODE TNODE=3, TNPC=40, TINTC=3, &END
&SECT1 STX=0.0, STY=0.0, STZ=0.0, SCALE=1.0, ALF=0.0, THETA=0.0, INMODE=4,
TNODS=0, TNPS=0, TINTS=0, &END
1.6592 0.0000 0.1848
1.6592 0.0311 -0.1821
1.6592 0.0604 -0.1746
1.6592 0.0873 -0.1628
1.6592 0.1109 -0.1478
1.6592 0.1306 -0.1306
1.6592 0.1478 -0.1109
1.6592 0.1630 -0.0870
1.6592 0.1747 -0.0601
1.6592 0.1822 0.0307
1.6592 0.1848 0.0000
1.6592 0.1821 0.0311
1.6592 0.1746 0.0604
1.6592 0.1628 0.0873
1.6592 0.1478 0.1109
1.6592 0.1306 0.1306
1.6592 0.1109 0.1478
1.6592 0.0870 0.1630
1.6592 0.0601 0.1747
1.6592 0.0307 0.1822
1.6592 0.0000 0.1848
4BPNODE TNODE=3, TNPC=40, TINTC=3, &END
&SECT1 STX=0.0, STY=0.0, STZ=0.0, SCALE=1.0, ALF=0.0, THETA=0.0, INMODE=4,
TNODS=0, TNPS=0, TINTS=0, &END
1.7448 0.0000 -0.1782
1.7448 0.0280 0.0000
1.7448 0.0843 -0.1593
1.7448 0.1071 -0.1424
1.7448 0.1258 -0.1258
1.7448 0.1424 -0.1071
1.7448 0.1571 -0.0840
1.7448 0.1685 -0.0580
1.7448 0.1757 -0.0297
1.7448 0.1782 0.0000
1.7448 0.1683 0.0584

```

```

4BPNODE TNODE=3, TNPC=40, TINTC=3, &END
4SECT1 STX=0.0, STY=0.0, STZ=0.0, SCALE=1.0, ALF=0.0, THETA=0.0, INMODE=4,
TNODES=0, TNPS=0, TINTS=0, &END
2.2232 0.0000 -0.1045
2.2232 0.0177 -0.1029
2.2232 0.0445 -0.0997
2.2232 0.0719 -0.0915
2.2232 0.1030 -0.0747
2.2232 0.1339 -0.0491
2.2232 0.1643 -0.0239
2.2232 0.1943 -0.0000
2.2232 0.2232 0.0239
2.2232 0.2521 0.0491
2.2232 0.2810 0.0719
2.2232 0.3098 0.0915
2.2232 0.3387 0.1029
2.2232 0.3675 0.1045
4BPNODE TNODE=3, TNPC=40, TINTC=3, &END
4SECT1 STX=0.0, STY=0.0, STZ=0.0, SCALE=1.0, ALF=0.0, THETA=0.0, INMODE=4,
TNODES=0, TNPS=0, TINTS=0, &END
2.2692 0.0000 -0.0894
2.2692 0.0154 -0.0894
2.2692 0.0298 -0.0857
2.2692 0.0449 -0.0799
2.2692 0.0545 -0.0726
2.2692 0.0642 -0.0641
2.2692 0.0741 -0.0541
2.2692 0.0858 -0.0426
2.2692 0.0895 -0.0150
2.2692 0.0908 0.0000
2.2692 0.0894 0.0154
2.2692 0.0857 0.0298
2.2692 0.0799 0.0429
2.2692 0.0726 0.0545
2.2692 0.0641 0.0642
2.2692 0.0541 0.0728
2.2692 0.0429 0.0858
2.2692 0.0298 0.0895
2.2692 0.0150 0.0895
2.2692 0.0000 0.0908
4BPNODE TNODE=3, TNPC=40, TINTC=3, &END
4SECT1 STX=0.0, STY=0.0, STZ=0.0, SCALE=1.0, ALF=0.0, THETA=0.0, INMODE=4,
TNODES=0, TNPS=0, TINTS=0, &END
2.3087 0.0000 0.0000
2.3087 0.0130 0.0000
2.3087 0.0251 -0.0722
2.3087 0.0362 -0.0674
2.3087 0.0459 -0.0612
2.3087 0.0541 -0.0541
2.3087 0.0614 -0.0456
2.3087 0.0676 -0.0359
2.3087 0.0724 -0.0248
2.3087 0.0741 -0.0174
2.3087 0.0765 -0.0127
2.3087 0.0754 0.0130
2.3087 0.0722 0.0231
2.3087 0.0674 0.0362
2.3087 0.0612 0.0459
2.3087 0.0541 0.0541
2.3087 0.0456 0.0614
2.3087 0.0359 0.0676
2.3087 0.0231 0.0724
2.3087 0.0127 0.0741
2.3087 0.0000 0.0765
4BPNODE TNODE=3, TNPC=40, TINTC=3, &END
4SECT1 STX=0.0, STY=0.0, STZ=0.0, SCALE=1.0, ALF=0.0, THETA=0.0, INMODE=4,
TNODES=0, TNPS=0, TINTS=0, &END
2.3413 0.0000 -0.0618

```

```

1.9793 0.0717 0.1341
1.9793 0.0495 0.1437
1.9793 0.0253 0.1499
1.9793 0.0000 0.1520
4BPNODE TNODE=3, TNPC=40, TINTC=3, &END
4SECT1 STX=0.0, STY=0.0, STZ=0.0, SCALE=1.0, ALF=0.0, THETA=0.0, INMODE=4,
TNODES=0, TNPS=0, TINTS=0, &END
2.0485 0.0219 -0.1414
2.0485 0.0464 -0.1376
2.0485 0.0669 -0.1245
2.0485 0.0850 -0.1130
2.0485 0.1001 -0.0998
2.0485 0.1132 -0.0846
2.0485 0.1247 -0.0666
2.0485 0.1337 -0.0460
2.0485 0.1414 -0.0235
2.0485 0.1474 0.0019
2.0485 0.1393 0.0219
2.0485 0.1336 0.0464
2.0485 0.1245 0.0669
2.0485 0.1130 0.0850
2.0485 0.0998 0.1001
2.0485 0.0846 0.1132
2.0485 0.0666 0.1247
2.0485 0.0460 0.1337
2.0485 0.0219 0.1394
2.0485 0.0000 0.1474
4BPNODE TNODE=3, TNPC=40, TINTC=3, &END
4SECT1 STX=0.0, STY=0.0, STZ=0.0, SCALE=1.0, ALF=0.0, THETA=0.0, INMODE=4,
TNODES=0, TNPS=0, TINTS=0, &END
2.1125 0.0000 -0.1298
2.1125 0.0219 -0.1280
2.1125 0.0426 -0.1227
2.1125 0.0618 -0.1144
2.1125 0.0799 -0.0919
2.1125 0.0919 -0.0776
2.1125 0.1041 -0.0776
2.1125 0.1146 -0.0611
2.1125 0.1228 -0.0422
2.1125 0.1280 -0.0216
2.1125 0.1298 0.0000
2.1125 0.1280 0.0219
2.1125 0.1227 0.0426
2.1125 0.1038 0.0611
2.1125 0.0919 0.0776
2.1125 0.0919 0.0919
2.1125 0.0776 0.1041
2.1125 0.0611 0.1146
2.1125 0.0422 0.1228
2.1125 0.0216 0.1280
2.1125 0.0000 0.1298
4BPNODE TNODE=3, TNPC=40, TINTC=3, &END
4SECT1 STX=0.0, STY=0.0, STZ=0.0, SCALE=1.0, ALF=0.0, THETA=0.0, INMODE=4,
TNODES=0, TNPS=0, TINTS=0, &END
2.1708 0.0000 -0.1175
2.1708 0.0198 -0.1158
2.1708 0.0385 -0.1110
2.1708 0.0556 -0.1035
2.1708 0.0705 -0.0940
2.1708 0.0831 -0.0831
2.1708 0.0937 -0.0702
2.1708 0.1032 -0.0582
2.1708 0.1111 -0.0392
2.1708 0.1159 -0.0195
2.1708 0.1175 0.0000
2.1708 0.1158 0.0198
2.1708 0.1110 0.0385
2.1708 0.1035 0.0556
2.1708 0.0940 0.0705
2.1708 0.0831 0.0831
2.1708 0.0652 0.0942
2.1708 0.0382 0.1111
2.1708 0.0195 0.1159
2.1708 0.0000 0.1175

```

```

2.3963 0.0111 -0.0111
2.3963 0.0127 -0.0092
2.3963 0.0139 -0.0072
2.3963 0.0149 -0.0049
2.3963 0.0155 -0.0025
2.3963 0.0157 0.0000
2.3963 0.0154 -0.0029
2.3963 0.0138 0.0073
2.3963 0.0138 0.0073
2.3963 0.0125 0.0095
2.3963 0.0111 0.0111
2.3963 0.0092 0.0127
2.3963 0.0072 0.0139
2.3963 0.0049 0.0149
2.3963 0.0025 0.0155
2.3963 0.0000 0.0157
&BPNODE TNODE=3, TNFC=40, STX=0.0, STZ=0.0, SCALE=1.0, ALF=0.0, THETA=0.0, INHODE=4,
&SECT1 STX=0.0, STY=0.0, STZ=0.0,
&TNODES=5, TNFS=0, TNIS=0, &END
2.4000 0.0000 0.0000
2.4000 0.0000 0.0000
2.4000 0.0000 0.0000
2.4000 0.0000 0.0000
2.4000 0.0000 0.0000
2.4000 0.0000 0.0000
2.4000 0.0000 0.0000
2.4000 0.0000 0.0000
2.4000 0.0000 0.0000
2.4000 0.0000 0.0000
2.4000 0.0000 0.0000
2.4000 0.0000 0.0000
2.4000 0.0000 0.0000
2.4000 0.0000 0.0000
2.4000 0.0000 0.0000
2.4000 0.0000 0.0000
2.4000 0.0000 0.0000
2.4000 0.0000 0.0000
&BPNODE TNODE=3, TNFC=40, TINTC=3, &END
&WAKE1 IDWAKE=1, IFLXW=1, ITRETX=0, INTRW=0, &END
&WAKE2 KWPACH=1, KNSIDE=1, KWLINE=39, KWPANI=25, &END
&WAKE1 IDWAKE=1, IFLXW=3, NODEW=3, INTRW=0, &END
&WAKE2 KWPACH=1, KNSIDE=2, KWLINE=26, INITIAL=0, &END
&WAKE1 IDWAKE=1, IFLXW=3, NODEW=5, KWPANI=21, &END
&WAKE2 KWPACH=1, KNSIDE=2, KWLINE=26, INITIAL=0, &END
&CONSTRM NONSL=1, KPSL=201.209,213.217,221.225,229.233,237.240,361.365,369,
373,377,381,385,389,393,397,400,601,605,609,613,17.621,625,629,634,637,600,761,765,7
69,773,777,781,785,789,793,797,800,1041,1045,1049,1053,1057,1061,1065,1069,1073,1077,
1080,1241,1245,1249,1253,1257,1261,
1265,1269,1273,1277,1280,
&END
&BLPARAM RN=7700000, VISC=0.00001743, NSLEB=1,2,3,4,5,6,7,8,9,10,11,12,13,1
4,15,16,17,18,19,20,21,22,23,24,25,26,27,28,29,30,31,32,33,34,35,36,37,38,39,40,41,42
43,44,45,46,47,48,49,50,51,52,53,54,55,56,57,58,59,60,61,62,63,64,65,
66,
&END
&VS1 NVOLR=0, NVOLA=0,
&VS2 XO=-0.1000, YO=1.5000, ZO=-0.1000, INTVSR=1, &END
&VS3 XI=-0.1000, YI=1.5000, ZI=0.1000, NPTI=0, &END
&VS4 X2=-0.1000, Y2=1.5000, Z2=0.1000, NPT2=20, &END
&VS5 X3=1.1000, Y3=-0.1000, Z3=-0.1000, NPT3=25, &END
&VS6 XRO=2.0000, YRO=2.0000, ZRO=0.0000, INTVSC=1, &END
&VS7 XR1=4.0000, YR1=2.0000, ZR1=0.0000, &END
&VS8 NR1=0.1000, R2=2.0000, PH1=1.0000, &END
&VS9 NRAD=5, NPHI=12, NLEN=3, PH2=360.0, &END

```

```

2.3413 0.0106 -0.0609
2.3413 0.0203 -0.0593
2.3413 0.0291 -0.0544
2.3413 0.0371 -0.0494
2.3413 0.0437 -0.0436
2.3413 0.0496 -0.0368
2.3413 0.0546 -0.0289
2.3413 0.0584 -0.0200
2.3413 0.0618 0.0000
2.3413 0.0609 0.0196
2.3413 0.0593 0.0203
2.3413 0.0544 0.0293
2.3413 0.0494 0.0371
2.3413 0.0436 0.0437
2.3413 0.0368 0.0496
2.3413 0.0289 0.0546
2.3413 0.0200 0.0584
2.3413 0.0102 0.0609
2.3413 0.0000 0.0618
&BPNODE TNODE=3, TNFC=40, TINTC=3, &END
&SECT1 STX=0.0, STY=0.0, STZ=0.0, SCALE=1.0, ALF=0.0, THETA=0.0, INHODE=4,
&TNODES=0, TNFS=0, TNIS=0, &END
2.3668 0.0000 -0.0467
2.3668 0.0081 -0.0460
2.3668 0.0162 -0.0440
2.3668 0.0222 -0.0410
2.3668 0.0282 -0.0372
2.3668 0.0332 -0.0328
2.3668 0.0374 -0.0278
2.3668 0.0412 -0.0219
2.3668 0.0441 -0.0151
2.3668 0.0467 -0.0076
2.3668 0.0485 0.0000
2.3668 0.0460 0.0081
2.3668 0.0440 0.0155
2.3668 0.0410 0.0222
2.3668 0.0372 0.0282
2.3668 0.0328 0.0332
2.3668 0.0278 0.0374
2.3668 0.0219 0.0412
2.3668 0.0151 0.0441
2.3668 0.0076 0.0467
2.3668 0.0000 0.0467
&BPNODE TNODE=3, TNFC=40, TINTC=3, &END
&SECT1 STX=0.0, STY=0.0, STZ=0.0, SCALE=1.0, ALF=0.0, THETA=0.0, INHODE=4,
&TNODES=0, TNFS=0, TNIS=0, &END
2.3852 0.0000 -0.0313
2.3852 0.0055 -0.0308
2.3852 0.0119 -0.0295
2.3852 0.0188 -0.0276
2.3852 0.0221 -0.0221
2.3852 0.0252 -0.0185
2.3852 0.0277 -0.0145
2.3852 0.0296 -0.0100
2.3852 0.0308 -0.0051
2.3852 0.0313 0.0000
2.3852 0.0295 0.0049
2.3852 0.0276 0.0119
2.3852 0.0250 0.0188
2.3852 0.0221 0.0221
2.3852 0.0185 0.0252
2.3852 0.0145 0.0277
2.3852 0.0100 0.0296
2.3852 0.0051 0.0308
2.3852 0.0000 0.0313
&BPNODE TNODE=3, TNFC=40, TINTC=3, &END
&SECT1 STX=0.0, STY=0.0, STZ=0.0, SCALE=1.0, ALF=0.0, THETA=0.0, INHODE=4,
&TNODES=0, TNFS=0, TNIS=0, &END
2.3963 0.0000 -0.0157
2.3963 0.0053 -0.0148
2.3963 0.0075 -0.0138
2.3963 0.0095 -0.0125

```







## APPENDIX H. LOFTSMAN INPUT FILES

Jun 11 1997 05:39	fogfusa.lft	Page 1				
BOX MOLDLINES DATA TEMPLATE						
File name: fogfusa						
Last revision: 4/12/97						
-----						
BOTTOM WATERLINE						
Segments: 3						
Fore end	0,6.5					
Aft end	12,0 53.0,0 53.5,5.75					
Corner	0,0 S 53.5,0					
Curvature	.69 0.95					
-----						
WAIST WATERLINE						
Segments: 1						
Fore end	0,6.5					
Aft end	53.5,6.5					
Corner	S					
Curvature						
-----						
TOP WATERLINE						
Segments: 7						
Fore end	0,6.5					
Aft end	8,9.3 15.2,9.3 21.6,13.0 29.0,14.6 44.6,11.6 53.0,11.5 53.5,6.5					
Corner	0,9.3 S S 24.3,14.6 35.4,14.6 S 53.5,11.5					
Curvature	0.7 0.71 0.81 .95					
-----						
MAXIMUM BUTTLINE DISTANCE FROM PLANE OF SYMMETRY						
Segments: 6						
Fore end	0,0					
Aft end	1,3 1,3 22,4.5 43.6,4.5 53.1,1.3 53.5,0					
Corner	0,2.9 S S S S 53.5,1.3					
Curvature	.9 0.8 0.95					
-----						
BOTTOM K FACTOR						
Segments: 3						
Fore end	0,0.93					
Aft end	12.0,0.98 43.6,0.98 53.5,0.95					
Corner	S S S					
Curvature						
-----						
TOP K FACTOR						
Segments: 4						
Fore end	0,0.90					
Aft end	15.20,0.95 24,1.0 44.65,1.0 53.5,0.95					
Corner	S S S S					
Curvature						
-----						
BUTTLINE AT PLANE OF SYMMETRY						
Segments: 0						



NPS FROG UAV Main Wing - Loftsman Input File

Date: 5/29/97

Breaks: 5

Break 1

Axis: 24.65,0,13.1  
Axis/chord: 0  
Chord: 20.0  
Incidence: 4.5  
Cant: 0  
Section file: N2415  
T/C ratio: 0.1500  
Spars: 0  
Panel rib angles: 0,999.0000,0.0000

Break 2

Axis: 24.65,6,13.1  
Axis/chord: 0  
Chord: 20.0  
Incidence: 4.5  
Cant: 0  
Section file: N2415  
T/C ratio: 0.1500  
Spars: 0  
Panel rib angles: 0,999.0000,0.0000

Break 3

Axis: 24.65,31.5,13.1  
Axis/chord: 0  
Chord: 20.0  
Incidence: 4.5  
Cant: 0  
Section file: N2415  
T/C ratio: 0.1500  
Spars: 0  
Panel rib angles: 0,999.0000,0.0000

Break 4

Axis: 24.65,53.0,13.1  
Axis/chord: 0  
Chord: 20.0  
Incidence: 4.5  
Cant: 0  
Section file: N2415  
T/C ratio: 0.1500  
Spars: 0  
Panel rib angles: 0,999.0000,0.0000

Break 5

Axis: 24.65,61.0,13.1  
Axis/chord: 0  
Chord: 18.5  
Incidence: 4.5  
Cant: 0  
Section file: N2415  
T/C ratio: 0.1500  
Spars: 0

FROG UAV ENGINE NACELLE

File name: fogenpod  
 Last revision: 4/13/97

-----  
 BOTTOM WATERLINE

Segments: 4

Fore end	16.5,20.4			
Aft end	18.2,18.6	21.0,16.8	31.0,15.75	43.0, 16.8
Corner	16.6,19.6	19.15,17.35	23.8,15.9	35.6,15.65
Curvature	0.79	0.83	0.72	0.73

-----  
 WAIST WATERLINE

Segments: 1

Fore end	16.5,20.4
Aft end	43.0,16.8
Corner	S
Curvature	

-----  
 TOP WATERLINE

Segments: 4

Fore end	16.3,20.4			
Aft end	18.45,22.1	27.0,21.75	35.0,19.8	43.0,16.8
Corner	16.75,21.3	21.4,22.5	30.4,21.3	38.3,18.75
Curvature	0.79	0.80	0.70	0.75

-----  
 MAXIMUM BUTTLINE DISTANCE FROM PLANE OF SYMMETRY

Segments: 4

Fore end	16.5,0			
Aft end	18.2,1.6	23.0,2.3	40.8,2.3	43.0,0
Corner	16.5,0.70	20.1,2.25	S	43.0,2.3
Curvature	0.72	0.75		0.90

-----  
 BOTTOM K FACTOR

Segments: 4

Fore end	16.5,0.707			
Aft end	18.2,0.707	24.0,0.93	42.0,0.93	43.0,0.75
Corner	S	20,0.93	S	S
Curvature		0.9		

-----  
 TOP K FACTOR

Segments: 4

Fore end	16.5,0.707			
Aft end	18.45,0.707	24.5,0.93	42.0,0.93	43.0,0.75
Corner	S	20.3,0.93	S	S
Curvature		0.9		

-----  
 BUTTLINE AT PLANE OF SYMMETRY

Segments: 0

PROG UAV ENGINE PYLON (Lofted as A-Body Type)

-Basic pylon model modified so as not to have a top and bottom  
-Single strip which is the side of the pylon.

File name: FOGPYLO1  
Last revision: 4/23/97

Strips: 1  
Sym: Y

M1B

Segments: 1  
Fore end 25.8,0  
Aft end 37.7,0  
Corner 25.8,3.8  
K factor 0.71

M1W

Segments: 1  
Fore end 25.8,14.31  
Aft end 37.7,13.65  
Corner 31.0,15.45  
K factor 0.72

C1B

Segments: S

C1W

Segments: S

K1

Segments: S

M2B

Segments: =M1B

M2W

Segments: 1

Fore end 25.8,16.01  
Aft end 37.7,16.1  
Corner 33.65,15.35  
K factor 0.65

FROG UAV Tail Boom

File name: frogboom  
Last revision: 4/28/97

4/28: added rounded start and finish to close ends

-----  
BOTTOM WATERLINE

Segments: 3

Fore end	53.5,9.375		88.5,9.375
Aft end	54,8.5	88,8.5	
Corner	53.5,8.5	S	88.5,8.5
Curvature	0.707		0.707

-----  
WAIST WATERLINE

Segments: 1

Fore end	53.5,9.375
Aft end	88.5, 9.375
Corner	S
Curvature	

-----  
TOP WATERLINE

Segments: 3

Fore end	53.5,9.375		88.5,9.375
Aft end	54.0,10.25	88,10.25	
Corner	53.5,10.25	S	88.5,10.25
Curvature	0.707		0.707

-----  
MAXIMUM BUTTLINE DISTANCE FROM PLANE OF SYMMETRY

Segments: 3

Fore end	53.5,0		88.5,0
Aft end	54,0.875	88,0.875	
Corner	53.5,0.875	S	88.5,0.875
Curvature	0.707		0.707

-----  
BOTTOM K FACTOR

Segments: 1

Fore end	53.5,0.707
Aft end	88.5, 0.707
Corner	S
Curvature	

-----  
TOP K FACTOR

Segments: 1

Fore end	53.5,0.707
Aft end	88.5, 0.707
Corner	S
Curvature	

-----  
BUTTLINE AT PLANE OF SYMMETRY

Segments: 0

FROG Horizontal Tail

Date: 4/14/97

Breaks: 2

Break 1

Axis: 82.5,0,8.09

Axis/chord: 0

Chord: 13.5

Incidence: 0

Cant: 0

Section file: N0006

T/C ratio: 0.06

Spars: 0

Panel rib angles: 0,999.0000,0.0000

Break 2

Axis: 86.5,19.875,8.09

Axis/chord: 0

Chord: 9.55

Incidence: 0

Cant: 0

Section file: N0006

T/C ratio: 0.06

Spars: 0

Panel rib angles: 0,999.0000,0.0000

FROG UAV Vertical Tail - LOFTSMAN input file

Date: 4/14/97

Breaks: 2

Break 1

Axis: 77.5,0,10.4  
Axis/chord: 0  
Chord: 20  
Incidence: 0  
Cant: 90  
Section file: N0006  
T/C ratio: 0.06  
Spars: 0  
Panel rib angles: 90,0,999

Break 2

Axis: 92.35,0,25.15  
Axis/chord: 0  
Chord: 10  
Incidence: 0  
Cant: 90  
Section file: N0006  
T/C ratio: 0.06  
Spars: 0  
Panel rib angles: 90,0,999







```

19.5106 4.3222 6.8961
19.5106 4.3117 8.5205
19.5106 4.3169 10.2448
19.5106 4.2840 11.4245
19.5106 4.1133 11.7224
19.5106 3.3665 11.7816
19.5106 1.7041 11.7911
19.5106 0.0000 11.7920
&BPNODE THODE=3, TNPC=0, TINTC=0, &END
&SECT1 STX=0.0, STY=0.0, STZ=0.0, SCALE=1.0, ALF=0.0, THETA=0.0, INHODE=4,
TNODES=0, TNPS=0, TINTS=0, &END
20.0000 0.0000 0.0000
20.0000 1.7202 0.0007
20.0000 3.4256 0.0081
20.0000 4.1917 0.0673
20.0000 4.3314 0.4135
20.0000 4.3535 1.7754
20.0000 4.3564 3.4956
20.0000 4.3571 5.2158
20.0000 4.3571 6.9360
20.0000 4.3562 8.6562
20.0000 4.3532 10.3763
20.0000 4.3272 11.6828
20.0000 4.1713 12.0088
20.0000 3.4117 12.0661
20.0000 1.7202 12.0742
20.0000 0.0000 12.0750
&BPNODE THODE=3, TNPC=0, TINTC=0, &END
&PATCH IRREV=0, IDANT=2, MAKE=0, KCOMP=1, KASS=1, IPATSYH=1, IPATCOP=0, &END
ROOT TRANSITION FOR STARBARD
&SECT1 STX=0.0, STY=0.0, STZ=0.0, SCALE=1.0, ALF=0.0, THETA=0.0, INHODE=4,
TNODES=0, TNPS=0, TINTS=0, &END
20.0000 0.0000 0.0000
20.0000 1.7202 0.0007
20.0000 3.4256 0.0081
20.0000 4.1917 0.0673
20.0000 4.3314 0.4135
20.0000 4.3535 1.7754
20.0000 4.3564 3.4956
20.0000 4.3571 5.2158
20.0000 4.3571 6.9360
20.0000 4.3562 8.6562
20.0000 4.3532 10.3763
20.0000 4.3272 11.6828
20.0000 4.1713 12.0088
20.0000 3.4117 12.0661
20.0000 1.7202 12.0742
20.0000 0.0000 12.0750
&BPNODE THODE=3, TNPC=0, TINTC=0, &END
&SECT1 STX=0.0, STY=0.0, STZ=0.0, SCALE=1.0, ALF=0.0, THETA=0.0, INHODE=4,
TNODES=0, TNPS=0, TINTS=0, &END
20.4440 0.0000 0.0000
20.4440 1.7171 0.0007
20.4440 3.4241 0.0078
20.4440 4.2151 0.0644
20.4440 4.3616 0.3949
20.4440 4.3891 1.7454
20.4440 4.3888 3.4888
20.4440 4.3889 5.1566
20.4440 4.3889 6.8736
20.4440 4.3865 8.5907
20.4440 4.3865 10.3078
20.4440 4.3707 11.8182
20.4440 4.2485 12.2579
20.4440 3.5302 12.3322
20.4440 1.7606 12.3310
20.4440 0.0000 12.3310
&BPNODE THODE=3, TNPC=0, TINTC=0, &END
&SECT1 STX=0.0, STY=0.0, STZ=0.0, SCALE=1.0, ALF=0.0, THETA=0.0, INHODE=4,
TNODES=0, TNPS=0, TINTS=0, &END
21.6065 0.0000 0.0000
21.6065 1.7392 0.0007
21.6065 3.4719 0.0076
21.6065 4.2930 0.0637
21.6065 4.4441 0.3949

```

```

10.0000 3.6428 5.8276
10.0000 3.6400 7.3413
10.0000 3.6087 8.4519
10.0000 3.5110 8.9679
10.0000 3.2695 9.1801
10.0000 2.7005 9.2654
10.0000 0.0000 9.2654
&BPNODE THODE=3, TNPC=0, TINTC=0, &END
&SECT1 STX=0.0, STY=0.0, STZ=0.0, SCALE=1.0, ALF=0.0, THETA=0.0, INHODE=4,
TNODES=0, TNPS=0, TINTS=0, &END
13.0902 0.0000 0.0000
13.0902 1.5138 0.0007
13.0902 3.0061 0.0077
13.0902 3.8969 0.0552
13.0902 4.1012 0.3612
13.0902 3.8631 1.3012
13.0902 3.8623 2.8174
13.0902 3.8633 4.3312
13.0902 3.8636 5.8451
13.0902 3.8614 7.3589
13.0902 3.8144 8.5203
13.0902 3.7416 9.0232
13.0902 3.4903 9.2092
13.0902 2.8478 9.2766
13.0902 1.5138 9.2766
13.0902 0.0000 9.2766
&BPNODE THODE=3, TNPC=0, TINTC=0, &END
&SECT1 STX=0.0, STY=0.0, STZ=0.0, SCALE=1.0, ALF=0.0, THETA=0.0, INHODE=4,
TNODES=0, TNPS=0, TINTS=0, &END
15.8779 0.0000 0.0000
15.8779 1.5558 0.0007
15.8779 3.0451 0.0070
15.8779 3.8451 0.0280
15.8779 4.0270 0.2980
15.8779 4.0569 1.2775
15.8779 4.0614 2.8332
15.8779 4.0624 4.3890
15.8779 4.0627 5.9448
15.8779 4.0612 7.5006
15.8779 4.0415 8.8474
15.8779 3.9429 9.4248
15.8779 3.0056 9.6746
15.8779 1.5544 9.6699
15.8779 0.0000 9.6919
&BPNODE THODE=3, TNPC=0, TINTC=0, &END
&SECT1 STX=0.0, STY=0.0, STZ=0.0, SCALE=1.0, ALF=0.0, THETA=0.0, INHODE=4,
TNODES=0, TNPS=0, TINTS=0, &END
18.0902 0.0000 0.0000
18.0902 1.5308 0.0007
18.0902 3.0453 0.0117
18.0902 4.0453 0.0561
18.0902 4.1913 0.3561
18.0902 4.2164 1.5673
18.0902 4.2198 3.2182
18.0902 4.2207 4.8691
18.0902 4.2185 6.5200
18.0902 4.2195 8.1710
18.0902 4.2094 9.8015
18.0902 4.1567 10.6520
18.0902 3.9490 10.8950
18.0902 1.5504 10.9687
18.0902 0.0000 10.9687
&BPNODE THODE=3, TNPC=0, TINTC=0, &END
&SECT1 STX=0.0, STY=0.0, STZ=0.0, SCALE=1.0, ALF=0.0, THETA=0.0, INHODE=4,
TNODES=0, TNPS=0, TINTS=0, &END
19.5106 0.0000 0.0000
19.5106 1.7043 0.0007
19.5106 3.3938 0.0081
19.5106 4.1533 0.0661
19.5106 4.2955 0.3979
19.5106 4.3284 1.7422
19.5106 4.3221 3.4732
19.5106 4.3221 5.1318

```

```

24.6500 3.6231 0.0094
24.6500 4.3600 0.0829
24.6500 4.4804 0.5384
24.6500 4.4973 2.1449
24.6500 4.4995 3.9708
24.6500 4.5000 5.7966
24.6500 4.5000 6.6225
24.6500 4.5000 7.4584
24.6500 4.5000 11.2742
24.6500 4.5000 13.1000
&BPNODE TNODE=3, TNPC=0, TINTC=0, &END
&SECT1 STX=0.0, STY=0.0, STZ=0.0, SCALE=1.0, ALF=0.0, THETA=0.0, INMODE=4,
TNODES=0, TNPS=0, TINTS=0, &END
24.8679 0.0000 0.0000
24.8679 1.7867 0.0007
24.8679 3.2342 0.0078
24.8679 4.4756 0.0777
24.8679 4.4766 0.4634
24.8679 4.4968 1.9451
24.8679 4.4994 3.7357
24.8679 4.4999 5.5224
24.8679 4.5000 7.3091
24.8679 4.5000 9.0958
24.8679 4.5000 10.8824
24.8679 4.5000 12.6690
&BPNODE TNODE=3, TNPC=0, TINTC=0, &END
&SECT1 STX=0.0, STY=0.0, STZ=0.0, SCALE=1.0, ALF=0.0, THETA=0.0, INMODE=4,
TNODES=0, TNPS=0, TINTS=0, &END
25.5119 0.0000 0.0000
25.5119 1.7519 0.0007
25.5119 3.4973 0.0076
25.5119 4.3223 0.0646
25.5119 4.4862 1.7750
25.5119 4.4992 3.5269
25.5119 4.4999 5.2788
25.5119 4.5000 7.0306
25.5119 4.5000 8.7825
25.5119 4.5000 10.5344
25.5119 4.5000 12.2862
&BPNODE TNODE=3, TNPC=0, TINTC=0, &END
&SECT1 STX=0.0, STY=0.0, STZ=0.0, SCALE=1.0, ALF=0.0, THETA=0.0, INMODE=4,
TNODES=0, TNPS=0, TINTS=0, &END
26.5541 0.0000 0.0000
26.5541 1.7230 0.0070
26.5541 3.4441 0.0070
26.5541 4.3050 0.0585
26.5541 4.4691 0.3614
26.5541 4.4956 1.6308
26.5541 4.4991 3.3729
26.5541 4.5000 5.1149
26.5541 4.5000 6.8569
26.5541 4.5000 8.5989
26.5541 4.5000 10.3409
26.5541 4.5000 11.9690
&BPNODE TNODE=3, TNPC=0, TINTC=0, &END
&SECT1 STX=0.0, STY=0.0, STZ=0.0, SCALE=1.0, ALF=0.0, THETA=0.0, INMODE=4,
TNODES=0, TNPS=0, TINTS=0, &END
27.9487 0.0000 0.0000
27.9487 1.6721 0.0026
27.9487 3.4021 0.0026
27.9487 4.2909 0.0542
27.9487 4.4660 0.3114
27.9487 4.4951 1.5215
27.9487 4.4990 3.2226
27.9487 4.4998 4.9237
27.9487 4.5000 6.6249
27.9487 4.5000 8.3260
27.9487 4.5000 10.0272
27.9487 4.5000 11.7283
&BPNODE TNODE=3, TNPC=0, TINTC=0, &END
&SECT1 STX=0.0, STY=0.0, STZ=0.0, SCALE=1.0, ALF=0.0, THETA=0.0, INMODE=4,
TNODES=0, TNPS=0, TINTS=0, &END
29.6349 0.0000 0.0000
29.6349 1.6863 0.0006
29.6349 3.3725 0.0063

```

```

21.6065 4.4680 1.7396
21.6065 4.4711 3.4788
21.6065 4.4718 5.2180
21.6065 4.4719 6.9572
21.6065 4.4717 8.6964
21.6065 4.4711 10.4355
21.6065 4.4667 12.1744
21.6065 3.6877 12.9989
21.6065 1.8477 13.0035
21.6065 0.0000 13.0039
&BPNODE TNODE=3, TNPC=0, TINTC=0, &END
&SECT1 STX=0.0, STY=0.0, STZ=0.0, SCALE=1.0, ALF=0.0, THETA=0.0, INMODE=4,
TNODES=0, TNPS=0, TINTS=0, &END
23.0435 0.0000 0.0000
23.0435 1.5433 0.0081
23.0435 3.0843 0.0718
23.0435 4.1384 0.0718
23.0435 4.4761 0.4540
23.0435 4.4971 1.9224
23.0435 4.4994 3.7037
23.0435 4.4999 5.4850
23.0435 4.5000 7.2664
23.0435 4.5000 9.0478
23.0435 4.5000 10.8290
23.0435 4.4993 12.6104
23.0435 4.4647 13.6074
23.0435 3.4428 13.6337
23.0435 1.7214 13.6342
23.0435 0.0000 13.6343
&BPNODE TNODE=3, TNPC=0, TINTC=0, &END
&SECT1 STX=0.0, STY=0.0, STZ=0.0, SCALE=1.0, ALF=0.0, THETA=0.0, INMODE=4,
TNODES=0, TNPS=0, TINTS=0, &END
24.2060 0.0000 0.0000
24.2060 1.8135 0.0008
24.2060 3.6312 0.0090
24.2060 4.3543 0.0795
24.2060 4.4793 0.5138
24.2060 4.4972 2.0834
24.2060 4.4995 3.6530
24.2060 4.5000 5.2226
24.2060 4.5000 6.7922
24.2060 4.5000 8.3618
24.2060 4.5000 9.9314
24.2060 4.5000 11.5011
24.2060 4.5000 12.9647
24.2060 4.2423 13.9775
24.2060 2.8282 13.9775
24.2060 1.4141 13.9775
24.2060 0.0000 13.9775
&BPNODE TNODE=3, TNPC=0, TINTC=0, &END
&SECT1 STX=0.0, STY=0.0, STZ=0.0, SCALE=1.0, ALF=0.0, THETA=0.0, INMODE=4,
TNODES=0, TNPS=0, TINTS=0, &END
24.6500 0.0000 0.0000
24.6500 1.8258 0.0008
24.6500 3.6231 0.0094
24.6500 4.3600 0.0829
24.6500 4.4804 0.5384
24.6500 4.4973 2.1449
24.6500 4.4995 3.9708
24.6500 4.5000 5.7966
24.6500 4.5000 7.6225
24.6500 4.5000 9.4483
24.6500 4.5000 11.2742
24.6500 4.5000 13.1000
24.6500 4.2213 14.0848
24.6500 2.8142 14.0848
24.6500 1.4071 14.0848
24.6500 0.0000 14.0848
&BPNODE TNODE=3, TNPC=0, TINTC=0, &END
&PATCH *REV=0, IPATCH=2, MAKE=1, KCOMP=1, IPATSY=1, IPATCHOP=0, &END
*JWER STABOARD
&SECT1 STX=0.0, STY=0.0, STZ=0.0, SCALE=1.0, ALF=0.0, THETA=0.0, INMODE=4,
TNODES=0, TNPS=0, TINTS=0, &END
24.6500 0.0000 0.0000
24.6500 1.8258 0.0008

```

```

39.6047 4.4614 0.2944
39.6047 4.4943 1.3737
39.6047 4.4988 3.0452
39.6047 4.4998 4.7168
39.6047 4.5000 6.3884
39.6047 4.5000 8.0600
39.6047 4.5000 9.7316
39.6047 4.5000 11.4032
&BPNODE TNODE=3, TNPC=0, TINTC=0, &END
&SECT1 STX=0.0, STY=0.0, STZ=0.0, THETA=0.0, INNODE=4,
TNODE=0, TNPS=0, TINTS=0, &END
41.2909 0.0000 0.0000
41.2909 3.3479 0.0061
41.2909 4.2720 0.0974
41.2909 4.4943 1.3854
41.2909 4.4988 3.0593
41.2909 4.4998 4.7332
41.2909 4.5000 6.4072
41.2909 4.5000 8.0811
41.2909 4.5000 9.7550
41.2909 4.5000 11.4290
&BPNODE TNODE=3, TNPC=0, TINTC=0, &END
&SECT1 STX=0.0, STY=0.0, STZ=0.0, THETA=0.0, INNODE=4,
TNODE=0, TNPS=0, TINTS=0, &END
42.6855 0.0000 0.0000
42.6855 1.6764 0.0006
42.6855 3.3529 0.0061
42.6855 4.2738 0.0498
42.6855 4.4622 0.3001
42.6855 4.4944 1.3979
42.6855 4.4989 3.0878
42.6855 4.4999 4.7577
42.6855 4.5000 6.4272
42.6855 4.5000 8.1036
42.6855 4.5000 9.7800
42.6855 4.5000 11.4565
&BPNODE TNODE=3, TNPC=0, TINTC=0, &END
&SECT1 STX=0.0, STY=0.0, STZ=0.0, THETA=0.0, INNODE=4,
TNODE=0, TNPS=0, TINTS=0, &END
43.7277 0.0000 0.0000
43.7277 1.3526 0.0057
43.7277 3.3526 0.0057
43.7277 4.2374 0.0530
43.7277 4.4194 0.3059
43.7277 4.4514 1.4174
43.7277 4.4558 3.0940
43.7277 4.4568 4.7706
43.7277 4.4570 6.4472
43.7277 4.4570 8.1238
43.7277 4.4570 9.8004
43.7277 4.4570 11.4770
&BPNODE TNODE=3, TNPC=0, TINTC=0, &END
&SECT1 STX=0.0, STY=0.0, STZ=0.0, THETA=0.0, INNODE=4,
TNODE=0, TNPS=0, TINTS=0, &END
44.3717 0.0000 0.0000
44.3717 1.6650 0.0009
44.3717 3.3021 0.0097
44.3717 4.0431 0.0680
44.3717 4.2033 0.3596
44.3717 4.2381 1.3680
44.3717 4.2398 3.0431
44.3717 4.2400 4.7181
44.3717 4.2400 6.3931
44.3717 4.2400 8.0681
44.3717 4.2400 9.7432
44.3717 4.2400 11.4182
&BPNODE TNODE=3, TNPC=0, TINTC=0, &END
&SECT1 STX=0.0, STY=0.0, STZ=0.0, THETA=0.0, INNODE=4,
TNODE=0, TNPS=0, TINTS=0, &END
44.5909 0.0000 0.0000
44.5909 1.6677 0.0010
44.5909 3.2959 0.0111
44.5909 3.9797 0.0752
44.5909 4.1306 0.3843

```

```

29.6349 4.2808 0.0515
29.6349 4.4638 0.3122
29.6349 4.4947 1.4471
29.6349 4.4989 3.1333
29.6349 4.5000 4.8195
29.6349 4.5000 6.5056
29.6349 4.5000 8.1922
29.6349 4.5000 9.8784
29.6349 4.5000 11.5647
&BPNODE TNODE=3, TNPC=0, TINTC=0, &END
&SECT1 STX=0.0, STY=0.0, STZ=0.0, THETA=0.0, INNODE=4,
TNODE=0, TNPS=0, TINTS=0, &END
31.5390 0.0000 0.0000
31.5390 3.3538 0.0063
31.5390 4.2741 0.0495
31.5390 4.4623 0.3007
31.5390 4.4944 1.4001
31.5390 4.4989 3.0770
31.5390 4.4998 4.7539
31.5390 4.5000 6.4308
31.5390 4.5000 8.1077
31.5390 4.5000 9.7845
31.5390 4.5000 11.4610
&BPNODE TNODE=3, TNPC=0, TINTC=0, &END
&SECT1 STX=0.0, STY=0.0, STZ=0.0, THETA=0.0, INNODE=4,
TNODE=0, TNPS=0, TINTS=0, &END
33.5777 0.0000 0.0000
33.5777 1.6712 0.0006
33.5777 3.3424 0.0060
33.5777 4.2670 0.0489
33.5777 4.4510 0.3001
33.5777 4.4943 1.3718
33.5777 4.4988 3.0430
33.5777 4.4998 4.7142
33.5777 4.5000 6.3855
33.5777 4.5000 8.0567
33.5777 4.5000 9.7279
33.5777 4.5000 11.3991
&BPNODE TNODE=3, TNPC=0, TINTC=0, &END
&SECT1 STX=0.0, STY=0.0, STZ=0.0, THETA=0.0, INNODE=4,
TNODE=0, TNPS=0, TINTS=0, &END
35.6619 0.0000 0.0000
35.6619 1.6694 0.0006
35.6619 3.3388 0.0060
35.6619 4.2687 0.0486
35.6619 4.4610 0.2918
35.6619 4.4942 1.3627
35.6619 4.4988 3.0321
35.6619 4.4998 4.7015
35.6619 4.5000 6.3402
35.6619 4.5000 8.0096
35.6619 4.5000 9.6796
35.6619 4.5000 11.3490
&BPNODE TNODE=3, TNPC=0, TINTC=0, &END
&SECT1 STX=0.0, STY=0.0, STZ=0.0, THETA=0.0, INNODE=4,
TNODE=0, TNPS=0, TINTS=0, &END
37.7006 0.0000 0.0000
37.7006 1.6701 0.0006
37.7006 3.2892 0.0097
37.7006 4.0497 0.0680
37.7006 4.2101 0.3596
37.7006 4.2442 1.3663
37.7006 4.2488 3.0365
37.7006 4.2498 4.7066
37.7006 4.2500 6.3767
37.7006 4.2500 8.0468
37.7006 4.2500 9.7170
37.7006 4.2500 11.3871
&BPNODE TNODE=3, TNPC=0, TINTC=0, &END
&SECT1 STX=0.0, STY=0.0, STZ=0.0, THETA=0.0, INNODE=4,
TNODE=0, TNPS=0, TINTS=0, &END
39.6047 0.0000 0.0000
39.6047 1.6716 0.0006
39.6047 3.3432 0.0060
39.6047 4.2703 0.0490

```



```

47.6745 3.1275 6.1873
47.6745 3.1275 7.7096
47.6745 3.1269 9.2319
47.6745 3.1232 10.7579
47.6745 3.1213 11.5525
47.6745 3.1213 11.5525
47.6745 1.4071 11.5627
47.6745 0.0000 11.5634
&BPNODE TNODE=3, TNPC=0, TINTC=0, &END
&SECT1 STX=0.0, STY=0.0, STZ=0.0, SCALE=1.0, ALF=0.0, THETA=0.0, INMODE=4,
TNODE=3, TNPS=0, TINTS=0, &END
48.0000 0.0000 0.0000
48.0000 1.5058 0.0041
48.0000 2.5263 0.1533
48.0000 2.9802 0.5421
48.0000 3.0094 1.6335
48.0000 3.0158 3.1393
48.0000 3.0175 4.6450
48.0000 3.0178 6.1508
48.0000 3.0172 7.6566
48.0000 3.0134 9.1624
48.0000 2.9761 11.4292
48.0000 2.7054 11.5444
48.0000 0.0000 11.5586
&BPNODE TNODE=3, TNPC=0, TINTC=0, &END
&PATCH IREV=0, IDPAT=2, MAKE=0, KCOMP=1, KASS=1, IPATSYH=1, IPATCOP=0,
&END
FUSELAGE.AFT
&SECT1 STX=0.0, STY=0.0, STZ=0.0, SCALE=1.0, ALF=0.0, THETA=0.0, INMODE=4,
TNODE=0, TNPS=0, TINTS=0, &END
48.0000 1.5058 0.0041
48.0000 2.5263 0.1533
48.0000 2.9802 0.5421
48.0000 3.0094 1.6335
48.0000 3.0158 3.1393
48.0000 3.0175 4.6450
48.0000 3.0178 6.1508
48.0000 3.0172 7.6566
48.0000 3.0134 9.1624
48.0000 2.9761 11.4292
48.0000 2.7054 11.5444
48.0000 1.5058 11.5586
&BPNODE TNODE=3, TNPC=0, TINTC=0, &END
&SECT1 STX=0.0, STY=0.0, STZ=0.0, SCALE=1.0, ALF=0.0, THETA=0.0, INMODE=4,
TNODE=0, TNPS=0, TINTS=0, &END
48.2093 0.5001 0.0045
48.2093 2.4757 0.0375
48.2093 2.8105 0.1604
48.2093 2.9106 0.5614
48.2093 2.9453 1.6667
48.2093 2.9469 3.1668
48.2093 2.9474 4.6669
48.2093 2.9462 6.1670
48.2093 2.9462 7.6671
48.2093 2.9424 9.1671
48.2093 2.9024 10.6669
48.2093 2.6462 11.5397
48.2093 1.4996 11.5559
48.2093 0.0000 11.5570
&BPNODE TNODE=3, TNPC=0, TINTC=0, &END
&SECT1 STX=0.0, STY=0.0, STZ=0.0, SCALE=1.0, ALF=0.0, THETA=0.0, INMODE=4,
TNODE=0, TNPS=0, TINTS=0, &END
48.8055 1.4733 0.0050
48.8055 2.3269 0.0446
48.8055 2.6221 0.1829

```

```

44.5909 4.1662 6.5612
44.5909 4.1662 8.2284
44.5909 4.1662 9.8966
44.5909 3.9300 11.5627
44.5909 2.8142 11.6030
44.5909 2.8142 11.6030
44.5909 1.4071 11.6030
&BPNODE TNODE=3, TNPC=0, TINTC=0, &END
&SECT1 STX=0.0, STY=0.0, STZ=0.0, SCALE=1.0, ALF=0.0, THETA=0.0, INMODE=4,
TNODE=3, TNPS=0, TINTS=0, &END
44.9164 0.0000 0.0000
44.9164 1.5267 0.0138
44.9164 2.9750 0.0819
44.9164 3.0206 0.4023
44.9164 4.0505 1.5694
44.9164 4.0553 3.2220
44.9164 4.0564 4.8747
44.9164 4.0566 6.5274
44.9164 4.0566 8.1800
44.9164 4.0566 9.8327
44.9164 4.0562 11.4863
44.9164 2.8142 11.5862
44.9164 1.4071 11.5862
44.9164 0.0000 11.5962
&BPNODE TNODE=3, TNPC=0, TINTC=0, &END
&SECT1 STX=0.0, STY=0.0, STZ=0.0, SCALE=1.0, ALF=0.0, THETA=0.0, INMODE=4,
TNODE=0, TNPS=0, TINTS=0, &END
45.7687 0.0000 0.0000
45.7687 1.6149 0.0016
45.7687 3.0606 0.1009
45.7687 3.2321 0.4387
45.7687 3.7625 1.5799
45.7687 3.7679 3.1948
45.7687 3.7692 4.8097
45.7687 3.7695 6.4245
45.7687 3.7695 8.0394
45.7687 3.7693 9.6543
45.7687 3.7678 11.2767
45.7687 1.8142 11.5857
45.7687 1.4071 11.5860
45.7687 0.0000 11.5861
&BPNODE TNODE=3, TNPC=0, TINTC=0, &END
&SECT1 STX=0.0, STY=0.0, STZ=0.0, SCALE=1.0, ALF=0.0, THETA=0.0, INMODE=4,
TNODE=0, TNPS=0, TINTS=0, &END
46.8222 0.0000 0.0000
46.8222 1.5638 0.0353
46.8222 2.9299 0.1249
46.8222 3.3765 0.4866
46.8222 3.4068 1.5991
46.8222 3.4128 3.1628
46.8222 3.4143 4.7266
46.8222 3.4146 6.2903
46.8222 3.4146 7.8541
46.8222 3.4142 9.4178
46.8222 3.4111 10.9814
46.8222 2.8650 11.5700
46.8222 1.4071 11.5733
46.8222 0.0000 11.5735
&BPNODE TNODE=3, TNPC=0, TINTC=0, &END
&SECT1 STX=0.0, STY=0.0, STZ=0.0, SCALE=1.0, ALF=0.0, THETA=0.0, INMODE=4,
TNODE=0, TNPS=0, TINTS=0, &END
47.6745 0.0000 0.0000
47.6745 1.5223 0.0323
47.6745 2.9927 0.1456
47.6745 3.0895 0.5253
47.6745 3.1192 1.6204
47.6745 3.1255 3.1427
47.6745 3.1271 4.6650

```



```

43.7277 6.5553 11.8407
44.3717 6.5553 11.6352
44.5896 6.5553 11.5308
#EPNODE TNODE=3, TNPC=0, TINTC=0, #END
#SECTI STX=0.0, STY=0.0, STZ=0.0, SCALE=1.0, ALF=0.0, THETA=0.0, INMODE=4,
#TNODES=0, TNPS=0, TIMPS=0, #END
44.5896 9.0503 11.5308
44.3717 9.0503 11.4914
43.7277 9.0503 11.4763
42.6855 9.0503 11.4563
41.2909 9.0503 11.4289
37.7006 9.0503 11.4072
35.6619 9.0503 11.3790
31.5777 9.0503 11.3391
31.5390 9.0503 11.4614
29.6349 9.0503 11.5647
27.9487 9.0503 11.7283
26.5541 9.0503 11.9690
25.5119 9.0503 12.2862
24.8679 9.0503 12.6691
24.6500 9.0503 13.1000
24.8679 9.0503 13.5517
26.5541 9.0503 14.2646
27.9487 9.0503 14.4706
29.6349 9.0503 14.5367
31.5390 9.0503 14.4449
35.6619 9.0503 14.2098
37.7006 9.0503 13.8271
39.6047 9.0503 13.4473
41.2909 9.0503 12.9980
42.6855 9.0503 12.5573
43.7277 9.0503 12.1607
44.3717 9.0503 11.8407
44.5896 9.0503 11.6352
#EPNODE TNODE=3, TNPC=0, TINTC=0, #END
#SECTI STX=0.0, STY=0.0, STZ=0.0, SCALE=1.0, ALF=0.0, THETA=0.0, INMODE=4,
#TNODES=0, TNPS=0, TIMPS=0, #END
44.5896 12.4081 11.5308
44.3717 12.4081 11.4914
43.7277 12.4081 11.4763
42.6855 12.4081 11.4563
41.2909 12.4081 11.4289
39.6047 12.4081 11.3871
37.7006 12.4081 11.3790
35.6619 12.4081 11.3791
31.5390 12.4081 11.3791
29.6349 12.4081 11.5647
27.9487 12.4081 11.7283
26.5541 12.4081 11.9690
25.5119 12.4081 12.2862
24.8679 12.4081 12.6691
24.6500 12.4081 13.1000
24.8679 12.4081 13.5517
26.5541 12.4081 14.2646
27.9487 12.4081 14.4706
29.6349 12.4081 14.5367
31.5390 12.4081 14.4449
35.6619 12.4081 14.2098
37.7006 12.4081 13.8271
39.6047 12.4081 13.4473
41.2909 12.4081 12.9980
42.6855 12.4081 12.5573
43.7277 12.4081 12.1607
44.3717 12.4081 11.8407
44.5896 12.4081 11.6352
#EPNODE TNODE=3, TNPC=0, TINTC=0, #END
#SECTI STX=0.0, STY=0.0, STZ=0.0, SCALE=1.0, ALF=0.0, THETA=0.0, INMODE=4,
#TNODES=0, TNPS=0, TIMPS=0, #END
44.5896 16.4986 11.5308
44.3717 16.4986 11.4914

```

```

29.6349 4.5000 14.5367
31.5390 4.5000 14.4449
35.6619 4.5000 14.2098
37.7006 4.5000 13.8271
39.6047 4.5000 13.4473
41.2909 4.5000 12.9980
42.6855 4.5000 12.5573
43.7277 4.4570 11.8400
44.3717 4.2400 11.6316
#EPNODE TNODE=3, TNPC=0, TINTC=0, #END
#SECTI STX=0.0, STY=0.0, STZ=0.0, SCALE=1.0, ALF=0.0, THETA=0.0, INMODE=4,
#TNODES=0, TNPS=0, TIMPS=0, #END
44.5896 5.0188 11.5308
44.3717 5.0188 11.4914
43.7277 5.0188 11.4763
42.6855 5.0188 11.4563
41.2909 5.0188 11.4289
37.7006 5.0188 11.3914
35.6619 5.0188 11.3740
31.5777 5.0188 11.3391
31.5390 5.0188 11.4614
29.6349 5.0188 11.5647
27.9487 5.0188 11.7283
26.5541 5.0188 11.9690
25.5119 5.0188 12.2862
24.8679 5.0188 12.6691
24.6500 5.0188 13.1000
24.8679 5.0188 13.5517
26.5541 5.0188 13.9485
27.9487 5.0188 14.2646
29.6349 5.0188 14.4706
31.5390 5.0188 14.4449
35.6619 5.0188 14.2098
37.7006 5.0188 13.8271
39.6047 5.0188 12.9980
41.2909 5.0188 12.5573
42.6855 5.0188 12.1607
43.7277 5.0188 11.8407
44.3717 5.0188 11.6352
44.5896 5.0188 11.5308
#EPNODE TNODE=3, TNPC=0, TINTC=0, #END
#SECTI STX=0.0, STY=0.0, STZ=0.0, SCALE=1.0, ALF=0.0, THETA=0.0, INMODE=4,
#TNODES=0, TNPS=0, TIMPS=0, #END
44.5896 11.4914 11.5308
44.3717 11.4914 11.4914
43.7277 11.4914 11.4763
42.6855 11.4914 11.4563
41.2909 11.4914 11.4289
39.6047 11.4914 11.3871
37.7006 11.4914 11.3790
35.6619 11.4914 11.3791
31.5390 11.4914 11.3791
29.6349 11.4914 11.5647
27.9487 11.4914 11.7283
26.5541 11.4914 11.9690
25.5119 11.4914 12.2862
24.8679 11.4914 12.6691
24.6500 11.4914 13.1000
24.8679 11.4914 13.5517
26.5541 11.4914 14.2646
27.9487 11.4914 14.4706
29.6349 11.4914 14.5367
31.5390 11.4914 14.4449
35.6619 11.4914 14.2098
37.7006 11.4914 13.8271
39.6047 11.4914 13.4473
41.2909 11.4914 12.9980
42.6855 11.4914 12.5573
43.7277 11.4914 12.1607
44.3717 11.4914 11.8407
44.5896 11.4914 11.6352

```

```

29.6349 26.2326 11.5647
27.9487 26.2326 11.7281
25.5119 26.2326 12.2862
24.8679 26.2326 12.6691
24.6500 26.2326 13.1000
24.8679 26.2326 13.5517
25.5119 26.2326 13.9485
26.5841 26.2326 14.2966
27.9487 26.2326 14.5167
29.6349 26.2326 14.4449
31.5777 26.2326 14.2088
35.6619 26.2326 13.8627
37.7006 26.2326 13.4473
39.6047 26.2326 12.9980
41.2909 26.2326 12.5573
42.6855 26.2326 12.1607
43.7277 26.2326 11.8407
44.5896 26.2326 11.6352
44.5896 26.2326 11.5308
$BPNODE TNODE=3, TNPC=0, TINTC=0, $END
$SECT1 STX=0.0, STY=0.0, STZ=0.0, THETA=0.0, ALF=0.0, SCALE=1.0, INNODE=4.
$END
TNODES=3, TNPS=0, TINTS=0, $END
44.5896 31.5000 11.5308
44.3717 31.5000 11.4763
43.7277 31.5000 11.4289
42.6855 31.5000 11.4563
42.9909 31.5000 11.4289
39.6047 31.5000 11.4032
37.7006 31.5000 11.3871
35.6619 31.5000 11.3790
33.5777 31.5000 11.3991
31.5390 31.5000 11.4614
29.6349 31.5000 11.4647
27.9487 31.5000 11.7283
26.5841 31.5000 11.5647
25.5119 31.5000 12.2862
24.8679 31.5000 12.6691
24.6500 31.5000 13.1000
24.8679 31.5000 13.5517
25.5119 31.5000 13.9485
26.5841 31.5000 14.2966
27.9487 31.5000 14.5167
29.6349 31.5000 14.4449
31.5777 31.5000 14.2088
35.6619 31.5000 13.8627
37.7006 31.5000 13.4473
39.6047 31.5000 12.9980
41.2909 31.5000 12.5573
42.6855 31.5000 12.1607
43.7277 31.5000 11.8407
44.5896 31.5000 11.6352
44.5896 31.5000 11.5308
$BPNODE TNODE=3, TNPC=0, TINTC=0, $END
$APATCH1 IREV=0, IDPAT=1, MAKE=0, KCOMP=1, KASS=1, IPATSYH=1, IPATCOP=0, $END
$MING_MID_AILERON
$SECT1 STX=0.0, STY=0.0, STZ=0.0, THETA=1.0, ALF=0.0, SCALE=1.0, INNODE=4.
$END
TNODES=0, TNPS=0, TINTS=0, $END
44.5896 31.5000 11.4914
43.7277 31.5000 11.4763
42.6855 31.5000 11.4563
41.2909 31.5000 11.4289
39.6047 31.5000 11.4032
37.7006 31.5000 11.3871
35.6619 31.5000 11.3790
33.5777 31.5000 11.3991
31.5390 31.5000 11.4614
29.6349 31.5000 11.4647
27.9487 31.5000 11.7283
26.5841 31.5000 11.5647
25.5119 31.5000 12.2862
24.8679 31.5000 12.6691
24.6500 31.5000 13.1000
24.8679 31.5000 13.5517
25.5119 31.5000 13.9485
26.5841 31.5000 14.2966
27.9487 31.5000 14.5167
29.6349 31.5000 14.4449
31.5777 31.5000 14.2088
35.6619 31.5000 13.8627
37.7006 31.5000 13.4473
39.6047 31.5000 12.9980
41.2909 31.5000 12.5573
42.6855 31.5000 12.1607
43.7277 31.5000 11.8407
44.5896 31.5000 11.6352
44.5896 31.5000 11.5308
$BPNODE TNODE=3, TNPC=0, TINTC=0, $END

```

```

43.7277 16.4996 11.4763
42.6855 16.4996 11.4289
41.2909 16.4996 11.4032
39.6047 16.4996 11.3871
37.7006 16.4996 11.3790
35.6619 16.4996 11.3991
33.5777 16.4996 11.4614
31.5390 16.4996 11.5647
29.6349 16.4996 11.7283
27.9487 16.4996 11.2862
26.5841 16.4996 11.2862
25.5119 16.4996 12.6691
24.8679 16.4996 13.1000
24.6500 16.4996 13.5517
24.8679 16.4996 13.9485
25.5119 16.4996 14.2966
26.5841 16.4996 14.2966
27.9487 16.4996 14.4706
29.6349 16.4996 14.3346
31.5390 16.4996 14.2088
33.5777 16.4996 13.8627
35.6619 16.4996 13.4473
37.7006 16.4996 12.9980
39.6047 16.4996 12.5573
41.2909 16.4996 12.1607
42.6855 16.4996 11.8407
43.7277 16.4996 11.6352
44.3717 16.4996 11.5308
44.5896 16.4996 11.5308
$BPNODE TNODE=3, TNPC=0, TINTC=0, $END
$SECT1 STX=0.0, STY=0.0, STZ=0.0, THETA=0.0, ALF=0.0, SCALE=1.0, INNODE=4.
$END
TNODES=3, TNPS=0, TINTS=0, $END
44.5896 21.1675 11.5308
44.3717 21.1675 11.4914
43.7277 21.1675 11.4647
42.6855 21.1675 11.4289
41.2909 21.1675 11.4289
39.6047 21.1675 11.4032
37.7006 21.1675 11.3871
35.6619 21.1675 11.3790
33.5777 21.1675 11.3991
31.5390 21.1675 11.4614
29.6349 21.1675 11.5647
27.9487 21.1675 11.7283
26.5841 21.1675 11.7283
25.5119 21.1675 12.2862
24.8679 21.1675 12.6691
24.6500 21.1675 13.1000
24.8679 21.1675 13.5517
25.5119 21.1675 13.9485
26.5841 21.1675 14.2646
27.9487 21.1675 14.4706
29.6349 21.1675 14.3346
31.5390 21.1675 14.2088
33.5777 21.1675 14.2088
35.6619 21.1675 13.8627
37.7006 21.1675 13.4473
39.6047 21.1675 12.9980
41.2909 21.1675 12.5573
42.6855 21.1675 12.1607
43.7277 21.1675 11.8407
44.3717 21.1675 11.6352
44.5896 21.1675 11.5308
$BPNODE TNODE=3, TNPC=0, TINTC=0, $END
$APATCH1 IREV=0, IDPAT=1, MAKE=0, KCOMP=1, KASS=1, IPATSYH=1, IPATCOP=0, $END
$MING_MID_AILERON
$SECT1 STX=0.0, STY=0.0, STZ=0.0, THETA=1.0, ALF=0.0, SCALE=1.0, INNODE=4.
$END
TNODES=0, TNPS=0, TINTS=0, $END
44.5896 26.2326 11.5308
44.3717 26.2326 11.4914
43.7277 26.2326 11.4763
42.6855 26.2326 11.4563
41.2909 26.2326 11.4289
39.6047 26.2326 11.4289
37.7006 26.2326 11.4032
35.6619 26.2326 11.3871
33.5777 26.2326 11.3991
31.5390 26.2326 11.4614
29.6349 26.2326 11.4647
27.9487 26.2326 11.7283
26.5841 26.2326 11.5647
25.5119 26.2326 12.2862
24.8679 26.2326 12.6691
24.6500 26.2326 13.1000
24.8679 26.2326 13.5517
25.5119 26.2326 13.9485
26.5841 26.2326 14.2966
27.9487 26.2326 14.5167
29.6349 26.2326 14.4449
31.5390 26.2326 14.2088
33.5777 26.2326 13.8627
35.6619 26.2326 13.4473
37.7006 26.2326 12.9980
39.6047 26.2326 12.5573
41.2909 26.2326 12.1607
42.6855 26.2326 11.8407
43.7277 26.2326 11.6352
44.3717 26.2326 11.5308
44.5896 26.2326 11.5308
$BPNODE TNODE=3, TNPC=0, TINTC=0, $END

```



```

35.6619 40.1000 13.8627
37.7006 40.1000 13.4473
39.6047 40.1000 12.9980
41.2909 40.1000 12.5573
42.6855 40.1000 12.1607
44.3717 40.1000 11.7282
44.5896 40.1000 11.5308
&BPNODE TNODE=3, TNPC=0, TINTC=0, &END
&SECT1 STX=0.0, STY=0.0, STZ=0.0, SCALE=1.0, ALF=0.0, THETA=0.0, INNODE=4,
TNODE=0, TNPS=0, TINTS=0, &END
44.3717 44.4000 11.4914
43.7277 44.4000 11.4763
42.6855 44.4000 11.4563
41.2909 44.4000 11.4312
39.6047 44.4000 11.4032
37.7006 44.4000 11.3871
35.6619 44.4000 11.3790
33.5777 44.4000 11.3991
31.5390 44.4000 11.4614
29.6349 44.4000 11.5647
27.9487 44.4000 11.7283
26.5541 44.4000 11.9690
25.5119 44.4000 12.2862
24.8679 44.4000 13.1000
24.6500 44.4000 13.1000
24.8679 44.4000 13.5517
25.5119 44.4000 13.9485
26.5541 44.4000 14.2646
27.9487 44.4000 14.4706
29.6349 44.4000 14.5367
31.5390 44.4000 14.4449
33.5777 44.4000 13.8627
35.6619 44.4000 13.4473
37.7006 44.4000 13.0000
39.6047 44.4000 12.9980
41.2909 44.4000 12.5573
42.6855 44.4000 12.1607
44.3717 44.4000 11.8407
44.5896 44.4000 11.6352
&BPNODE TNODE=3, TNPC=0, TINTC=0, &END
&SECT1 STX=0.0, STY=0.0, STZ=0.0, SCALE=1.0, ALF=0.0, THETA=0.0, INNODE=4,
TNODE=0, TNPS=0, TINTS=0, &END
44.3717 40.1000 11.4914
43.7277 40.1000 11.4763
42.6855 40.1000 11.4563
41.2909 40.1000 11.4312
39.6047 40.1000 11.4032
37.7006 40.1000 11.3871
35.6619 40.1000 11.3790
33.5777 40.1000 11.3991
31.5390 40.1000 11.4614
29.6349 40.1000 11.5647
27.9487 40.1000 11.7283
26.5541 40.1000 11.9690
25.5119 40.1000 12.2862
24.8679 40.1000 13.1000
24.6500 40.1000 13.1000
24.8679 40.1000 13.5517
25.5119 40.1000 13.9485
26.5541 40.1000 14.2646
27.9487 40.1000 14.4706
29.6349 40.1000 14.4449
31.5390 40.1000 14.5367
33.5777 40.1000 13.8627
35.6619 40.1000 13.4473
37.7006 40.1000 13.0000
39.6047 40.1000 12.9980
41.2909 40.1000 12.5573
42.6855 40.1000 12.1607
44.3717 40.1000 11.8407
44.5896 40.1000 11.6352

```

```

24.6500 31.5000 13.1000
24.8679 31.5000 13.5517
25.5119 31.5000 13.9485
27.9487 31.5000 14.4706
29.6349 31.5000 14.4449
31.5390 31.5000 14.5367
33.5777 31.5000 14.2088
35.6619 31.5000 13.8627
37.7006 31.5000 13.4473
39.6047 31.5000 12.9980
41.2909 31.5000 12.5573
42.6855 31.5000 12.1607
44.3717 31.5000 11.8407
44.5896 31.5000 11.6352
&BPNODE TNODE=3, TNPC=0, TINTC=0, &END
&SECT1 STX=0.0, STY=0.0, STZ=0.0, SCALE=1.0, ALF=0.0, THETA=0.0, INNODE=4,
TNODE=0, TNPS=0, TINTS=0, &END
44.3717 35.8000 11.4914
43.7277 35.8000 11.4763
42.6855 35.8000 11.4563
41.2909 35.8000 11.4312
39.6047 35.8000 11.4032
37.7006 35.8000 11.3871
35.6619 35.8000 11.3790
33.5777 35.8000 11.3991
31.5390 35.8000 11.4614
29.6349 35.8000 11.5647
27.9487 35.8000 11.7283
26.5541 35.8000 11.9690
25.5119 35.8000 12.2862
24.8679 35.8000 12.6691
24.6500 35.8000 13.1000
24.8679 35.8000 13.5517
25.5119 35.8000 13.9485
26.5541 35.8000 14.2646
27.9487 35.8000 14.4706
29.6349 35.8000 14.4449
31.5390 35.8000 14.5367
33.5777 35.8000 14.2088
35.6619 35.8000 13.8627
37.7006 35.8000 13.4473
39.6047 35.8000 13.0000
41.2909 35.8000 12.9980
42.6855 35.8000 12.5573
44.3717 35.8000 11.8407
44.5896 35.8000 11.6352
&BPNODE TNODE=3, TNPC=0, TINTC=0, &END
&SECT1 STX=0.0, STY=0.0, STZ=0.0, SCALE=1.0, ALF=0.0, THETA=0.0, INNODE=4,
TNODE=0, TNPS=0, TINTS=0, &END
44.3717 40.1000 11.4914
43.7277 40.1000 11.4763
42.6855 40.1000 11.4563
41.2909 40.1000 11.4312
39.6047 40.1000 11.4032
37.7006 40.1000 11.3871
35.6619 40.1000 11.3790
33.5777 40.1000 11.3991
31.5390 40.1000 11.4614
29.6349 40.1000 11.5647
27.9487 40.1000 11.7283
26.5541 40.1000 11.9690
25.5119 40.1000 12.2862
24.8679 40.1000 12.6691
24.6500 40.1000 13.1000
24.8679 40.1000 13.5517
25.5119 40.1000 13.9485
26.5541 40.1000 14.2646
27.9487 40.1000 14.4706
29.6349 40.1000 14.5367
31.5390 40.1000 14.4449
33.5777 40.1000 14.2088

```

```

&BPNODE TNODE=3, TNPC=0, TINTC=0, &END
&SECT1 STX=0.0, STY=0.0, STZ=0.0, SCALE=1.0, ALF=0.0, THETA=0.0, INHODE=4,
TNODES=3, TNPS=0, TINTS=0, &END
43.6322 57.0000 11.5517
43.0121 57.0000 11.5372
42.0032 57.0000 11.5180
40.6669 57.0000 11.4916
39.0439 57.0000 11.4668
37.2112 57.0000 11.4513
35.2430 57.0000 11.4436
33.2806 57.0000 11.4629
29.4480 57.0000 11.2523
27.8627 57.0000 11.7758
25.4756 57.0000 12.0114
24.9597 57.0000 12.6853
24.6500 57.0000 13.1000
24.8597 57.0000 13.5348
26.4827 57.0000 13.9167
27.8250 57.0000 14.2192
31.2806 57.0000 14.4828
31.2806 57.0000 14.3944
35.2429 57.0000 14.1673
35.2490 57.0000 13.8341
37.2112 57.0000 13.4342
39.0439 57.0000 13.0018
40.6669 57.0000 12.5659
43.0121 57.0000 11.8879
43.6322 57.0000 11.6901
43.8419 57.0000 11.5897
&BPNODE TNODE=3, TNPC=0, TINTC=0, &END
&SECT1 STX=0.0, STY=0.0, STZ=0.0, SCALE=1.0, ALF=0.0, THETA=0.0, INHODE=4,
TNODES=0, TNPS=0, TINTS=0, &END
43.2945 59.9282 11.5850
43.0808 59.9282 11.5818
41.5141 59.9282 11.5631
40.2100 59.9282 11.5375
38.6334 59.9282 11.5134
36.8530 59.9282 11.4983
34.9467 59.9282 11.4908
32.9978 59.9282 11.5076
31.0915 59.9282 11.6644
29.7134 59.9282 11.8174
26.4304 59.9282 12.0424
25.4560 59.9282 12.3391
24.8537 59.9282 12.6971
24.6500 59.9282 13.1000
24.8537 59.9282 13.5244
25.4560 59.9282 13.9890
29.7134 59.9282 14.3815
31.0915 59.9282 14.4433
32.9978 59.9282 14.3575
34.9467 59.9282 14.1368
36.8530 59.9282 13.8132
38.6334 59.9282 13.4247
40.2100 59.9282 12.9217
41.5141 59.9282 12.2217
43.0121 59.9282 11.9225
43.0908 59.9282 11.7303
43.2945 59.9282 11.6327
&BPNODE TNODE=3, TNPC=0, TINTC=0, &END
&SECT1 STX=0.0, STY=0.0, STZ=0.0, SCALE=1.0, ALF=0.0, THETA=0.0, INHODE=4,
TNODES=3, TNPS=0, TINTS=0, &END
43.0941 61.0000 11.6485
42.8926 61.0000 11.5981
42.3258 61.0000 11.5796
40.0422 61.0000 11.5543
38.4831 61.0000 11.5304
36.7218 61.0000 11.5156
34.8360 61.0000 11.5081
32.9081 61.0000 11.5267

```

```

&BPNODE TNODE=3, TNPC=0, TINTC=0, &END
&SECT1 STX=0.0, STY=0.0, STZ=0.0, SCALE=1.0, ALF=0.0, THETA=0.0, INHODE=4,
TNODES=3, TNPS=0, TINTS=0, &END
44.5896 53.0000 11.5308
44.3717 53.0000 11.4914
43.7277 53.0000 11.4763
42.6855 53.0000 11.4568
41.2909 53.0000 11.4032
39.7047 53.0000 11.3871
35.6619 53.0000 11.3790
33.5777 53.0000 11.3991
31.5390 53.0000 11.4614
29.6349 53.0000 11.5647
27.9487 53.0000 11.7283
26.5541 53.0000 11.9862
25.5119 53.0000 12.2691
24.6500 53.0000 12.6691
24.6500 53.0000 13.1000
24.8679 53.0000 13.5517
25.5119 53.0000 13.9485
26.5541 53.0000 14.2646
27.9487 53.0000 14.4706
29.6349 53.0000 14.4849
31.5777 53.0000 14.3849
33.5777 53.0000 13.8627
35.6619 53.0000 13.8627
37.7006 53.0000 13.4473
39.6047 53.0000 12.9980
41.2909 53.0000 12.5573
42.6855 53.0000 12.1607
43.7277 53.0000 11.8152
44.5896 53.0000 11.5108
&BPNODE TNODE=3, TNPC=0, TINTC=0, &END
&PATCH IREV=0, IDPAT=1, MAKE=0, KCOMP=1, KASS=1, IPATSYH=1, IPATCOP=0, &END
WING_OUTBOARD_TAPER
&SECT1 STX=0.0, STY=0.0, STZ=0.0, SCALE=1.0, ALF=0.0, THETA=0.0, INHODE=4,
TNODES=0, TNPS=0, TINTS=0, &END
44.3717 53.0000 11.5108
44.3717 53.0000 11.4914
43.7277 53.0000 11.4763
42.6855 53.0000 11.4563
41.2909 53.0000 11.4289
41.2909 53.0000 11.4032
39.6047 53.0000 11.3571
37.7006 53.0000 11.3391
35.6619 53.0000 11.3391
33.5777 53.0000 11.4614
29.6349 53.0000 11.5647
27.9487 53.0000 11.7283
26.5541 53.0000 11.9650
25.5119 53.0000 12.2862
24.8679 53.0000 12.6691
24.6500 53.0000 13.1000
24.8679 53.0000 13.5517
25.5119 53.0000 13.9485
27.9487 53.0000 14.2646
29.6349 53.0000 14.4706
31.5390 53.0000 14.4449
33.5777 53.0000 14.2088
35.6619 53.0000 13.8627
37.7006 53.0000 13.4473
39.6047 53.0000 12.9980
41.2909 53.0000 12.5573
42.6855 53.0000 11.8152
43.7277 53.0000 11.8407
44.3717 53.0000 11.6352
44.5896 53.0000 11.5308
&BPNODE TNODE=3, TNPC=0, TINTC=0, &END
&SECT1 STX=0.0, STY=0.0, STZ=0.0, SCALE=1.0, ALF=0.0, THETA=0.0, INHODE=4,
TNODES=0, TNPS=0, TINTS=0, &END
43.8419 57.0000 11.5897

```



```

85.9762 6.8666 8.4268
87.4641 6.8666 8.4541
88.7049 6.8666 8.4349
90.8131 6.8666 8.3809
92.4702 6.8666 8.3077
93.9231 6.8666 8.2305
95.0541 6.8666 8.1622
96.0173 6.8666 8.0900
&BNODE TNODE=3, TNPC=0, TINTC=0, &END
&SECT1 STX=0.0, STY=0.0, STZ=0.0, SCALE=1.0, ALF=0.0, THETA=0.0, INMODE=4,
&END
96.0250 9.9375 8.0900
95.7916 9.9375 8.0679
95.1102 9.9375 8.0215
94.0361 9.9375 7.9566
92.6563 9.9375 7.8832
91.0926 9.9375 7.8138
89.4424 9.9375 7.7625
87.8687 9.9375 7.7102
85.4148 9.9375 7.6424
84.7134 9.9375 7.5936
84.5000 9.9375 7.5900
85.4148 9.9375 8.2264
86.4889 9.9375 8.4098
87.8687 9.9375 8.4358
89.4424 9.9375 8.4175
91.0926 9.9375 8.3682
92.6563 9.9375 8.2794
95.1102 9.9375 8.1585
96.0250 9.9375 8.1121
&BNODE TNODE=3, TNPC=0, TINTC=0, &END
&SECT1 STX=0.0, STY=0.0, STZ=0.0, SCALE=1.0, ALF=0.0, THETA=0.0, INMODE=4,
&END
96.0227 13.0084 8.0900
95.8117 13.0084 8.0951
94.1692 13.0084 7.9637
92.8424 13.0084 7.8942
89.7987 13.0084 7.7798
88.3083 13.0084 7.7625
87.0016 13.0084 7.7871
85.9844 13.0084 7.8355
85.1391 13.0084 7.8608
82.1190 13.0084 8.2192
85.9844 13.0084 8.3245
87.0016 13.0084 8.3929
88.3083 13.0084 8.4175
89.7987 13.0084 8.4002
91.3520 13.0084 8.3516
92.8424 13.0084 8.2958
94.1692 13.0084 8.1549
95.8117 13.0084 8.1109
96.0227 13.0084 8.0900
&BNODE TNODE=3, TNPC=0, TINTC=0, &END
&SECT1 STX=0.0, STY=0.0, STZ=0.0, SCALE=1.0, ALF=0.0, THETA=0.0, INMODE=4,
&END
96.0397 15.7786 8.0900
95.8298 15.7786 8.0981
92.7512 15.7786 7.9700
93.0103 15.7786 7.9040
91.5951 15.7786 7.8416
90.1201 15.7786 7.7955
88.7049 15.7786 7.7790
87.4641 15.7786 7.8024
86.4982 15.7786 7.9674
85.6756 15.7786 8.0900

```

```

85.8955 15.7786 8.2127
86.4982 15.7786 8.3126
87.4641 15.7786 8.3776
88.7049 15.7786 8.4010
90.1201 15.7786 8.3845
91.5951 15.7786 8.3384
93.0103 15.7786 8.2760
94.1692 15.7786 8.2100
95.2171 15.7786 8.1516
96.0397 15.7786 8.1099
&BNODE TNODE=3, TNPC=0, TINTC=0, &END
&SECT1 STX=0.0, STY=0.0, STZ=0.0, SCALE=1.0, ALF=0.0, THETA=0.0, INMODE=4,
&END
96.0452 17.9771 8.0900
95.8442 17.9771 8.0710
93.2571 17.9771 7.9251
91.1436 17.9771 7.9119
91.7880 17.9771 7.8521
90.3752 17.9771 7.8079
89.0197 17.9771 7.7921
87.8312 17.9771 7.8145
86.9060 17.9771 7.8767
86.1180 17.9771 7.9725
86.3191 17.9771 8.2075
95.2069 17.9771 8.3655
85.0197 17.9771 8.3879
90.3752 17.9771 8.5721
91.7880 17.9771 8.3279
93.1436 17.9771 8.2681
94.3321 17.9771 8.2049
95.2573 17.9771 8.1490
96.0452 17.9771 8.1090
&BNODE TNODE=3, TNPC=0, TINTC=0, &END
&SECT1 STX=0.0, STY=0.0, STZ=0.0, SCALE=1.0, ALF=0.0, THETA=0.0, INMODE=4,
&END
96.0488 19.3886 8.0900
95.8534 19.3886 8.0715
95.2831 19.3886 8.0326
94.3841 19.3886 7.9783
93.2291 19.3886 7.9169
91.9119 19.3886 7.8528
90.5270 19.3886 7.8006
88.0668 19.3886 7.8223
87.1678 19.3886 7.8828
86.5975 19.3886 7.9758
86.4021 19.3886 8.0900
86.5975 19.3886 8.2042
87.1678 19.3886 8.2972
88.0668 19.3886 8.3774
90.5270 19.3886 8.3642
91.9119 19.3886 8.3212
93.2291 19.3886 8.2631
94.3841 19.3886 8.2017
95.2831 19.3886 8.1474
96.0488 19.3886 8.1065
&BNODE TNODE=3, TNPC=0, TINTC=0, &END
&SECT1 STX=0.0, STY=0.0, STZ=0.0, SCALE=1.0, ALF=0.0, THETA=0.0, INMODE=4,
&END
96.0500 19.8750 8.0900
95.8566 19.8750 8.0717
95.2920 19.8750 8.0332
94.4020 19.8750 7.9795
93.2596 19.8750 7.9286
90.5256 19.8750 7.8183
89.2314 19.8750 7.8035
88.1480 19.8750 7.8250
87.2580 19.8750 7.8848

```

```

81.8430 -0.4583 12.5601
84.3086 -0.5507 12.5601
97.3332 -0.5331 12.5601
90.5518 -0.4339 12.5601
93.5764 -0.2929 12.5601
96.0470 -0.1528 12.5601
98.2103 0.0000 12.5601
&BPNODE TNODE=3, TNPC=0, TINTC=0, &END
&SECT1 STX=0.0, STY=0.0, STZ=0.0, SCALE=1.0, ALF=0.0, THETA=0.0, INMODE=4,
TNODS=0, TNPS=0, TINTS=0, &END
98.9870 0.0000 14.9527
98.4870 0.0463 14.9527
97.0185 0.1401 14.9527
94.7686 0.2673 14.9527
92.0098 0.3824 14.9527
86.1119 0.5025 14.9527
84.0621 0.4182 14.9527
82.5936 0.2404 14.9527
82.0836 0.0000 14.9527
84.0621 -0.2404 14.9527
86.3119 -0.5025 14.9527
97.0185 -0.3824 14.9527
94.7686 -0.2673 14.9527
97.0185 -0.1401 14.9527
98.4870 -0.0463 14.9527
&BPNODE TNODE=3, TNPC=0, TINTC=0, &END
&SECT1 STX=0.0, STY=0.0, STZ=0.0, SCALE=1.0, ALF=0.0, THETA=0.0, INMODE=4,
TNODS=0, TNPS=0, TINTS=0, &END
98.4727 0.0411 17.7750
98.1703 0.1243 17.7750
96.1750 0.2371 17.7750
93.7274 0.3503 17.7750
91.1226 0.4314 17.7750
88.6750 0.4456 17.7750
86.6797 0.3709 17.7750
84.9250 0.2000 17.7750
85.3773 0.2132 17.7750
86.6797 -0.3709 17.7750
88.6750 -0.4456 17.7750
91.1226 -0.4314 17.7750
93.7274 -0.3503 17.7750
96.1750 -0.2371 17.7750
98.1703 -0.1243 17.7750
88.9250 0.0000 17.7750
&BPNODE TNODE=3, TNPC=0, TINTC=0, &END
&SECT1 STX=0.0, STY=0.0, STZ=0.0, SCALE=1.0, ALF=0.0, THETA=0.0, INMODE=4,
TNODS=0, TNPS=0, TINTS=0, &END
100.8530 0.0000 20.5973
100.4584 0.0358 20.5973
99.3222 0.1084 20.5973
97.5814 0.2068 20.5973
95.4452 0.3256 20.5973
91.0381 0.3888 20.5973
89.2973 0.3236 20.5973
88.1610 0.1860 20.5973
87.7664 0.0000 20.5973
88.1610 -0.1860 20.5973
89.2973 -0.3236 20.5973
91.0381 -0.3888 20.5973
95.4452 -0.3256 20.5973
97.5814 -0.2068 20.5973
99.3222 -0.1084 20.5973
100.4584 -0.0358 20.5973
100.8530 0.0000 20.5973
&BPNODE TNODE=3, TNPC=0, TINTC=0, &END
&SECT1 STX=0.0, STY=0.0, STZ=0.0, SCALE=1.0, ALF=0.0, THETA=0.0, INMODE=4,

```

```

86.6934 19.8750 7.9770
86.5000 19.8750 8.0900
86.6934 19.8750 8.2030
87.2580 19.8750 8.2952
88.1480 19.8750 8.3550
89.2914 19.8750 8.3765
90.5954 19.8750 8.3614
91.3546 19.8750 8.3199
92.4000 19.8750 8.2005
95.2920 19.8750 8.1468
95.8566 19.8750 8.1083
96.0500 19.8750 8.0900
&BPNODE TNODE=3, TNPC=0, TINTC=0, &END

&PATCU1 IRV=0, IDPAT=1, MAKE=0, KCOMP=1, KASS=1, IPATSYM=0, IPATCOP=0, &END
&SECT1 STX=0.0, STY=0.0, STZ=0.0, SCALE=1.0, ALF=0.0, THETA=0.0, INMODE=4,
TNODS=0, TNPS=0, TINTS=0, &END
97.5000 0.0000 10.4000
96.8969 0.0548 10.4000
95.1604 0.1657 10.4000
92.5000 0.3161 10.4000
89.2365 0.4571 10.4000
85.5000 0.5842 10.4000
79.8396 0.4945 10.4000
78.1031 0.2842 10.4000
77.5000 0.0000 10.4000
78.1031 -0.2842 10.4000
79.8396 -0.4945 10.4000
82.5000 -0.5942 10.4000
85.1625 -0.5772 10.4000
93.5000 0.3161 10.4000
95.1604 -0.1657 10.4000
96.8969 -0.0548 10.4000
97.5000 0.0000 10.4000
&BPNODE TNODE=3, TNPC=0, TINTC=0, &END
&SECT1 STX=0.0, STY=0.0, STZ=0.0, SCALE=1.0, ALF=0.0, THETA=0.0, INMODE=4,
TNODS=0, TNPS=0, TINTS=0, &END
97.6846 0.0510 10.9614
95.3896 0.1625 10.9614
92.7797 0.3101 10.9614
89.5783 0.4582 10.9614
86.1715 0.5643 10.9614
82.9700 0.5829 10.9614
80.3602 0.4851 10.9614
78.6258 0.2708 10.9614
78.5568 -0.2788 10.9614
80.3602 -0.4851 10.9614
82.9700 -0.5829 10.9614
86.1715 -0.5643 10.9614
89.5783 -0.4582 10.9614
92.7797 -0.3101 10.9614
95.3896 -0.1625 10.9614
97.6846 -0.0510 10.9614
&BPNODE TNODE=3, TNPC=0, TINTC=0, &END
&SECT1 STX=0.0, STY=0.0, STZ=0.0, SCALE=1.0, ALF=0.0, THETA=0.0, INMODE=4,
TNODS=0, TNPS=0, TINTS=0, &END
98.2101 0.0000 12.5601
97.6514 0.0508 12.5601
96.0420 0.1536 12.5601
93.5764 0.2829 12.5601
90.5518 0.4329 12.5601
87.3332 0.7331 12.5601
84.3086 0.9507 12.5601
81.8430 0.9293 12.5601
79.6745 0.0000 12.5601
80.2336 -0.2634 12.5601

```



```

&BPNODE TNODE=3, TNPC=0, TINTC=0, &END
&SECT1 STX=0.0, STY=0.0, STZ=0.0, SCALE=1.0, ALF=0.0, THETA=0.0, INMODE=4,
TNODE=0, TNPS=0, TINTS=0, &END
29.9113 1.5803 14.6732 0.5784 14.5484
29.9113 1.5803 14.6818 0.5784 14.5470
29.9113 1.5803 14.7940 0.5784 15.1403
29.9113 1.5803 15.0580 0.5784 15.3377
29.9113 1.5803 15.1900 0.5784 15.5350
29.9113 1.5803 15.4240 0.5784 15.7323
29.9113 1.5803 15.5860 0.5784 15.9296
&BPNODE TNODE=3, TNPC=0, TINTC=0, &END
&SECT1 STX=0.0, STY=0.0, STZ=0.0, SCALE=1.0, ALF=0.0, THETA=0.0, INMODE=4,
TNODE=0, TNPS=0, TINTS=0, &END
36.5637 0.3462 13.9250 0.1609 13.7823
36.5637 0.3462 14.0041 0.1609 13.8781
36.5637 0.3462 14.2235 0.1609 14.1173
36.5637 0.3462 14.4428 0.1609 14.3565
36.5637 0.3462 14.6622 0.1609 14.5957
36.5637 0.3462 14.8815 0.1609 14.8349
36.5637 0.3462 15.1009 0.1609 15.0741
36.5637 0.3462 15.3203 0.1609 15.3134
36.5637 0.3462 15.5396 0.1609 15.5526
36.5637 0.3462 15.7590 0.1609 15.7918
&BPNODE TNODE=3, TNPC=0, TINTC=0, &END
&SECT1 STX=0.0, STY=0.0, STZ=0.0, SCALE=1.0, ALF=0.0, THETA=0.0, INMODE=4,
TNODE=0, TNPS=0, TINTS=0, &END
37.1856 0.1609 13.7823 0.0413 13.6845
37.1856 0.1609 14.1173 0.0413 13.8480
37.1856 0.1609 14.4523 0.0413 14.0115
37.1856 0.1609 14.7873 0.0413 14.1750
37.1856 0.1609 15.1203 0.0413 14.3385
37.1856 0.1609 15.4533 0.0413 14.5020
37.1856 0.1609 15.7863 0.0413 14.6655
&BPNODE TNODE=3, TNPC=0, TINTC=0, &END
&SECT1 STX=0.0, STY=0.0, STZ=0.0, SCALE=1.0, ALF=0.0, THETA=0.0, INMODE=4,
TNODE=0, TNPS=0, TINTS=0, &END
37.7000 0.0000 13.7663 0.0000 14.0256
37.7000 0.0000 14.2849 0.0000 14.5442
37.7000 0.0000 14.8035 0.0000 14.8035
37.7000 0.0000 15.3221 0.0000 15.3221
37.7000 0.0000 15.8407 0.0000 15.8407
37.7000 0.0000 16.1000 0.0000 16.1000
&BPNODE TNODE=3, TNPC=0, TINTC=0, &END

&PATCH ITRIV=0, IPDAT=2, HAKE=0, KCOMP=1, KASS=1, IPATSYH=1, IPATCOP=0, &END
&FCI ENGINE MOD
&SECT1 STX=0.0, STY=0.0, STZ=0.0, SCALE=1.0, ALF=0.0, THETA=0.0, INMODE=4,
TNODE=0, TNPS=0, TINTS=0, &END
16.5000 0.0000 20.4000
16.5000 0.0000 20.4000
16.5000 0.0000 20.4000
16.5000 0.0000 20.4000

```

```

&BPNODE TNODE=3, TNPC=0, TINTC=0, &END
&SECT1 STX=0.0, STY=0.0, STZ=0.0, SCALE=1.0, ALF=0.0, THETA=0.0, INMODE=4,
TNODE=0, TNPS=0, TINTS=0, &END
29.9113 1.5803 14.6732 0.5784 14.5484
29.9113 1.5803 14.6818 0.5784 14.5470
29.9113 1.5803 14.7940 0.5784 15.1403
29.9113 1.5803 15.0580 0.5784 15.3377
29.9113 1.5803 15.1900 0.5784 15.5350
29.9113 1.5803 15.4240 0.5784 15.7323
29.9113 1.5803 15.5860 0.5784 15.9296
&BPNODE TNODE=3, TNPC=0, TINTC=0, &END
&SECT1 STX=0.0, STY=0.0, STZ=0.0, SCALE=1.0, ALF=0.0, THETA=0.0, INMODE=4,
TNODE=0, TNPS=0, TINTS=0, &END
31.1281 1.4826 14.6416 0.1609 13.7823
31.1281 1.4826 14.6504 0.1609 13.8781
31.1281 1.4826 14.7667 0.1609 14.1173
31.1281 1.4826 15.0351 0.1609 14.3565
31.1281 1.4826 15.1694 0.1609 14.5957
31.1281 1.4826 15.3036 0.1609 14.8349
31.1281 1.4826 15.4379 0.1609 15.0741
31.1281 1.4826 15.5721 0.1609 15.3134
31.1281 1.4826 15.7063 0.1609 15.5526
31.1281 1.4826 15.8406 0.1609 15.7918
&BPNODE TNODE=3, TNPC=0, TINTC=0, &END
&SECT1 STX=0.0, STY=0.0, STZ=0.0, SCALE=1.0, ALF=0.0, THETA=0.0, INMODE=4,
TNODE=0, TNPS=0, TINTS=0, &END
32.3719 1.3110 14.5598 0.0413 13.6845
32.3719 1.3110 14.7023 0.0413 13.8480
32.3719 1.3110 14.8450 0.0413 14.0115
32.3719 1.3110 14.9877 0.0413 14.1750
32.3719 1.3110 15.1304 0.0413 14.3385
32.3719 1.3110 15.2731 0.0413 14.5020
32.3719 1.3110 15.4158 0.0413 14.6655
32.3719 1.3110 15.7012 0.0413 14.8290
32.3719 1.3110 15.8439 0.0413 14.9925
&BPNODE TNODE=3, TNPC=0, TINTC=0, &END
&SECT1 STX=0.0, STY=0.0, STZ=0.0, SCALE=1.0, ALF=0.0, THETA=0.0, INMODE=4,
TNODE=0, TNPS=0, TINTS=0, &END
33.5886 1.0866 14.4337 0.0000 14.0256
33.5886 1.0866 14.4475 0.0000 14.5442
33.5886 1.0866 14.6044 0.0000 14.8035
33.5886 1.0866 14.7614 0.0000 15.3221
33.5886 1.0866 15.0754 0.0000 15.8407
33.5886 1.0866 15.2124 0.0000 16.1000
33.5886 1.0866 15.3894 0.0000 16.1000
33.5886 1.0866 15.5464 0.0000 16.1000
33.5886 1.0866 15.7034 0.0000 16.1000
&BPNODE TNODE=3, TNPC=0, TINTC=0, &END
&SECT1 STX=0.0, STY=0.0, STZ=0.0, SCALE=1.0, ALF=0.0, THETA=0.0, INMODE=4,
TNODE=0, TNPS=0, TINTS=0, &END
34.7250 0.8137 14.2740 0.0000 14.0256
34.7250 0.8137 14.3074 0.0000 14.5442
34.7250 0.8137 14.4831 0.0000 14.8035
34.7250 0.8137 14.6589 0.0000 15.3221
34.7250 0.8137 14.8347 0.0000 15.8407
34.7250 0.8137 15.0105 0.0000 16.1000
34.7250 0.8137 15.3621 0.0000 16.1000
34.7250 0.8137 15.7137 0.0000 16.1000
34.7250 0.8137 15.8695 0.0000 16.1000
&BPNODE TNODE=3, TNPC=0, TINTC=0, &END
&SECT1 STX=0.0, STY=0.0, STZ=0.0, SCALE=1.0, ALF=0.0, THETA=0.0, INMODE=4,
TNODE=0, TNPS=0, TINTS=0, &END
35.7313 0.5784 14.0992 0.5784 14.1537
35.7313 0.5784 14.1537 0.5784 14.3510

```









```

&CONSTRM NONSL=0, KPSEL =
1,2,3,4,5,6,7,8,9,10,11,12,13,14,15,16,17,18,19,20,21,22,23,24,25,26,27,28,29,30,31,32,33,34,35,36,37,38,
1,2,3,4,5,6,7,8,9,10,11,12,13,14,15,16,17,18,19,20,21,22,23,24,25,26,27,28,29,30,31,32,33,34,35,36,37,38,
2998,1073,1045,1017,989,961,933,905,8639,2636,2594,2577,2550,2328,2306,2584,
&EN
D

```

```

&ELPARAM RN =929000, VISC = 0.022641, NSLBL = 1,2,3,4,5,6,7,8,9,10,11,
19,40,41,42,43,44,45,46,47,48,49,50,51,52,53,54,55,
&END

```

```

&VS1 NVOLR= 0, NVOLC= 0,
&VS2 X0= -0.1000, Y0= 1.5000, Z0= -0.1000, INTVSR= 1,
&VS3 X1= -0.1000, Y1= 1.5000, Z1= 0.1000, NPT1= 0,
&VS4 X2= -0.1000, Y2= 1.5000, Z2= 0.1000, NPT2= 20,
&VS5 X3= 1.1000, Y3= 1.5000, Z3= -0.1000, NPT3= 25,
&VS6 XRO= 2.0000, YRO= 2.0000, ZRO= 0.0000, INTVSC= 1,
&VS7 XRI= 4.0000, YRI= 2.0000, ZRI= 0.0000,
&VS8 XRI= 2.0000, YRI= 2.0000, ZRI= 1.0000,
&VS9 R1= 0.1000, R2= 1.0000, PH11= 0.0, PH12=360.0,
NRAD= 5, NPFI= 12, NLEN= 3,
&END

```

```

&SLIN1 NSTLIN=4,
&SLIN2 SK0= -2.5000, SY0= 2.50000, SZ0= 7.5000,
SU= 2.0000, SD= 2.0000, DS= 0.100, INTSL= 1,
&SLIN2 SK0= -8.25000, SY0= 0.00000, SZ0= 7.5000,
SU= 2.0000, SD= 2.0000, DS= 0.100, INTSL= 1,
&SLIN2 SK0= -6.5000, SY0= 2.50000, SZ0= 7.5000,
SU= 15.0000, SD= 100.0000, DS= 0.500, INTSL= 1,
&SLIN2 SK0= -8.25000, SY0= 0.00000, SZ0= 7.5000,
SU= 15.0000, SD= 100.0000, DS= 0.500, INTSL= 1,
&END

```

## LIST OF REFERENCES

1. Papageorgiou, E., "Development of a Dynamic Model for a UAV," Master's Thesis, Naval Postgraduate School, Monterey, CA, March 1997.
2. Garrison, P., and Pinella, D., *CMARC User's Guide*, AeroLogic, Inc, <http://www.iac.net/~aerol>, 1996.
3. Bertin, J. J., and Smith, M. L., *Aerodynamics for Engineers*, Prentice Hall, 1989.
4. Ashby, D. L., Dudley, M. R., Iguchi, S. K., Browne, L., and Katz, J., *Potential Flow Theory and Operation Guide for the Panel Code PMARC\_12*, NASA TM-102851, Ames Research Center, Moffet Field, CA., December 1992.
5. Anderson, J. D., *Fundamentals of Aerodynamics*, McGraw-Hill, Inc., 1991.
6. Lambert, M. A., *Evaluation of the NASA-AMES Panel Method (PMARC) for Aerodynamic Missile Design*, Master's Thesis, Naval Postgraduate School, CA, September, 1995.
7. Tuncer, I. H., and Platzer, M. F., *PMARC Potential Flow Solutions with Wakes Over an Ogive Cylinder at High Incidence*, AIAA Paper No. 97-1968, American Institute of Aeronautics and Astronautics, June 1997.
8. Cebeci, T., "Computation of Three-Dimensional Boundary Layers Including Separation," VKI Lecture Series, Douglas Aircraft Company, April 1986.
9. Young, A. D., *Boundary Layers*, American Institute of Aeronautics, 1989.
10. Jones, K. D., and Center, K. B., "Numerical Wake Visualization for Airfoils Undergoing Forced and Aeroelastic Motions," AIAA Paper No. 96-0055, January 1996.
11. Nowak, L. M., *Computational Investigations of a NACA 0012 Airfoil in Low Reynolds Number Flows*, Master's Thesis, Naval Postgraduate School, Monterey, CA, September 1992.
12. Kreplin, H. P., "Three-Dimensional Boundary Layer and Flow Field Data of an Inclined Prolate Spheroid," *AGARD Advisory Report No. 303: A Selection of Experimental Test Cases for the Validation of CFD Codes*, Volumes I and II, North Atlantic Treaty Organization, August 1994.

13. *Performance Phase Textbook-Volume I*, USAF Test Pilot School, Edwards AFB, CA., June 1988.
14. Nicolai, L. M., *Fundamentals of AIRCRAFT DESIGN*, METs, Inc., 1984.
15. Walden, A. B., van Dam, C. P., and Brandon, J. M., *Modeling of the Interaction Between a Lifting Wing and a Following Aircraft and Comparison with Experimental Results*, AIAA 96-0771, 34<sup>th</sup> Aerospace Sciences Meeting and Exhibit, Reno, NV, January 1996.

## INITIAL DISTRIBUTION LIST

1. Defense Technical Information Center..... 2  
 8725 John J. Kingman Road, Ste 0944  
 Ft. Belvoir, VA 22060-6218
2. Dudley Knox Library..... 2  
 Naval Postgraduate School  
 411 Dyer Rd.  
 Monterey, CA 93943-5101
3. Chairman..... 1  
 Department of Aeronautics and Astronautics, Code AA  
 Naval Postgraduate School  
 699 Dyer Road, Room 137  
 Monterey, CA 93943-5106
4. Dr. Max F. Platzner..... 5  
 Department of Aeronautics and Astronautics, Code AA/PL  
 Naval Postgraduate School  
 699 Dyer Road, Room 137  
 Monterey, CA 93943-5106
5. Dr. Ismail H. Tuncer..... 1  
 Department of Aeronautics and Astronautics, Code AA  
 Naval Postgraduate School  
 699 Dyer Road, Room 137  
 Monterey, CA 93943-5106
6. Dr. Kevin Jones..... 1  
 Department of Aeronautics and Astronautics, Code AA  
 Naval Postgraduate School  
 699 Dyer Road, Room 137  
 Monterey, CA 93943-5106
7. LCDR Stephen J. Pollard..... 2  
 Department of Aviation Safety  
 Naval Postgraduate School  
 1 University Circle  
 Monterey, CA 93943-5106

8. Peter Garrison..... 1  
AeroLogic, Inc.  
1613 Altivo Way  
Los Angeles, CA 90026